AN EXPERIMENTAL INVESTIGATION OF PARTICLE MOTION IN LIQUID FLUIDIZED BEDS

Thesis by

Charles Arthur Willus

In Partial Fulfillment of the Requirements

For the Degree of

Doctor of Philosophy

California Institute of Technology

Pasadena, California

1970

(Submitted August 10, 1970)

ACKNOWLEDGMENTS

It is a pleasure to express my gratitude and appreciation to Professor W. Duncan Rannie for the sound guidance, advice, and encouragement he provided during the course of this study.

Special appreciation is due to Mr. Frank T. Linton for his skilled help both in the fabrication of the test equipment for this study and also in the preparation of the figures. Notes of appreciation are also due to Mr. Carl Eastvedt for his expert advice on photographic problems and to Mrs. Roberta Duffy for typing the manuscript.

During the course of this study the writer was supported through a NASA Traineeship, an NSF Traineeship, and a special fellowship of the California Institute of Technology.

This work is dedicated to the writer's wife, Susan, and his parents, who shared all vicissitudes stemming from an endeavor of this type.

ABSTRACT

A laboratory study was made on particle motion in liquid fluidized beds. In Part 1, experiments made in a bed of 4-inch inside diameter with a large length-to-diameter ratio of 24 to 1 are described. Particle motion in the bed was found to be essentially a diffusion process. Diffusion coefficients for motion in the vertical direction were measured for glass beads of .236-inch diameter at a range of average bead concentrations. Vertical diffusion was independent of radial position in the bed.

The experimental findings on particle diffusion in the bed were compared to principles of diffusion of a turbulent fluid. A significant correlation between two successive vertical step lengths of short duration suggested that a bead is within an eddy of beads and fluid for a short time. The diffusion coefficients of the beads were much larger than the diffusion coefficients of the turbulent fluid in the absence of the beads, indicating that particles in a liquid fluidized bed augment instabilities.

Steady and quasi-steady patterns of particle circulation were observed in both a cylindrical bed with a length-to-diameter ratio of 5 to 1 and in beds of conical shape, and are described in Part 2. Weak waves also formed in this cylindrical bed; the observed propagating speed compared roughly to that estimated using the theory of kinematical waves.

Photographic materials on pages 17 , 18 , 65 , and 94 are essential and will not reproduce clearly on Xerox copies. Photographic copies should be ordered.

TABLE OF CONTENTS

LIST OF FIGURES

INTRODUCTION

A fluidized bed is a suspension of particles supported in the gravity field by a fluid which flows upwards through the particles. The weight of the particles is balanced by the drag exerted on them by the fluid in addition to buoyant forces. A porous bottom forms the lower boundary of the suspension and allows the fluid to enter the bed. At a given fluid flow rate, the height of the suspension remains steady, and the particles of the suspension are dispersed somewhat uniformly. The upper boundary of the suspension is flat and resembles a free surface, as there is a sharp demarcation between the suspension and the fluid above, devoid of particles. Although the suspension as a whole assumes specific boundaries, the particles of the suspension are in agitated and complex forms of motion.

With no flow through the column, the particles are at rest supported by the bottom. Their transformation to a fluidized state is reached only at a sufficiently large fluid flow rate. At a very small flow rate, the particles remain motionless, for the drag forces resulting from the flow are not sufficient to support their weight. This is referred to as a fixed bed; flow through a fixed bed is similar to that through a porous medium. As the fluid flow is increased, the bed swells slightly and a flow rate is reached at which some of the particles begin to shift, and the top of the bed begins to move. With a slight further increase in fluid flow, all the particles are set in motion. The irregular disturbance at the top of the bed increases as the bed begins to expand. This condition is known as incipient fluidization. Any further increase in the fluid flow rate results in an upward

surge of the top of the bed. The height of the bed stabilizes when the expansion of the solids is sufficient to accommodate the specific flow rate applied. Now the particles are suspended by the flow in a state of fluidization. If the fluid flow velocity is increased to a value greater than the free fall velocity of a single particle, the particles are carried upward and the bed is emptied.

Rapid development in fluidized beds was made in the 1940's by the petroleum industry as devices for the catalytic cracking of raw petroleum. A fluid consisting of some reacting species is used to fluidize a bed of particles which serves as the catalyst for the reaction. The use of fluidized beds in catalytic reaction processes remains today as a major application. However, the large surface area of the particles in a fluidized bed and also the agitation provided by the particles facilitate the application of fluidized beds as a means of temperature control (constant temperature bath) and also as a heat exchanger.

When a fluidized bed is used as a catalytic reactor or as a heat exchanger, regeneration of particles is usually required. For instance, the catalyst in a petroleum cracking process eventually becomes coated with unwanted chemicals and loses its effectiveness. The regeneration of particles is typically affected by continuously adding a fresh charge at the top of the bed while at the same time removing wasted particles at the bottom in order to keep the bed height constant. Particle diffusion coefficients, investigated in this study, are thus a parameter of important practical value, for a knowledge of diffusion coefficients allows an estimation to be made of the charac-

teristics of the residence time of a particle in a catalytic reactor or heat exchanger.

The theory of fluidized beds is in a primitive state, and the experimental data that do exist are concerned primarily with gross average behavior. The purpose of the experiments made here was to provide data of a more fundamental nature on the unsteady random motion within a fluidized bed.

The properties basic to a fluidized bed as a whole, such as bed height for a given fluid mass flow rate, fluid velocity at incipient fluidization, and pressure drop in the fixed bed regime, have been investigated empirically and rather extensively by many authors. Several textbooks have been published in recent years: Leva[1], Zabrodsky[2], and Zenz and Othmer[3] summarize the experimental findings and present generalized correlations. A series of three articles by Botterill[4] covers the important papers on fluidization of the early 1960's in abstract form. From a macroscopic viewpoint, the average properties of fluidized beds can be deduced from correlations of dimensionless variables based on experimental findings. In defining these basic properties, it is sufficient in dealing with the particles to assume that they are distributed uniformly and are at rest with drag forces balancing buoyant weight. An average particle concentration (volume fraction) is used to characterize the entire bed.

In a real fluidized bed, however, the solids are not necessarily distributed uniformly, nor are they at rest but assume various types of motion dependent upon the actual fluidizing apparatus employed. As a primary classification, microscopic bed behavior can

be divided into two general categories, aggregative and particulate. In gas-fluidized beds, some gas rises as particle-free voids or bubbles which can be observed as they burst at the upper free surface. The bubbles agitate the bed considerably, creating a high degree of non-uniformity in particle concentration, evidenced by a bed height which fluctuates markedly. This behavior, called aggregative fluidization, is dealt with in a book by Davidson and Harrison[5]. In contrast to gas-fluidized beds, the particles in a liquid fluidized bed space themselves more or less uniformly, exhibiting particulate fluidization. The experiments described here were confined to liquid beds.

Although the particles are distributed rather uniformly in liquid beds, they do assume various forms of movement. Visual examination of the microstructure of a liquid fluidized bed reveals an eddy type of motion with clumps of particles moving together, similar in appearance to eddies of fluid in a turbulent flow field. Two other types of particle motion commonly occurring in liquid fluidized beds are steady patterns of particle recirculation and also weak waves. The scale of the recirculation patterns is the size of the bed, and their shape as well as their presence is very sensitive to bed geometry. The waves appear as narrow strata of slightly varying particle concentration propagating upwards at a somewhat regular rate in a bed of otherwise uniform concentration. They have a one-dimensional character and a much weaker concentration variation than the bubbles found in gas-fluidized beds. All three characteristics of particle movement in liquid-fluidized beds were examined.

A specific liquid-fluidized bed was developed, and experiments were made to examine the random motion of individual particles and to measure particle diffusion coefficients for the vertical direction. Position data on the motion of a few individual particles in the bed were recorded by means of motion picture photography. From these data, distributions of step lengths were reduced for varying time intervals, for statistical analysis.

Glass beads of 0.236-inch diameter were used for the particles along with a glass fluidizing column 8 feet long and 4-inch inside diameter. Beads to be tracked on film were colored and made visible anywhere in the column by utilizing a fluid* with the same refractive index as that of the uncolored beads. Without matching the refractive indices of the beads and the fluid, it was impossible to see a colored bead that was even a few bead diameters from the wall of the column.

It is believed that the random motion of an individual bead is generated by its capture in eddies of beads and fluid that are created and destroyed over time. The experimental findings as well as the appearance of the microstructure of the bed suggested such a physical process; two successive steps of short duration separated by a short time were found statistically correlated, indicating that a bead resides in an eddy for a short time. Vertical step lengths of longer duration were normally distributed and could be interpreted in terms of a diffusion coefficient as for a random walk process. Particle diffusion coefficients for the vertical direction were measured at several average bed particle concentrations. These diffusion coefficients are much larger than would be found in the fluid alone at the same flow

*See page 15.

rate; the particles in a fluidized bed tend to increase instabilities appreciably.

Carlos and Richardson[6], Handley, et al.[7], and Rowe, et al.[8] have also measured particle diffusion coefficients in liquid fluidized beds. The physical properties of the fluid and the particles in the present experiment differed from those in the other experiments, increasing the range of bed properties for which diffusion coefficients have been measured. Also, the three other experiments had some inherent weaknesses; the present experiment incorporated several features which allowed very careful measurements to be made. The most important feature was the use of a fluidizing column long in length in comparison to its diameter, which eliminated gross steady patterns of particle recirculation and also permitted measurements to be taken far away from the special effects of the ends of the bed.

The presence of steady patterns of particle recirculation in a shallow bed of glass beads fluidized by water made it impossible to observe random motion in that bed because of the difficulty in separating it from the steady currents. Circulation patterns are still very important, for they provide a large amount of fluid-particle mixing. Experiments on circulation patterns as well as weak waves in a shallow cylindrical bed with a length-to-diameter ratio of 5 to 1 and also conical beds of glass beads fluidized by water are discussed in Part 2; Part 1 is devoted to the diffusion experiments.

PART 1

PARTICLE DIFFUSION IN LIQUID FLUIDIZED BEDS

I. AVERAGE BED PROPERTIES

In the experiments on particle diffusion, important macroscopic parameters are the average particle size, density, shape, and concentration; the temperature, density, and viscosity of the fluid; and the superficial fluid velocity (the average fluid velocity at bed inlet). The average particle concentration is the fraction of the total volume of the bed occupied by the particles and is determined from the bed height, the cross-sectional area of the fluidizing column, and the density and overall weight of the beads. During an experiment, the height of the bed remained quite steady, with fluctuation less than $\frac{1}{2}$ percent. The temperature of the fluid fixes the values of the physical properties of the fluid; an operating temperature of $30^{o}C$ was maintained in each diffusion experiment.

For a given average particle concentration and operating temperature, the superficial fluid velocity is fixed. Superficial fluid velocity, U_o, was measured for average particle concentrations, C_o, ranging from 0.120 to 0.415, and the results are plotted in Figure 1. The vertical axis is the natural logarithm of the ratio, U_o/U_t, of the superficial fluid velocity to the free-fall velocity of a bead in a quiescent fluid; utilizing drag coefficient data for rigid spheres reported by Haberman and Morton[9], U_t was calculated to be 0.56 ft/sec for a Reynolds number, R_t, of 61, based on particle diameter. The horizontal axis is the natural logarithm of particle voidage, $1-C_o$, or the volume fraction of the fluid. The plot is constructed to facilitate comparison of the experimental findings to the empirical formula, $U_o = U_t(1-C_o)^n$, a simple and widely recognized correlation devised by Richardson and

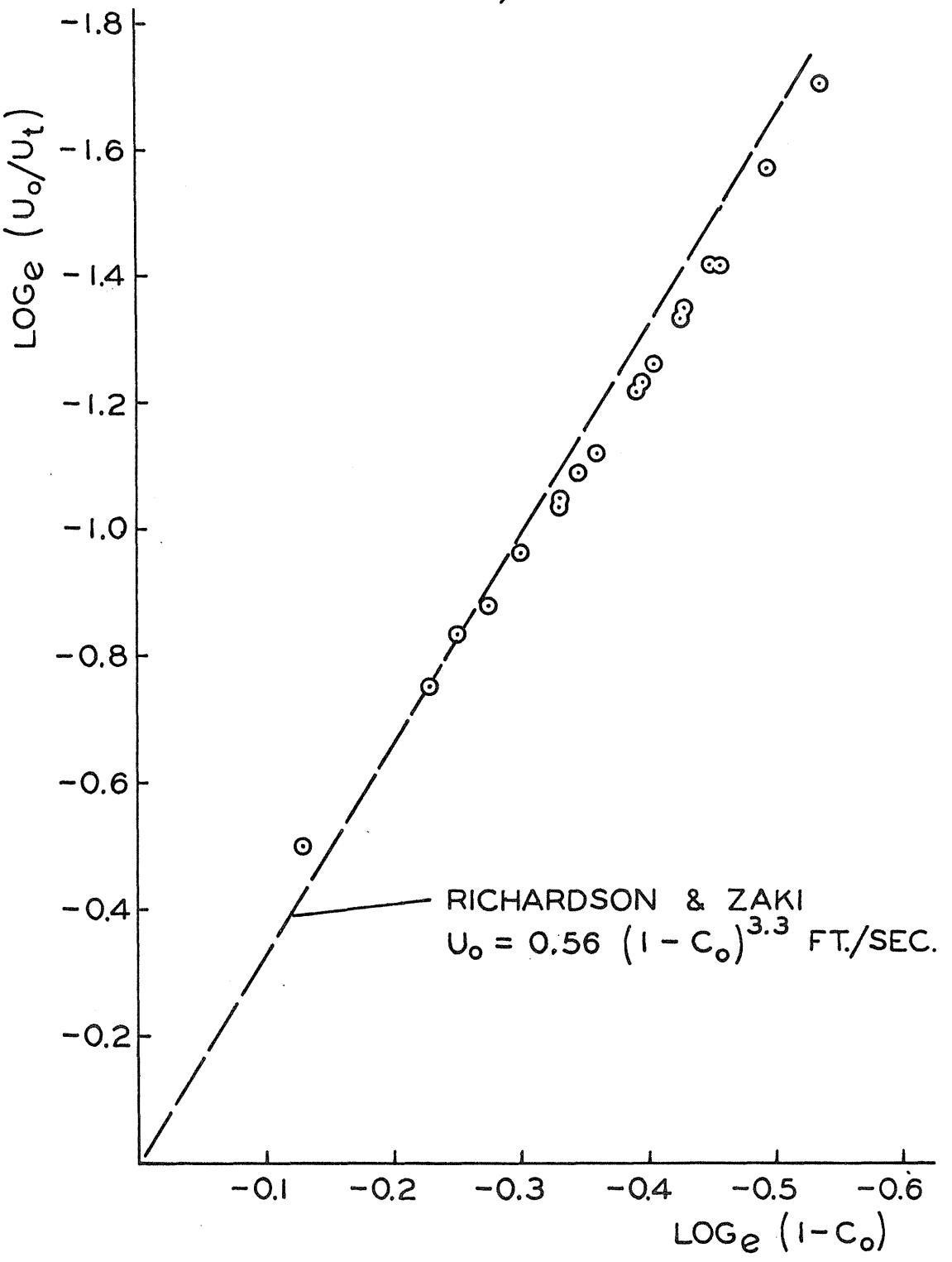

Figure 1. Superficial Fluid Velocity, U_o, as a Function of Average Particle Voidage, $1-C_o$, at 30°C.

Zaki[10]. The exponent, n, is a function of R_t and the ratio of bead-to-bed diameter and generally can be evaluated from other empirical formulas reported by Richardson and Zaki in their paper. However, in the current case, the diameter ratio is 0.06 and is larger than 0.04, the maximum value at which the formulas remain valid. Instead of using the formulas, the exponent was estimated directly from a plot of Richardson and Zaki's data and was found to be 3.3. This estimate is somewhat crude, as the number of data points was rather deficient in the neighborhood of $R_t = 61$ and a diameter ratio of 0.06.

The experimental values agree fairly well with those predicted, utilizing the correlation of Richardson and Zaki; however, two areas of disagreement are noticeable from the plot. The curve representing the data is slightly curved, while that formed by the empirical formula is a straight line. At the smaller voidages, the data form a straight line parallel to but lying below that of the empirical formula; as the voidage is increased, the curve formed by the data bends upwards intersecting the line predicted by Richardson and Zaki. The fact that the curve representing the data has a shape is not surprising, for in some cases, the curves representing the raw data of Richardson and Zaki, upon which their correlation is based, were also similarly shaped. However, in those cases, the exponent in the empirical formula and the slope of the curve formed by their raw data matched better at the larger voidages, not the smaller voidages as in the current example; the exponent in the empirical formula would have to be smaller in order to better match the slope of the curve formed by the

current data at the larger voidages. Perhaps this discrepancy, which is only of a rather small magnitude, is due to the crude way in which the exponent was estimated.

The other area of disagreement between the experimental findings and the empirical formula regards the multiplication factor, U_t. If one imagines the curve representing the data extended to intersect the vertical axis, the intercept value would be less than unity; the multiplication factor in the empirical formula is too large. This means that as the voidage approaches unity, the superficial velocity approaches a value less than the free-fall velocity of a single bead in a quiescent fluid. As the voidage tends to unity, the fluid in the column is not quiescent. Although the Reynolds number, based on the diameter of the column, approaches a value on the order of 1000, suggesting a laminar flow, there is probably a fair degree of turbulence present also due to the agitation of even a few particles. Though no data on the free-fall velocity of spheres in a turbulent field are known to the author, it is expected that it would provide a better means of estimating the multiplication factor.

II. EXPERIMENTAL APPARATUS AND PROCEDURE

The experiment was designed to measure particle diffusion coefficients in a fluidized bed by observing the random motion of an individual tagged particle. A fluidized bed was developed which enabled the positions of a few colored particles to be observed directly. The bed was made transparent by using glass particles combined with a liquid of the same refractive index as the glass. (This transparent bed technique has been used by others[6, 7, 11, 12] to locate particles in fluidized beds.) Motion pictures were made to record the position of a colored particle in the bed as a function of time.

In the early stages of the experiment, another approach to measuring particle diffusion coefficients in this apparatus had been considered. Instead of photographing the random motion of an individual particle, a diffusing front of particles could have been observed, but for several reasons this method was deemed impractical. For statistical purposes, a given experiment would have to be repeated many time, and to separate the tagged particles from the untagged particles after each experimental run would have proved time consuming and difficult. The nature of the working fluid is such that it is irritating to the skin, and in the presence of even a small amount of water becomes very corrosive. Removal of the particles for the purpose of separation without exposing the system to water vapor in the atmosphere would have entailed complicated procedures. In addition, the problem of adding tagged particles to the bed without disturbing the state of fluidization would have been difficult, if not impossible, to overcome.

A. Particles and Working Fluid

Kimble kimax glass beads of .236 in. average diameter were chosen for the particles. These beads were of nearly uniform size and had an average sphericity of ± 3 percent, expressed as the maximum variation in diameter relative to the average diameter. Their average density of 138 lb./cu. ft. was determined by measuring the water displacement of a known weight of beads. The manufacturer reported their refractive index (na-D line at 20°C) as 1.491. A disadvantage of using these beads was that tiny air bubbles in them made the fluid-particle system optically non-uniform. The density of air bubbles was not large enough, however, to reduce significantly the resolution on film of a marked bead deep in the column. This problem will be discussed in more detail in the section dealing with photographic techniques.

Tagged beads were identified by exposing them to high intensity γ-radiation, a process which colored them dark brown without affecting their size or density. In the preliminary stages, before this technique was discovered, attempts at coloring by chemical treatment proved unsatisfactory. Details on the γ-radiation technique, as well as the chemical methods that were tried, are described in Appendix A-1.

The working fluid was a clear mixture of 1, 1, 2, 2, tetrabromoethane (commonly called acetylene tetrabromide or ATB), purchased from the Dow Chemical Company, and an organic fluid, UCON LB-65, manufactured by the Union Carbide Corporation. The refractive indices of these two compounds straddle that of the glass beads, ATB

having the higher refractive index. The use of ATB as the solute in a mix designed to match the refractive index of glass beads was suggested by Lemlich and Manoff[13]. The mix that had the same refractive index as that of the glass beads contained 18.8 percent acetylene tetrabromide and 81.2 percent UCON fluid LB-65 by volume at 30°C. This was determined by titrating ATB into the UCON fluid, which had previously been added to the experimental apparatus. A match was achieved when the contours of individual beads disappeared under the actual experimental lighting conditions at the operating temperature of 30°C. The volume fractions of the components of the mix were determined later (assuming no change of volume on mixing) by measuring the densities at 30°C of the mix, the ATB, and the UCON fluid; the density of the mix was assumed to be the sum of the densities of the individual components weighted by their respective volume fractions.

Details of experiments performed to determine the density and viscosity of the working fluid at a range of temperatures near the operating temperature of 30°C are described in Appendix A-2. Viscosities were measured using a falling ball viscosimeter, and densities were determined using a pycnometer. Property data on the individual components of the working fluid can be found in references 14, 15, and 16. Pertinent data on the physical properties of the particles and the working fluid have been summarized in Table 1 for easy reference.

Certain properties of ATB and UCON fluid had an effect on the practicality of their application to the experiment. The choice

PROPERTIES OF WORKING FLUID

(at 30°C)

Composition:	18.8% by volume 1, 1, 2, 2 $C_2H_2Br_4$
	81.2% by volume UCON fluid LB-65
Density:	83.004 lb./cu. ft.
Viscosity:	22.2 cp.
Viscosity - Temperature Dependence	- .885 cp./°C

PROPERTIES OF PARTICLES

Type:	Kimble kimax glass spheres
Average Diameter:	.236 inches
Density:	138 lb./cu. ft.
Refractive Index:	1.491 for Na-D line at 20°C

TABLE 1. Summary of Important Working Fluid and Particle Properties.

of UCON fluid as the solvent did not create any problems. It was safe to use, stable, non-corrosive to metals, and relatively inexpensive. ATB, on the other hand, had both desirable and undesirable qualities, some of which are discussed in a Dow report[15]. Also, valuable information was obtained from direct communication with Cokelet[17], who had experience working with ATB. Although acetylene tetrabromide is toxic if taken internally, vapor concentrations at ordinary room temperatures are not dangerous. Also, it does not create a fire hazard; in fact, it is sometimes used as a fire retardant. However, ATB hydrolyzes in the presence of water and corrodes certain metals. Not only was it essential to keep water out of the apparatus, but extreme care had to be taken in the selection of materials (stainless steel, teflon, glass, brass) for use in constructing the apparatus. For more detailed information on this corrosive effect, refer to Appendix A-3. In addition, ATB discolors slightly at high temperatures. This discoloration was observed as a result of an accident discussed in Appendix A-4.

B. Apparatus

Photographs of the experimental installation are presented in Figures 2 and 3. Basically, this apparatus consists of the fluidized bed itself and the equipment which maintains and controls a flow through the bed. The fluidized bed apparatus will be discussed in terms of its two basic elements, the fluidizing column and the entrance section. Following this will be a description of the elements in the flow circuit.

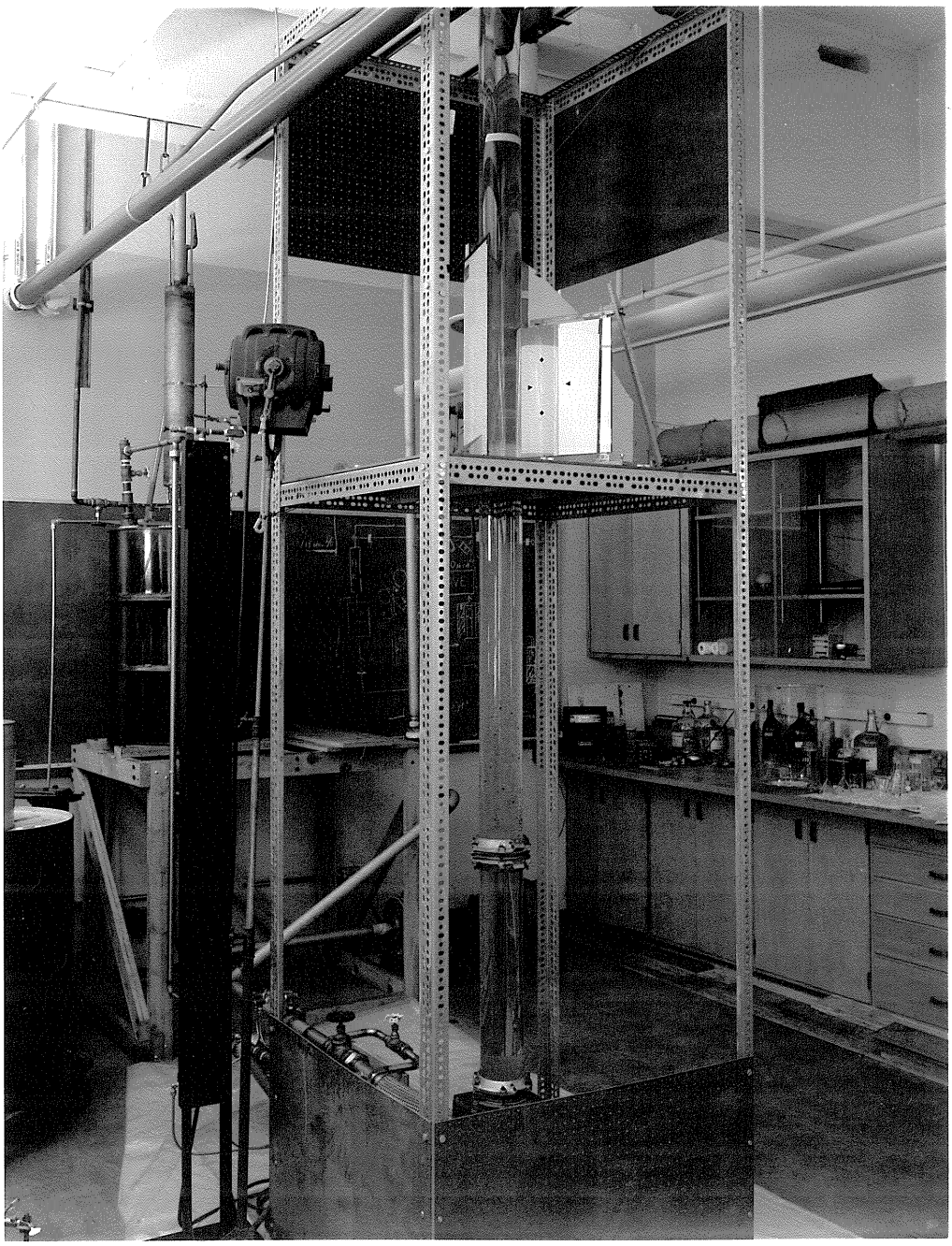

Figure 2. Experimental Installation with the Fluidizing Column in the Foreground.

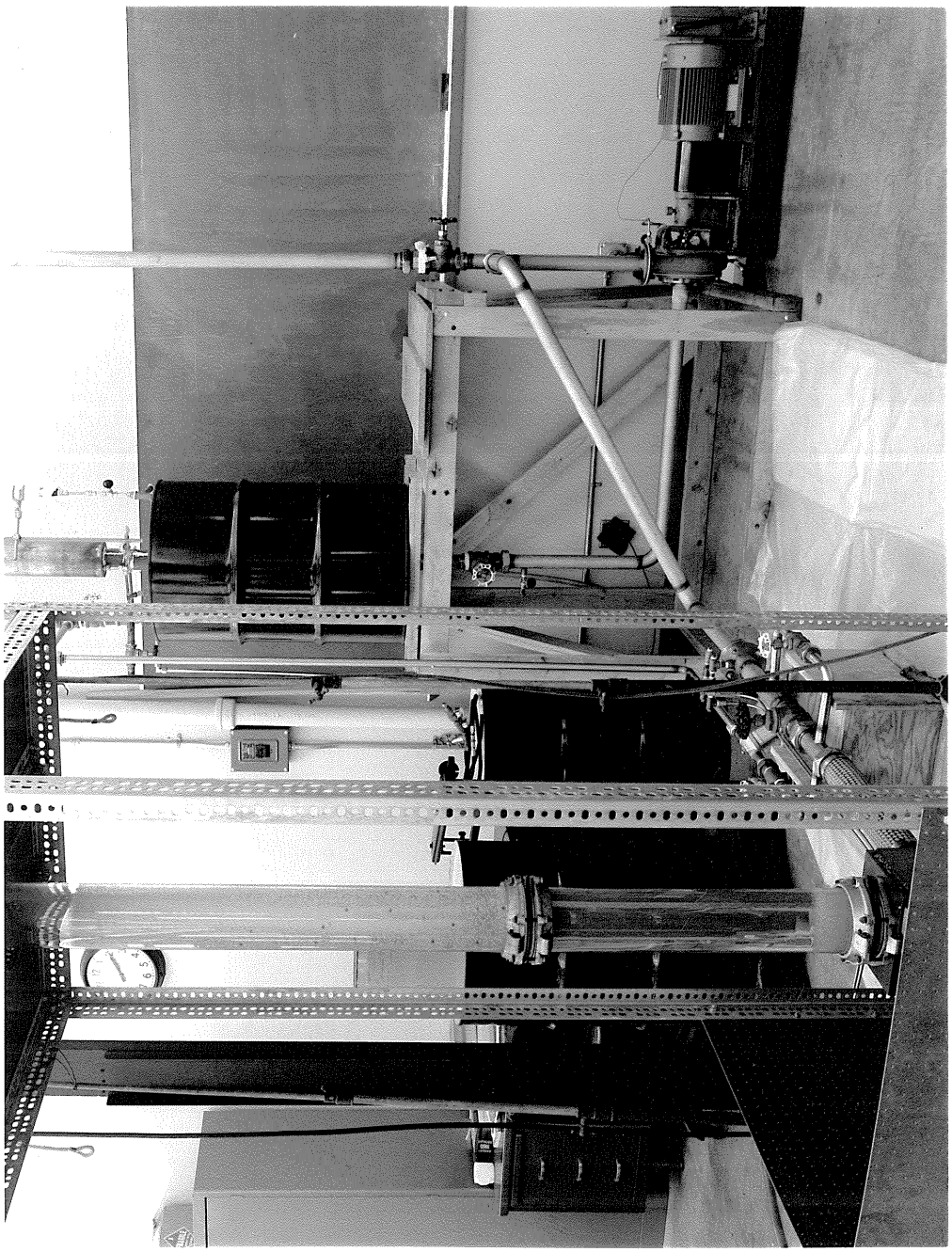

Figure 3. Experimental Installation Detailing Elements of the Flow Circuit.

The fluidizing column is a Corning pyrex pipe, 8 ft. in length and 4 in. inside diameter. This column, having a relatively large ratio of length to diameter, helped provide the experiment with two important features. The use of a long column enabled measurements to be taken at a position along the length of the column away from the influence of bed end effects. In addition, preliminary studies performed by following the motion of tagged beads gave no indication of large-scale, steady patterns of collective particle circulation. In earlier experiments, the presence of these patterns in a short column of particles fluidized by water precluded the use of the short column for diffusion studies. In that apparatus, it was found impossible to observe random particle motion because of the difficulty in separating it from the steady circulation patterns. It is believed that the use of a column with a large length-to-diameter ratio is a major factor in inhibiting the formation of steady circulation patterns in this experiment. Carlos and Richardson[6] and Handley, et al.[7], who also measured particle diffusion coefficients in liquid fluidized beds, employed columns in their apparatus of much smaller length-to-diameter ratios than that of the present study (2.5 to 1 and 3.3 to 1 as compared to the 24 to 1 here).

Another factor helpful in the suppression of steady circulation patterns was the application of a novel entrance section.* The entrance section consisted of a Corning pyrex pipe 2 ft. long and 4 in. inside diameter, containing approximately four pounds of .12 in. di-

*The design of the entrance section was suggested by R. Puzyrewski of the Institute of Fluid Flow Machinery, Gdansk, while Research Fellow at the California Institute of Technology in 1965-1966.

ameter glass beads. A 30-mesh stainless steel screen was mounted on the bottom of the section, and a 40-mesh screen was mounted on the top. These screens prevented particles from leaving the section. (The upper screen also served as a support for the particles in the major fluidizing column.) With upward flow of the fluid, some of the particles became packed against the upper screen, while the rest of the particles were suspended in a fluidized state. Apparently, this combined action produced a uniform velocity at the inlet to the major fluidizing column, which tended to suppress the circulation patterns.

The fluidizing column was hung from the ceiling, and the entrance section was supported on the floor by four legs of adjustable length. Standard Corning fittings and gaskets were used to connect flexible tubing to the inlet at the entrance section and the outlet at the top of the fluidizing column. This mounting arrangement provided a means of adjusting the vertical alignment of the column. It also facilitated disassembly of the column from the entrance section in order to change the amount of beads in the column.

The flow circuit is shown schematically in Figure 4. The drum, of a fifty-five gallon capacity and with a baked epoxy lining, feeds the pump. The centrifugal pump, manufactured by Worthington, was of stainless steel with a maximum capacity of 130 gpm. at 42 ft. of water, and a maximum head of 72 ft. of water. A General Electric motor of 5 h. p. drives the pump at 1750 rpm. The pump supplies two major pipelines, one of which feeds the fluidized bed and also contains the filter in an auxiliary branch, and the other a by-pass line. Except for the filter line, all pipes were stainless steel tubing, 2 in. o. d.

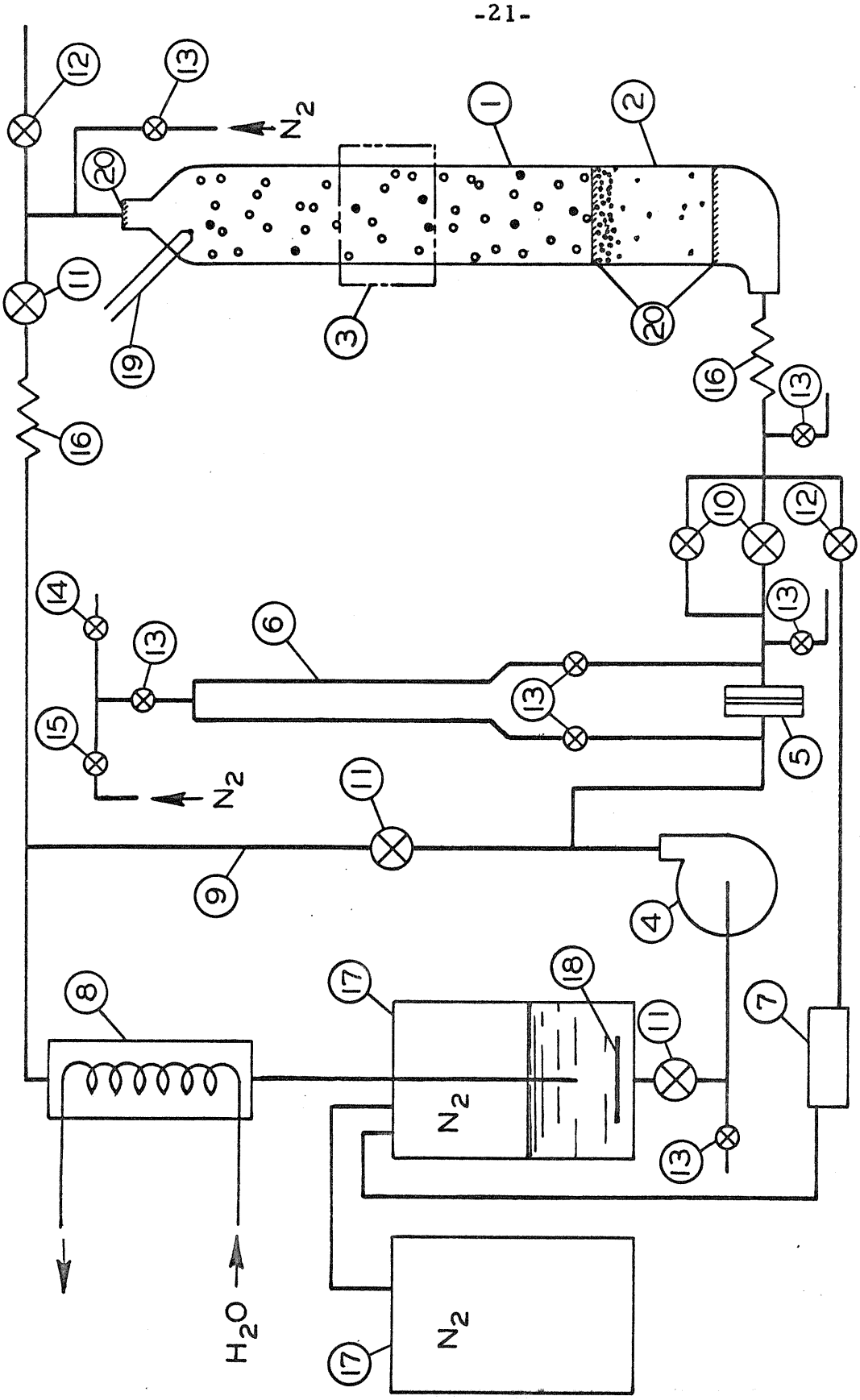

Figure 4. Schematic Diagram of the Flow Circuit.

FLOW CIRCUIT LEGEND

1. Fluidizing Column
2. Entrance Section
3. Test Section
4. Pump
5. Orifice Meter
6. U-Tube Manometer
7. Filter
8. Heat Exchanger
9. By-Pass Line
10. Bed Control Valves -- Globe Valves, 1 in. and 2 in.
11. Gate Valve, 2 in.
12. Gate Valve, 1 in.
13. Valve, 0.25 in.
14. Pressure Relief Valve, 0.25 in.
15. Check Valve, 0.25 in.
16. Flexible Tube
17. Drum, 55 gal.
18. Baffle
19. Thermocouple Probe
20. Screen

Figure 4 (continued)

by .035 in. wall. The circuit is completed by returning the flow from these lines to the drum.

The filter was installed to remove fine debris found in the fluid as a result of the accident described in Appendix A-4. It was manufactured by Commercial Filters Corporation and has a replaceable cotton cartridge capable of removing particles as small as 1 micron. Having a low flow capacity, it was placed in an auxiliary line branching from the line that feeds the bed. Since this branching occurs downstream from the orifice meter, the filter was not used while an experiment was in progress.

To prevent an excessive rise in the temperature of the fluid as it passed through the pump, the pump was operated at high flow rate. The flow rate through the bed was therefore controlled by adjusting the valves feeding the bed in conjunction with the valve to the by-pass line. For example, if a lower flow rate was desired in the bed, not only was its valve(s) closed somewhat, but also the by-pass valve was opened. This allowed the pump to operate at constant capacity. Other elements of the circuit provided means for flow measurement, temperature control, and the prevention of corrosion.

The temperature of the working fluid was adjusted by controlling the flow rate of water through the coils of the heat exchanger. The coils were of .375 in. stainless-steel tubing and had an unwound length of eighty feet. They were set between large concentric brass tubes, the central tube being sealed at both ends; the working fluid was forced across the coils in the remaining annular space. The inside diameter of the outer brass tube was 4.75 in., and the thickness

of the annulus was .5 in. Fluid temperature was measured with a thermocouple at the top of the fluidizing column. The .005 in. copper-constantan wires of the thermocouple were set in a small glass test tube with epoxy. The tip of this tube was injected directly into the fluid stream. An operating temperature of 30°C was maintained, for at that temperature, the refractive index of the fluid matched that of the beads.

An orifice meter was installed in the pipeline which fed the fluidized bed. Sharp-edged orifice plates of .658 in. and .814 in. diameter were utilized for the smaller and the larger fluidizing velocities, respectively. Pressure taps of .031 in. diameter were located one inch from each face of the plate, and a U-tube manometer, five feet in length, was employed to measure the pressure differentials. Although the orifice plates, the flanges, and the location of pressure taps were according to NACA standard specifications[18], standard lengths of entrance and exit pipe were not installed due to space limitations. Therefore, standard orifice coefficients could not be used, necessitating calibration of the meter specific to the pipe installation used. Details of the calibration procedure are discussed in Appendix A-5.

In addition to the use of special materials in the fabrication of the apparatus, further precautions were taken to inhibit the corrosive effects of the working fluid. Before the fluid was originally added to the apparatus, any water present was removed; warm air was circulated through all passages,which were then purged and replenished with dry nitrogen. With the addition of about 25 gallons of UCON fluid

and $5\frac{1}{2}$ gallons of ATB to the apparatus, a dry nitrogen atmosphere was created above the fluid level in the drum. The nitrogen atmosphere was increased by connecting an additional 55-gallon drum of nitrogen, also containing a few pounds of silica gel. At times it was necessary to repurge various portions of the system with nitrogen; this was done, for example, as part of the procedure when exchanging orifice plates or altering the weight of beads in the column. A baffle placed between the inlet and outlet pipes in the drum served to remove any nitrogen bubbles which had combined with the fluid when it re-entered the purged sections.

C. Photographic Technique and Experimental Procedure

In a typical experiment, a known weight of beads, which included approximately twenty tagged beads, was expanded to a height close to the full height of the column. After about an hour and a half warm-up, an equilibrium temperature of 30°C was reached. At this time, an accurate measure of the height of the fluidized particles was taken, and the pressure differential across the orifice was noted. The motion of tagged beads in a portion of the column away from the influence of bed end effects was recorded on movie film. The test section was 12 in. long and located about ten column diameters from either boundary of the bed. A plan view of the test section and the photographic arrangement is shown in Figure 5.

A total of five or six rolls of film, each containing 100 feet of film, was used in a given experiment. A roll of film was shot continuously as long as at least one bead and not more than four appeared in the test section. When this condition was not met, the camera was

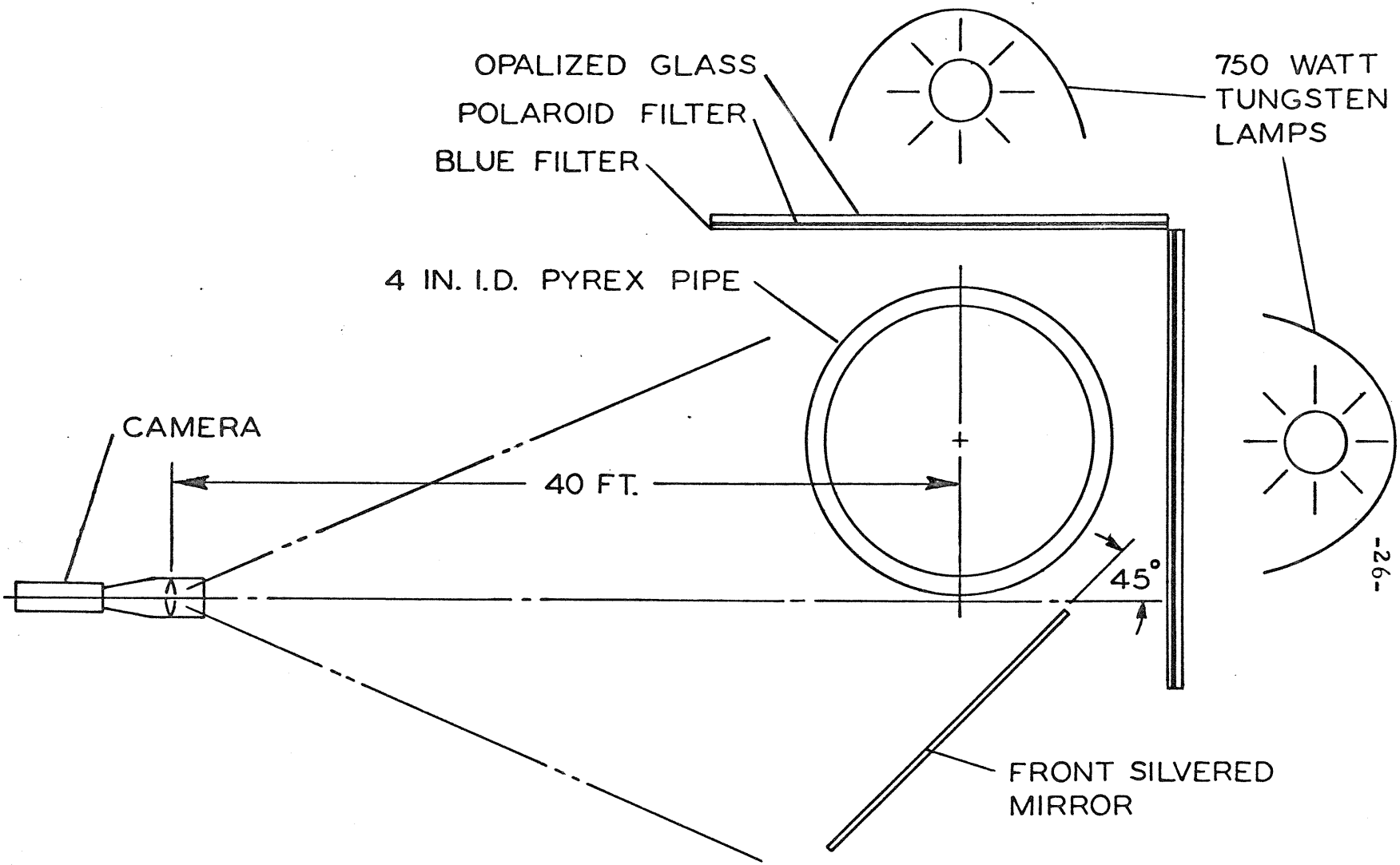

Figure 5. Plan View of the Test Section.

stopped; filming resumed when the proper number of tagged beads reappeared in the test section. Most of the time, it was possible to shoot about fifty feet in this manner.

The data were recorded by means of a 16-mm Bolex movie camera, model H-16 Rex, using a 300-mm Omnitar f/5 telephoto lens. Use of this long lens reduced perspective errors by allowing a distance of forty feet between the camera and test section. At this distance, sufficient depth of field could be obtained with an aperture setting of f/8. A framing rate of 24 frames per second was maintained by a synchronous motor. Light from two flood lamps of 750 watts each, operating at a color temperature of 3000^{o}K, illuminated the test section and mirror. The light was filtered to enhance the resolution of a tagged bead on film. Opalized glass and polaroid filters reduced scattering of light from tiny air bubbled entrained in the glass beads; a blue acetate filter provided a background against which the contrast of the brown beads was increased. One hundred-foot rolls of Eastman Double X negative Type 7222 film were used. Under the above conditions, this film was chosen to produce an image of high contrast and fine grain.

A front surface mirror (14 in. by 11 in.) was mounted on the right of the test section, enabling a side view of the column to be recorded in addition to the front view. Using the position of a tagged bead in each of these views, along with information concerning the optical system employed and its geometrical relationship to the column and mirror, it is possible to determine the location of the bead in the column. The focal length of the camera lens and the factor by

which the size of an object in sharp focus is reduced to its size on the film image (reduction factor) define the optical system. Four triangular marks indicating the endpoints of two perpendicular lines of known length (vertical, 5.143 in.; horizontal, 3.985 in.) were painted on the mirror and provided a fiducial scale. The reduction factor was derived from the vertical reference marks upon which the camera was focused. The horizontal reference marks were used to determine the angle formed by the mirror and the focal plane of the camera. This was the essential factor needed in determining the geometrical relationship of the column and mirror to the optical system. To obtain a very sharp image of the mirror marks on film, the last few feet of a given experiment were filmed with filters removed and the aperture stopped down to f/22. It was absolutely necessary that the vertical alignment of the focal plane, the vertical mirror marks, and the fluidizing column be adjusted precisely. To double-check this alignment, test footage was shot prior to a given experiment.

III. RESULTS OF EXPERIMENTS

A. Position Analysis

Four experiments were filmed obtaining data at average particle concentrations (volume fractions), C_o, of 0.120, 0.203, 0.286, and 0.365, with the working fluid at 30°C. Each experiment involved an analysis of the vertical positions of a tagged bead. In addition, in one experiment, $C_o = 0.120$, polar positions were determined for each vertical position to see if vertical diffusion depended upon radial position.

A frame of film was displayed on the screen of a microfilm reader, and raw position data for a tagged bead were recorded on an IBM card. An IBM 360/75 computer was used to apply corrections and convert the raw data to a real position in the fluidizing column. Details of this process are described in Appendices B-1 and B-2; B-1 deals with vertical position and B-2 with polar position. A large amount of data was processed effectively by these means.

Though the film was shot at 24 frames per second, the vertical distance traveled by a tagged bead in one twenty-fourth of a second was too small to be determined accurately. Positions were noted after skipping a regular number of frames; two basic frame rates, a short time rate, T_1, and a long time rate, T_2, were employed for each experiment.* For example, at $C_o = 0.120$, some positions were noted every fifth frame, or every 0.208 seconds, and others every tenth frame, or 0.417 seconds. As estimated in Appendix B-1, the variance (error) in measuring two successive positions on film is

*At $C_o = 0.365$, only one frame rate was employed.

0.06 inches, approximately. At the short frame rate, the error in determining the vertical distance traveled was about 20 percent on the average.

A run (denoted by superscript R) is defined as the sequence of successive vertical positions, Z_i^R, $(i = 1, \ldots, M^R)$, of a tagged bead at either a short or a long frame rate. Vertical positions were measured relative to the horizontal mirror marks, fixed at a height of 4 feet above the inlet to the fluidizing column. A run terminated when the tagged bead either left the test section or moved to a location in the column where it seemed to vanish from both the front and mirror views. The lens effect of the cylindrical column causes total reflection of objects at certain locations in the column; these blind spots are discussed in Appendix B-2 as a detail of polar position reduction. On the average, a run contained approximately 100 successive positions at the long frame rate or 150 positions at the short frame rate. A given experiment consisted of a number of runs. For instance, the experiment $C_o = 0.120$ was a composite of four runs at five frame intervals to yield a total of approximately 650 vertical positions and also six runs at ten frame intervals to yield 600 positions, approximately. In addition, approximately 350 positions at ten frame intervals could be derived from the four runs at five frame intervals. Appendix B-3 explains the coding process used to locate a run on the original film; the run number, the frame rate, and the number of positions recorded are tabulated for each run of a given experiment. A computer plot of the vertical positions occupied by the tagged bead of run number 172, as a function of time, is presented in

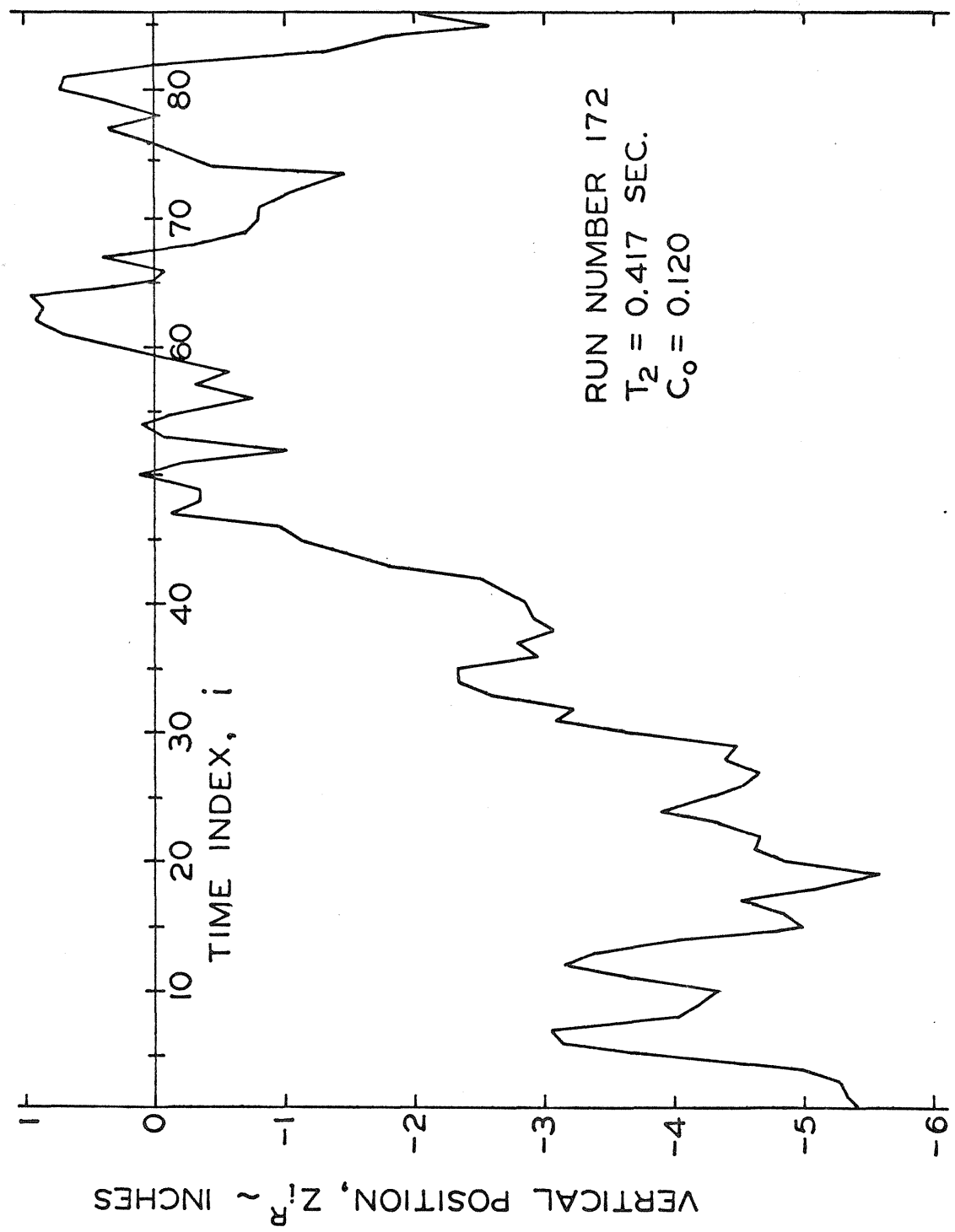

Figure 6a. Track of Vertical Positions.

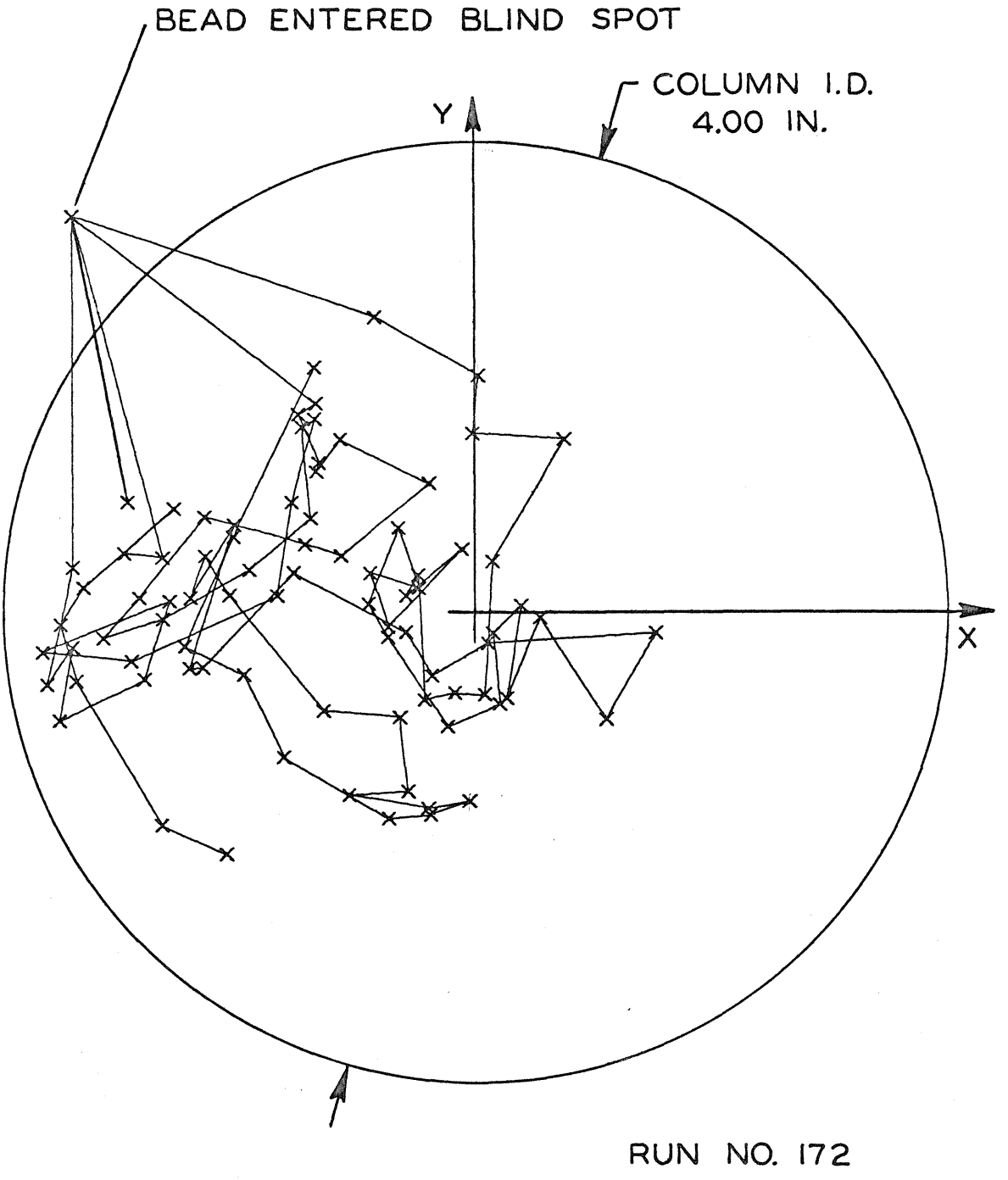

Figure 6b. Track of Polar Positions.

Figure 6a; corresponding polar positions are presented in Figure 6b.

For each run, sequences of successive step lengths, $\lambda_i^R(k)$, were computed at varying time intervals, τ_k. The time index, k, ranges from one to generally not more than ten in the application of the sequences to further calculations. The time interval in seconds for all steps in a given sequence is

$$\tau_k = (T_1 \text{ or } T_2)(k) ,$$

depending upon whether the positions of the particular run were recorded at the short or the long basic frame rate. The sequences are defined by use of the formula

$$\lambda_i^R(k) = Z^R_{ki+1} - Z^R_{k(i-1)+1}$$

$$i = 1, \ldots, N^R(k)$$

$$N^R(k) = \frac{(M^R - 1)}{k} \quad .^*$$

Four computer routines were developed to manipulate data and perform calculations throughout this work. CORPO was developed to convert raw data to real positions; FILM2 was used primarily to obtain diffusion coefficients; CORLN, primarily to compute time-wise correlations of vertical step data; and RADCO, primarily to investigate radial correlations.

B. Diffusion Coefficients

In a given experiment, a diffusion coefficient was derived from the analysis of distributions of step lengths grouped at various time intervals. A group with time index, k, was composed of step

---

*If this term if fractional, it is rounded down to the nearest integer.

lengths, $\lambda_i(k)$: $k = 1, \ldots, N(k)$, from the pooling of all runs at a given basic frame rate, T_1 or T_2. In this way, two sets of groups were constructed, one from the runs at the short frame rate, the other from the runs at the long frame rate. In addition, runs at the short frame rate were utilized to increase the size of a group at the long frame rate.* For example, at $C_o = 0.120$, groups ranging in size from 635 elements with $\tau_1 = 0.208$ seconds to 125 elements with $\tau_5 = 1.04$ seconds were formed from the runs at the short frame rate of 0.208 seconds. Runs at the short frame rate were combined with those at the long frame rate of 0.417 seconds to form groups ranging in size from 952 elements with $\tau_1 = 0.417$ seconds to 113 elements at $\tau_8 = 3.33$ seconds. For statistical precision in the calculations which follow, a group size of approximately 100 elements was the smallest considered.

In the analysis of a given group, step lengths were sorted into an array of increasing order, and a histogram was constructed. The shape of a histogram suggested that the step lengths in a given group are distributed normally. Further, in a given experiment, analysis of histograms constructed from step lengths grouped at various time intervals suggested that the width of a distribution increases with time. Figures 7a, 7b, and 7c present histograms at $C_o = 0.120$ for three increasing time intervals, 0.417 seconds, 1.25 seconds, and 2.08 seconds, from runs at the long frame rate of 0.417 seconds.

---

*The long frame rate was twice as large as the short frame rate for the experiments at $C_o = 0.120$ and $C_o = 0.203$. At $C_o = 0.286$, runs at the short frame rate were not utilized to increase the size of a group at the long frame rate; the basic frame rates employed did not combine evenly.

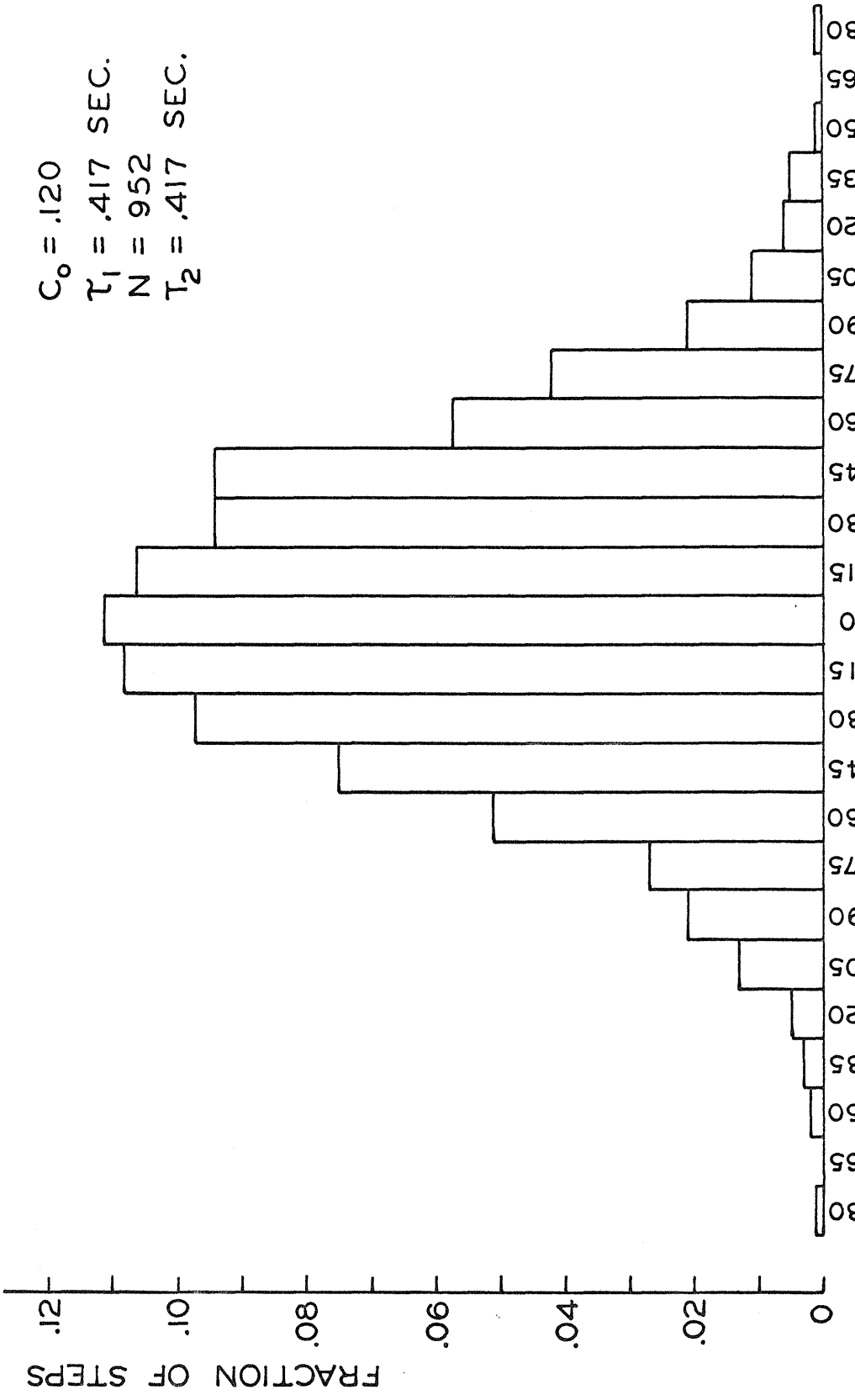

Figure 7a. Histogram of Step Lengths Grouped at Same Time Interval.

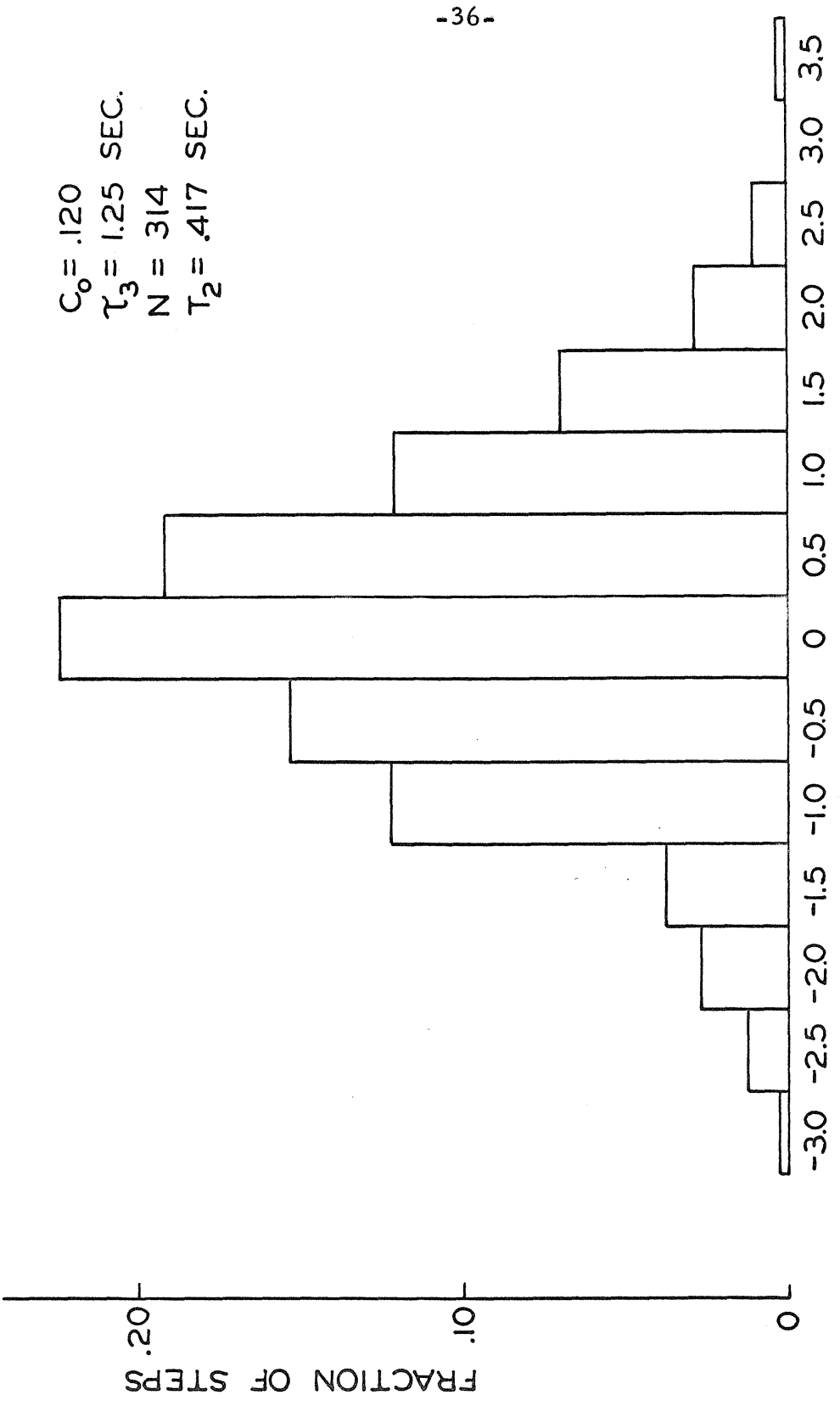

Figure 7b. Histogram of Step Lengths Grouped at Same Time Interval (contd.)

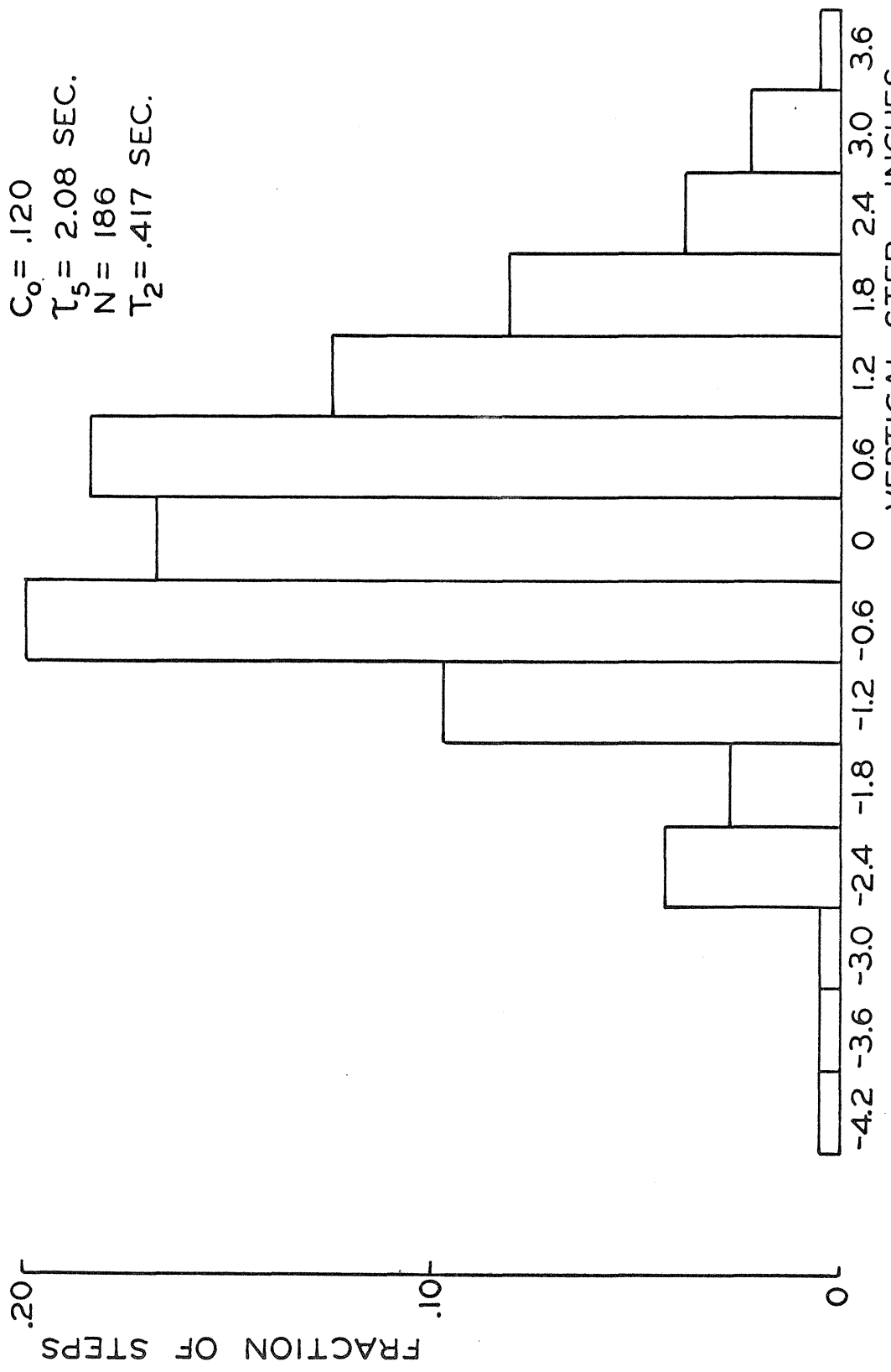

Figure 7c. Histogram of Step Lengths Grouped at Same Time Interval (contd.).

For each group, the mean square step length, $\overline{\lambda^2(k)}$ was computed by use of the formula

$$\overline{\lambda^2(k)} = \frac{1}{N(k)} \sum_{i=1}^{N(k)} [\lambda_i(k) - \overline{\lambda(k)}]^2 ,$$

where

$$\overline{\lambda(k)} = \frac{1}{N(k)} \sum_{i=1}^{N(k)} \lambda_i(k) .$$

In Appendix C, mean square step lengths, time intervals, and group sizes are tabulated for each experiment. Mean step lengths, $\overline{\lambda(k)}$, assumed very small values due to statistical fluctuations resulting from the use of a finite group size, N(k); because they were so near to the ideal of zero, it was concluded that tagged beads had no appreciable drift. Figure 8 presents plots of mean square step length as a function of time for each experiment. A straight line fitted the data in a given experiment fairly well. Each curve tends to intersect the time axis at a small positive value, suggesting the mean square step is negative at zero time in contradiction to its definition; this small time effect is discussed in the next section dealing with time-wise correlations of vertical step data. There is some evidence of small deviation from straight lines in a somewhat wave-like shape, and this is also discussed in the next section. Otherwise, the scatter is consistent statistically.

A mean square step length, $\overline{\lambda^2(k)}$, was formed from a group of size N(k) and is itself a random variable. The chi-square distribution was utilized to place confidence limits on the mean square step lengths. Details are discussed in Appendix D, which includes a table

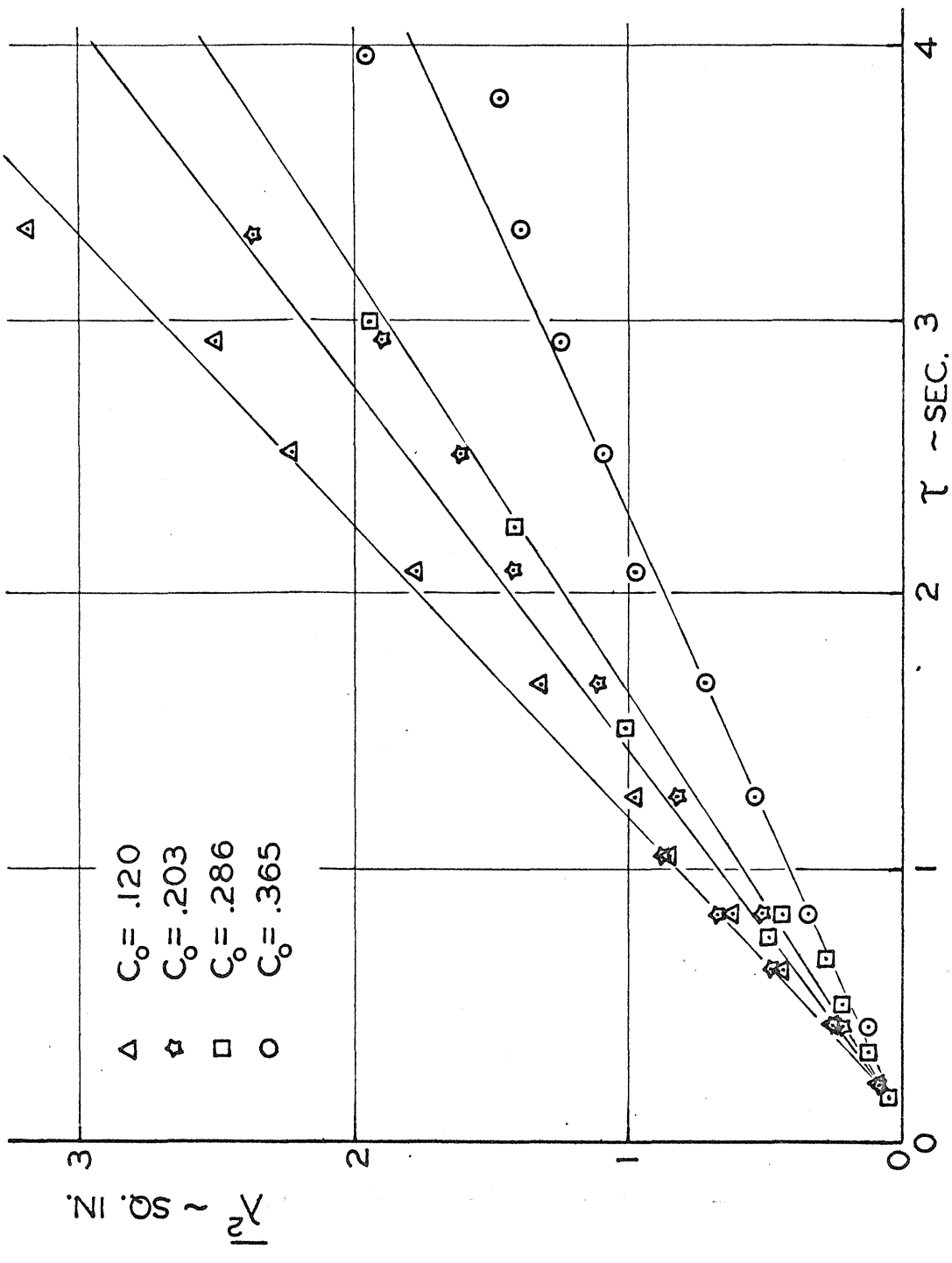

Figure 8. Vertical Mean Square Step Length as a Function of Time.

of confidence limits at the 90 percent level, for each of the mean square step lengths in the experiment $C_o = 0.203$. Considering runs at the short frame rate in a given experiment, the mean square step length at the shortest time interval was formed from a group of 600 steps, approximately; confidence limits at the 90 percent level on this mean square step length are ±9 percent. (Considering runs at the long frame rate, the mean square step length at the shortest time interval was formed from a group of 1000 steps, approximately; confidence limits at the 90 percent level on this mean square step length are ±6.5 percent.) As the time interval increases, the size of a group decreases in direct proportion, and the confidence limits widen. Thus, confidence limits at the 90 percent level on the mean square step, formed from a group of approximately 100 steps at the longest time interval in a given experiment, are + 26 percent and - 20 percent, regardless of the frame rate.

Considering diffusion processes in general, a familiar result is that the mean square displacement of a particle in one dimension is directly proportional to the time, the constant of proportionality being twice the diffusion coefficient. Einstein[19], for instance, found this result in describing the irregular or Brownian movement of particles suspended in a liquid. It is also a result of applying probability theory to a random walk problem, which in the limit, passes into a diffusion: see, for instance, Feller[20]. In comparing this result to the experimental findings presented in Figure 8, it is concluded that the movement of beads in the bed is essentially a diffusion process. For time intervals sufficiently large, the slight shift

of a straight line from the origin in Figure 8 can be neglected; then, the mean square step lengths of a bead proceeds in direct proportion to the time, namely,

$$\overline{\lambda^2} = 2D_z \tau \quad ,^*$$

where D_z is the coefficient of diffusion in the vertical direction of particles in a liquid fluidized bed. Diffusion coefficients were deduced from the curves of Figure 8; Table 2 lists C_o, U_o, and D_z in each experiment.

C. Time-wise Correlations

Visual observations of solid particles in liquid fluidized beds suggest that they may behave similarly to particles of fluid in a turbulent flow field. This possibility was investigated by using the step length sequences to construct a correlation coefficient, $K_j(k)$, defined by

$$K_j(k) = \frac{1}{\overline{\lambda^2(k)}} \frac{\sum_R \sum_{i=1}^{N(k)-j} [\lambda_i^R(k) - \overline{\lambda(k)}][\lambda_{i+j}^R(k) - \overline{\lambda(k)}]}{\sum_R [N^R(k)-j]}$$

for runs at either the short or long basic frame rate. This is a measure of the statistical dependency of a step, $\lambda_{i+j}^R(k)$, on that which originated at a time, $j\tau_k$, earlier. It is normalized by $\overline{\lambda^2(k)}$ and

$$K_o = 1 \quad .$$

Although it is desirable to employ steps of very short duration in this analysis, there is a lower limit on the duration of a step

---

*The notation using time index k was dropped in this formula as the formula represents continuous movement.

C_o	U_o (ft./sec.)	D_z ($ft.^2$/sec.)
0.120	0.347	3.3×10^{-3}
0.203	0.258	2.7×10^{-3}
0.286	0.190	2.3×10^{-3}
0.365	0.136	1.6×10^{-3}

TABLE 2. Diffusion Coefficients in Each Experiment.

that permits the length of a step to be measured accurately. The variance in a measurement, $\lambda_i^R(k)$, is estimated to be about 0.06 inches (see Appendix B-1); thus, the smallest step duration without excessive error was that in the short frame rate of a given experiment.

In each experiment, $K_j(1)$ was computed from runs at the short frame rate, and the results are plotted as a function of j in Figure 9. Two trends are evident in the plot for a given experiment. K_1 assumes a significant value, for instance, 0.48 in the experiment at $C_o = 0.120$; as j is increased, K_j decays to zero rapidly. Then it assumes a wave-like pattern of small varying amplitude with an irregular, though somewhat uniform, period. The significant correlation of two steps (for small values of j) originating at a time of $j\tau_1$ apart, indicates that a bead is within an eddy for a short time, a behavior expected of fluid particles in a turbulent flow field.

Taylor[20] assumes a specific model for the diffusion in one space dimension, z, of a fluid particle in a turbulent field; included

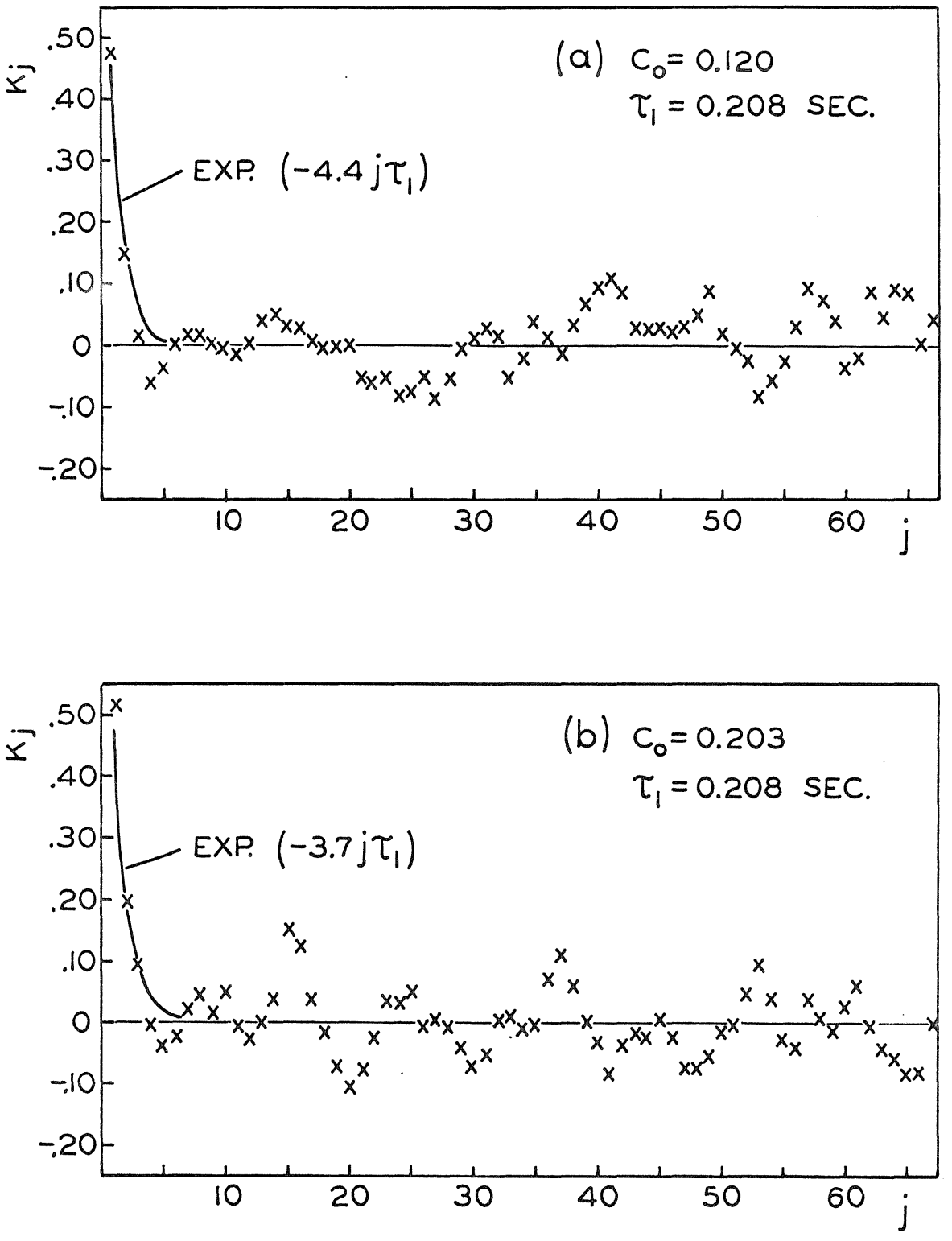

Figure 9a, b. Time-wise Correlations in Vertical Step Length Data for Each Experiment.

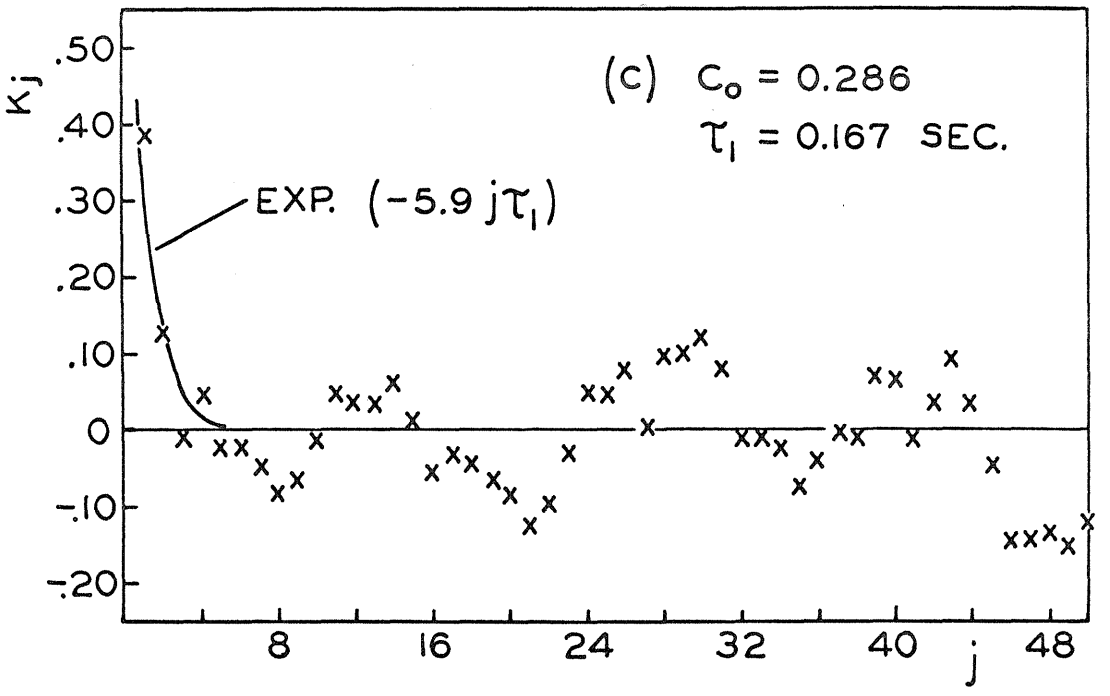

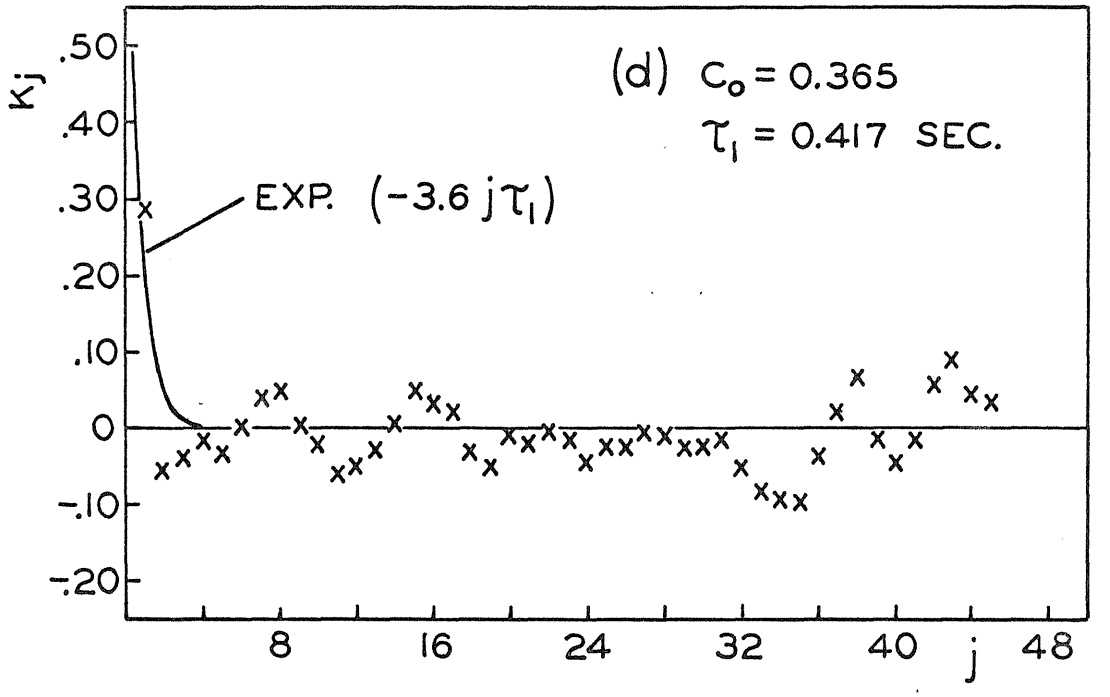

Figure 9c, d. Time-wise Correlations in Vertical Step Length Data for Each Experiment (continued).

is the assumption that the direction of a step of infinitesimal length is correlated to that at a time, τ later, by a correlation coefficient, $\widetilde{K}(\tau)$ defined by the formula

$$\widetilde{K}(\tau) = e^{-\tau/\tau^*} .$$

Taylor derives a relationship of the mean square step length, $\overline{\lambda^2(\tau)}$, as a function of step time, τ, defined by

$$\overline{\lambda^2(\tau)} = 2D_z(\tau - \tau^* + \tau^* e^{-\tau/\tau^*}) .$$

Assuming the results of Taylor's analysis can be applied to the fluidized beads, it explains the behavior, mentioned previously, of the mean square step data at small time, Figure 8. The point at which a line intersects the time axis is, in fact, τ^*; the line for each experiment intersects this axis at 0.15 seconds, approximately. The correlation coefficient of Taylor's model can also be compared to the experimental findings. Using a regression technique[22], curves $\widetilde{K}(\tau)$ were fitted to the data, K_j, in each experiment (shown in Figure 9), and the following values of τ^* were found:

C_o	τ^* (sec.)
.120	.23
.203	.27
.286	.17
.365	.28

The differences in the results of calculating the parameter τ^* in these two ways suggest that Taylor's model may not apply to the motion of the immersed beads. However, owing to the scatter from one experiment to another in the results of the latter calculation and the

dubious accuracy at which the intercept was measured in the former calculation, a definite conclusion concerning the suitability of applying Taylor's model to the particles in a fluidized bed cannot be drawn.

The oscillatory nature of the correlation coefficient probably can be attributed to the presence of weak waves in the bed. The occurrence of weak waves seems to be an intrinsic feature of fluidized beds. They were observed in the shallow, water - glass bead, fluidized bed to be discussed in Part 2 and appeared as narrow strata propagating upwards at a somewhat regular rate in a bed of otherwise uniform concentration. There is an obvious difficulty in observing weak waves in the present transparent system. However, early in the experimental program, before the ATB was titrated into the UCON fluid, their presence was observed: waves were also observed in the process of purging the system with acetone. Although waves using acetone were observed in a Reynolds' number range different than that at which the diffusion experiments were run (viscosity of acetone is one hundred times smaller and density 40 percent less than that of the working fluid), waves using UCON fluid were observed in a similar Reynolds' number range.

The periodic behavior of the correlation coefficient data implies that a given step is made up of two parts, a random part and a small oscillatory part. This explains, qualitatively, the wave-like variation in the mean square step data presented as a function of time in Figure 8 for a given experiment. Since the periods of oscillation in each correlation coefficient were so irregular, the correction to the raw position data, which would remove the waves for the purpose

of diffusion analysis, was too complex and was not warranted.

D. Radial Effects

The vertical diffusion coefficients, D_z, were determined assuming they were uniform on the cross section of the fluidizing column. Though a dependency was not expected, polar positions were reduced for each vertical position from the data of one experiment, $C_o = 0.120$, to investigate the possibility of a correlation between vertical diffusion and radial position.

For each time interval, τ_k, vertical step lengths, $\lambda_i(k)$, were plotted as a function of the radial position, R, at the start of each step. If the tagged bead was located in a blind spot in either the front or mirror views, plotting was suppressed, for the exact radial position could not be reduced from the data. Figures 10a, 10b, and 10c are the plotted distributions of vertical step length as a function of radial position at $C_o = 0.120$ for three increasing time intervals, 0.417 seconds, 1.25 seconds, and 2.08 seconds, from runs at the long frame rate of 0.417 seconds. It is apparent that vertical diffusion is not correlated with radial position, for the width of a given distribution is uniform, radially. Note that the distributions in Figures 10a, 10b, and 10c were derived from those groups of vertical steps used in the construction of the histograms in Figures 7a, 7b, and 7c; both the histograms and the radial plots present the same results, since vertical diffusion is not dependent on radial position.

The polar position data were also utilized to obtain a distribution of starting positions on the cross section for vertical steps at the

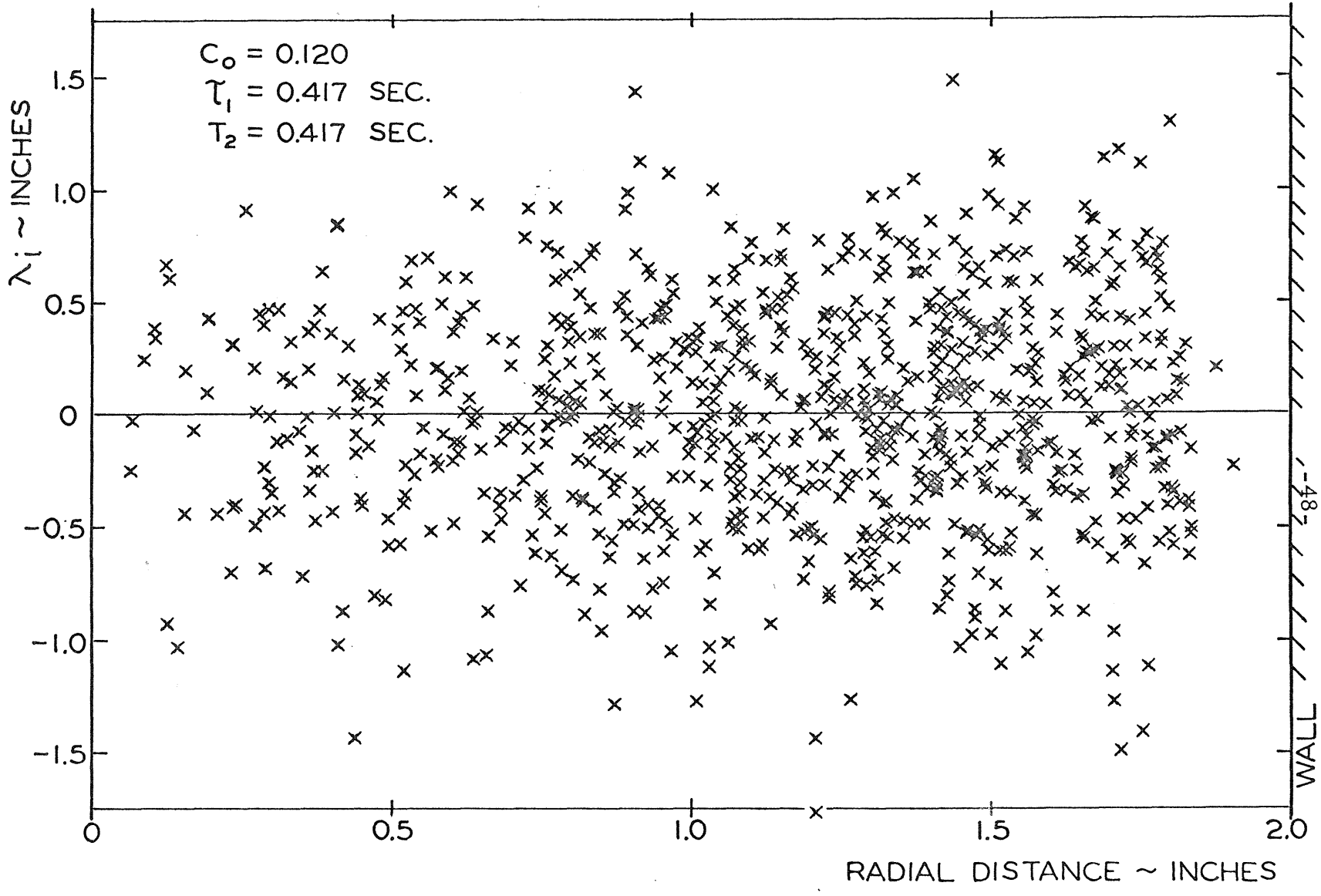

Figure 10a. Vertical Step Length as Function of Radial Position.

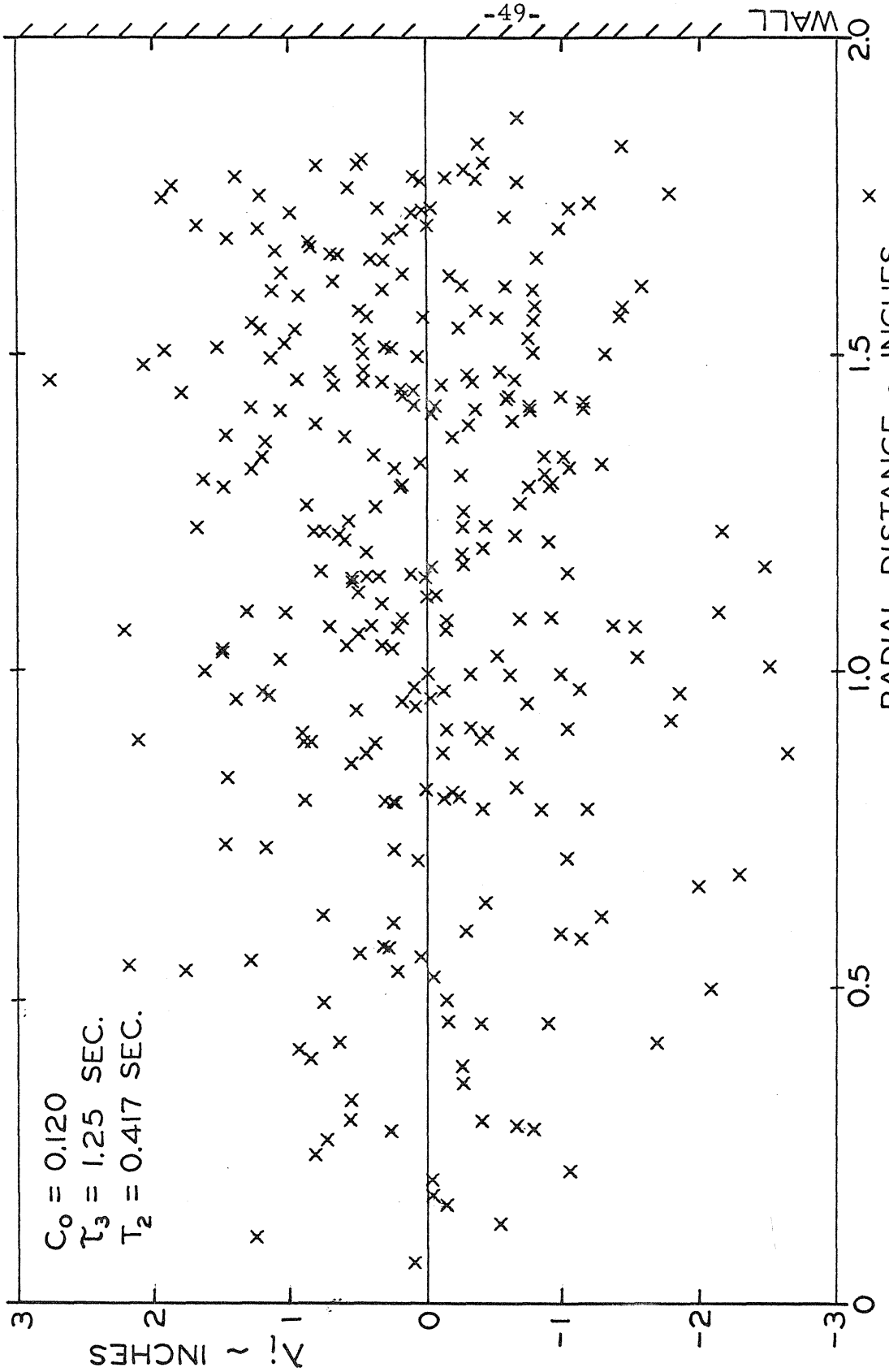

Figure 10b. Vertical Step Length as Function of Radial Position (continued).

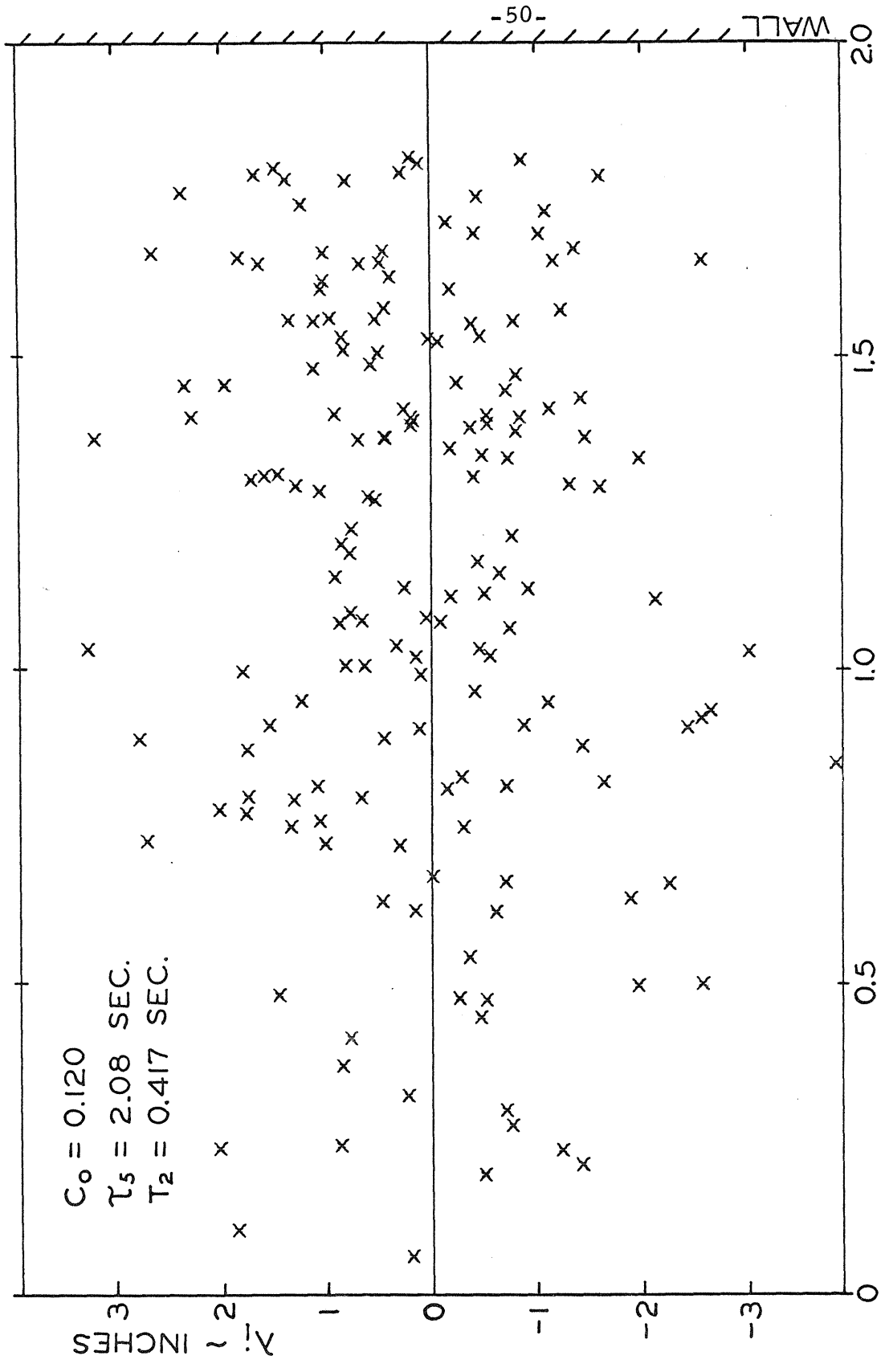

Figure 10c. Vertical Step Length as a Function of Radial Position (continued).

same time, τ_k. The cross section was divided into grids of equal area and the fraction of steps with starting positions in a given grid was computed; Figure 11 presents this density of polar sampling for the time interval 0.417 seconds from runs at the long frame rate. Each quadrant is divided into annuli, each with an area one twenty-eighth that of the cross-sectional area of the column, except for the outer annuli in quadrants I, II, and III, which have areas three times as large to include blind spot regions. As presented in the figure for the time interval 0.417 seconds, indicative of all time intervals, the sampling density was greatest in quadrants III and IV, the front of the column relative to the camera. This phenomenon can be explained by the bias in the selection of runs in a given experiment, originally; although an attempt was made to obtain a uniform sample, there was a tendency to favor runs with starting positions close to the front of the column because of their greater resolution on film. The sampling density was nearly constant radially, however, as shown by the totals in each concentric ring.

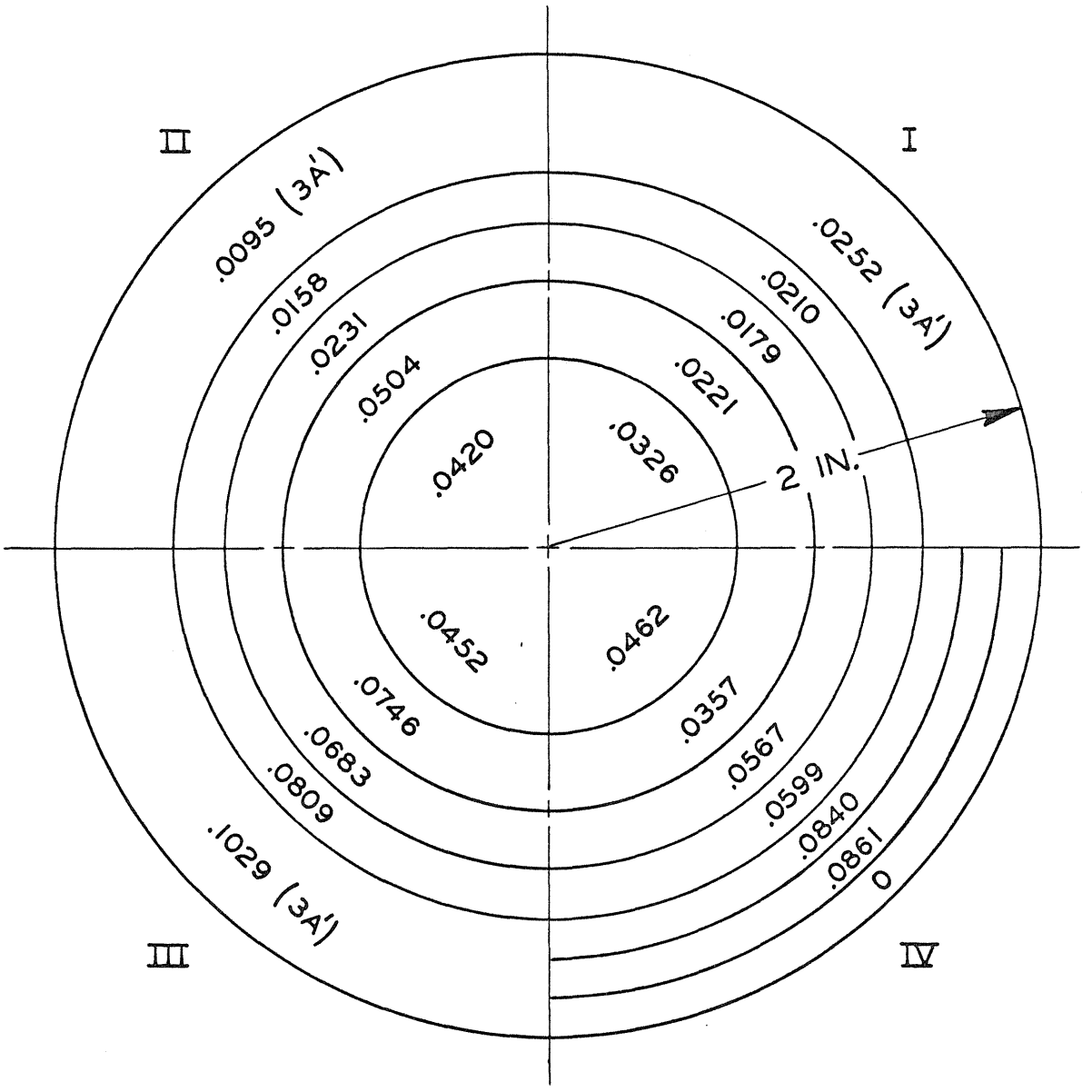

Figure 11. Polar Sampling Density of Vertical Steps.

IV. COMPARISON WITH OTHER EXPERIMENTS

Three other investigators have measured particle diffusion coefficients in liquid beds. Handley, et al.[7] employed a technique similar to that of the current experiment; matching the refractive index of crushed soda glass particles with methyl benzoate, particle diffusion coefficients were determined by the application of Brownian motion analysis to film data on colored particles. However, in contrast to the current experiment, Handley, et al. utilized a short bed with a length-to-diameter ratio of 3.3 to 1, raising suspicion that the effects of particle recirculation may have influenced his measurements. In fact, it is quite possible that Handley, et al. did not measure random particle motion as much as particle motion in the steady patterns of recirculation. Rowe, et al.[8] fluidized copper shot with water and determined particle diffusion coefficients by following a diffusing front of nickel particles (copper and nickel have nearly the same density). At the start of an experiment, a narrow strip of nickel particles was placed on the bottom of the settled bed. The bed was then fluidized and scanned with a coil, the inductance of which was recorded continuously. Diffusion coefficients were deduced from the time required for the nickel particles to distribute themselves uniformly. The major drawback of this technique is that the effect of transients is included in the measurements while the bed comes to an equilibrium height; there is usually much mixing by means other than diffusion during this time.

Carlos and Richardson[6] matched the refractive index of glass beads with dimethyl phthalate and determined particle diffusion coefficients by following a diffusing front of opaque beads on film. Initially,

100 opaque beads were placed at the bottom of the bed, and the fluid velocity was adjusted to a value slightly less than that required for fluidization; then the flow rate was sharply increased to the desired value. The weaknesses in the techniques of both Handley, et al. and Rowe, et al. were combined by Carlos and Richardson: a short bed with a length-to-diameter ratio of 2.5 to 1 was utilized, and transient effects were included in the measurements.

Dimensions and physical properties relating to the fluidizing column, the fluid, and the particles employed in each of these three experiments, as well as in the current experiment, are summarized in Tables 3a and 3b. Plots of particle diffusion coefficients as a function of Reynolds number, R_o, based on superficial fluid velocity and column diameter, are shown in Figure 12; Figure 13 presents plots of particle diffusion coefficients as a function of particle voidage. In their article, Carlos and Richardson present diffusion coefficient data as a function of superficial velocity and voidage; Rowe, et al., however, present them only as a function of superficial velocity; and Handley, et al. present them only as a function of voidage. The superficial velocity function of Richardson and Zaki[10] was estimated for the experiment of Handley, et al. in order to convert voidages to superficial velocities in preparing Figure 12, and for the experiment of Rowe, et al. in order to convert superficial velocities to voidages in preparing Figure 13. Since it is such a useful average property of a liquid fluidized bed, Richardson and Zaki's superficial velocity functions are included in Table 3b for each experiment.

In comparing the particle diffusion coefficient data of all four

	Fluidizing Column		Fluid Properties*			
	diameter (inches)	height / diameter	name	viscosity (cp.)	density ($\frac{\text{lb.}}{\text{cu. ft.}}$)	operating temperature (°C)
Carlos and Richardson	4.00	2.5	dimethyl phthalate	10.0	72.4	30
Handley, et al.	3.00	3.3	methyl benzoate	2.07**	67.8	30.5
Rowe, et al.	4.00	6	water	1.0	62.4	†
Willus	4.00	24	18.8% ATB, 81.2% UCON LB-65	22.2	83.0	30

*Values of properties are those reported by each author and are evaluated at the operating temperature unless noted otherwise.

**At 20°C.

†Neither temperature nor properties reported; 20°C assumed.

TABLE 3a. Parameters of Experiments on Diffusion Coefficients -- Fluid and Fluidizing Column.

	Particle Properties			
	Type	Diameter (inches)	Density (lb./cu. ft)	Richardson-Zaki* Superficial Velocity (ft./sec.)
Carlos and Richardson	glass beads	.35	155	$1.6(1-C_o)^{2.4}$
Handley, et al.	crushed glass	14-16 mesh ~.043	155	$.28(1-C_o)^{3.2}$
		10-12 mesh ~.059	155	$.39(1-C_o)^{3.0}$
Rowe, et al.	Cu shot	.015	545	$.59(1-C_o)^{3.0}$
Willus	glass beads	.236	138	$.56(1-C_o)^{3.3}$

*Free-fall velocity for rigid spheres estimated with use of drag coefficient data reported by Haberman and Morton[9]; Handley measured free-fall velocity of a particle of mean size.

TABLE 3b. Parameters of Experiments on Diffusion Coefficients -- Particles and Velocity Function.

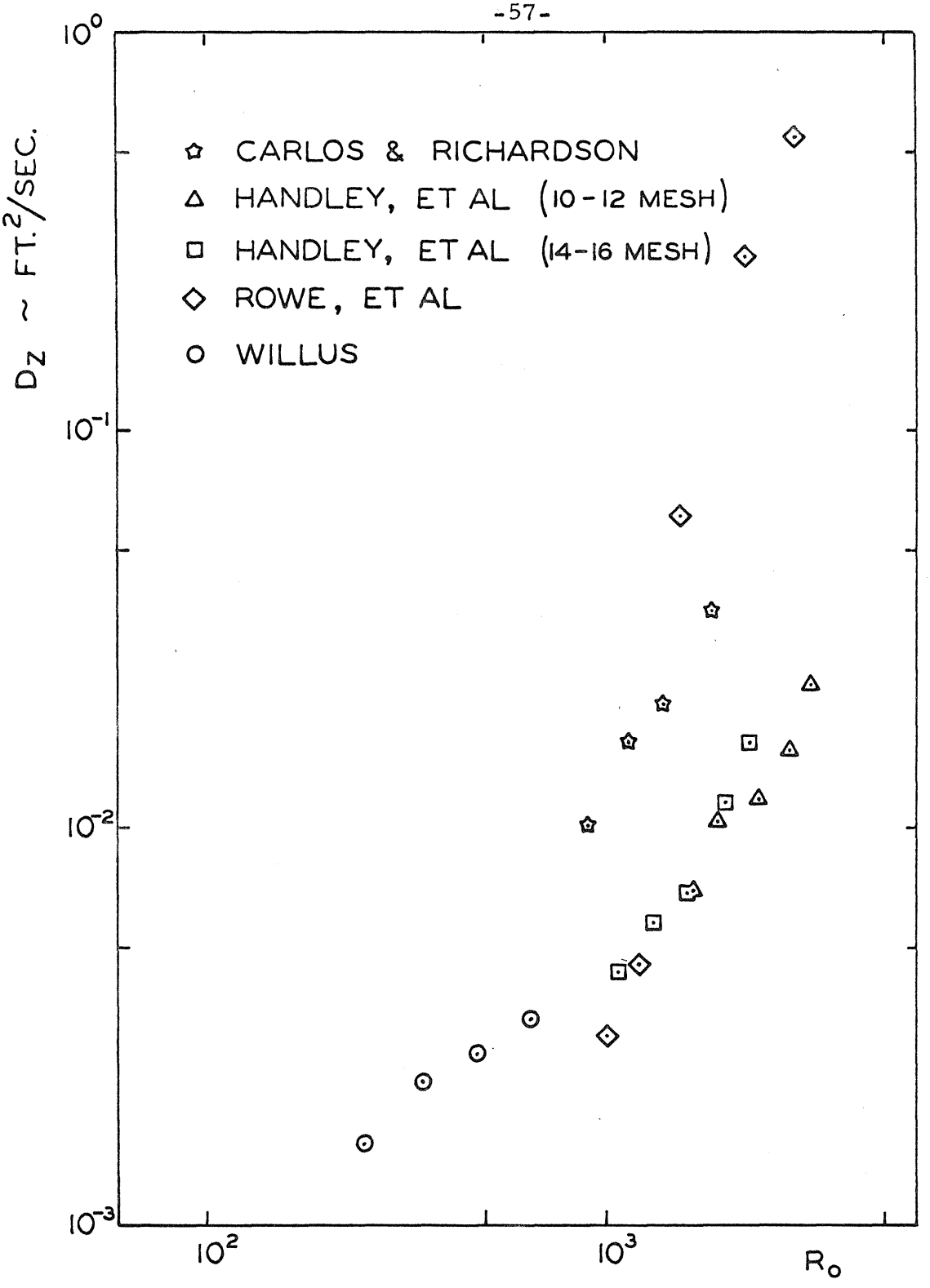

Figure 12. Particle Diffusion Coefficients as a Function of Superficial Reynolds Number Based on Column Diameter.

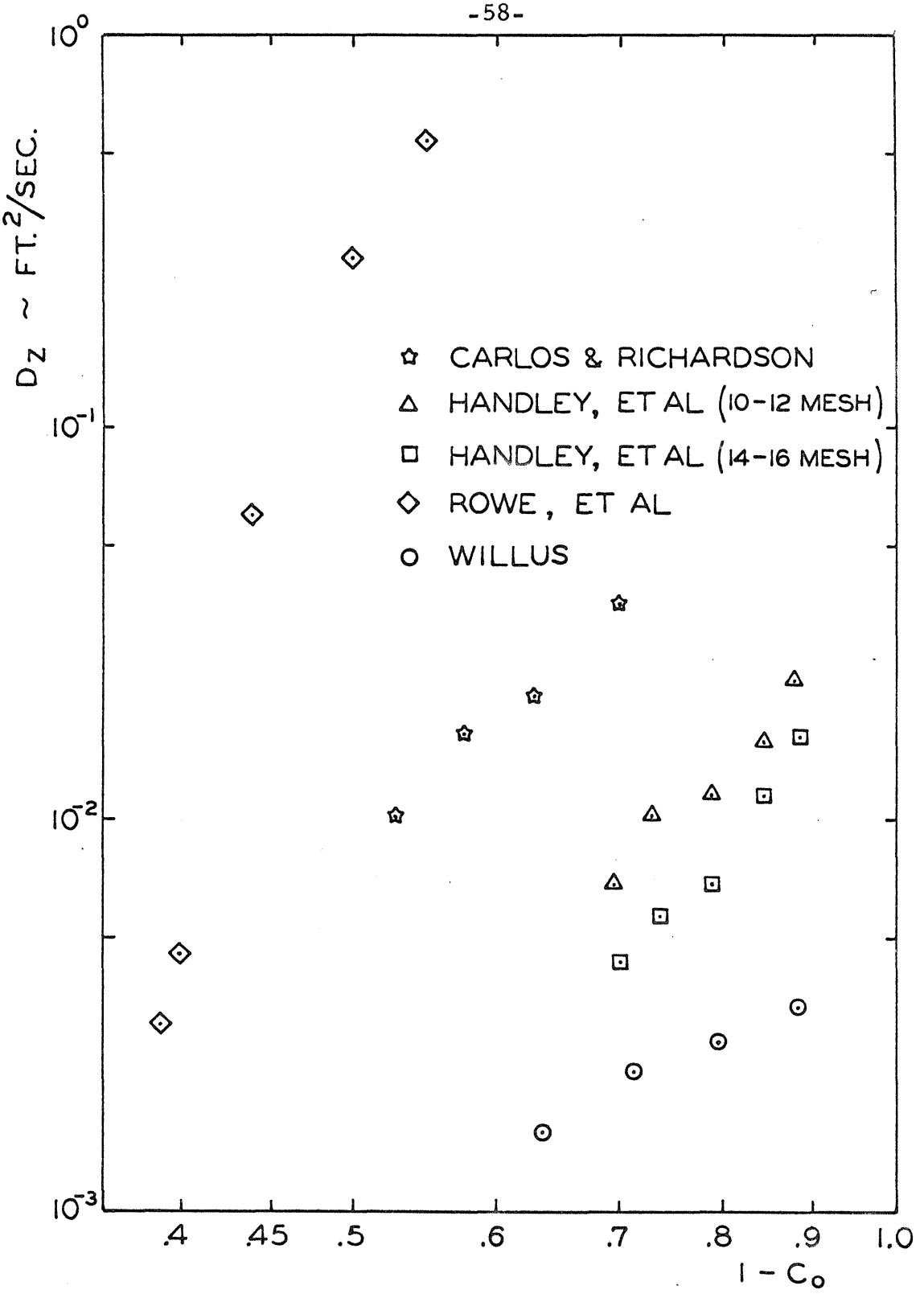

Figure 13. Particle Diffusion Coefficients as a Function of Voidage.

experiments, the writer was unable to untangle the appropriate length and time scales required to correlate the data. At least part of the difficulty in doing so rests on the doubt concerning the validity of diffusion coefficients quoted by three of the investigators. Clearly, more experiments are needed, preferably with particles of different sizes in the same apparatus.

A noteworthy observation was made in comparing the diffusion coefficients of the beads determined in the current experiment with the estimated eddy viscosity of the fluid in the absence of the particles. The eddy viscosity of the fluid was evaluated in the limit, as the particle concentration tends to zero or approximately at the free fall velocity, U_t, of a single particle in a quiescent fluid. (U_t = 0.56 ft./sec., as discussed in Chapter I.) At this condition, the Reynolds number of the fluid is approximately 1000, based on the diameter of the fluidizing column. Although a laminar flow is predicted at a Reynolds number, R, of 1000, the flow is probably somewhat turbulent due to the presence of even a few particles. To obtain a crude estimate of the eddy viscosity, suppose that it is evaluated for the turbulent flow of a fluid in a pipe. Turbulence in pipe flow and the turbulence of the fluid in the bed as the particle concentration tends to zero are not of the same mechanism, but the supposition is made merely to obtain a rough estimate of the fluid eddy viscosity in the bed. For the turbulent flow of a fluid in a pipe, the eddy viscosity, ε_f, taken at its maximum value on the cross section of the pipe, can be evaluated with use of a semi-empirical correlation of Schlichting[23],

$$\varepsilon_f = .04\, U^* D_{bed} \qquad \text{ft.}^2/\text{sec.} \quad ,$$

where D_{bed} is the diameter of the fluidizing column, and U^* is the turbulent friction velocity. In terms of the friction factor, f, the friction velocity is given by

$$U^* = \frac{U}{2}\sqrt{\frac{f}{2}} \quad ,$$

where U is the average fluid velocity in the pipe. The Blasius formula[24] for the friction factor, namely,

$$f = \frac{0.316}{R^{.25}} \quad ,$$

is valid at Reynolds numbers (based on pipe diameter) less than 10^5. In estimating the eddy viscosity in the bed, further suppose that the friction factor is calculated at a Reynolds number of 2000, the minimum Reynolds number at which turbulence forms in a pipe; the fluid velocity was taken at U_t. A value, $\epsilon_f = .00058$ ft.^{2}/sec. was found. At the smallest average bead concentration at which an experiment was made ($C_o = 0.120$), a diffusion coefficient of the beads, $D_z = 0.0033$ ft.^{2}/sec. , was measured. At $C_o = 0.120$,

$$D_z/\epsilon_f = 5.7 \quad .$$

Even if the eddy viscosity of the fluid in the bed is evaluated in this rough way, the addition of only 12 percent by volume of beads increases the level of instabilities significantly. Instabilities in a fluidized bed are not due to those of the fluid alone, uninfluenced by the presence of the particles. Rather, the combined action of the particles and the fluid create instabilities by a mechanism as yet not fully understood.

PART 2

CIRCULATION PATTERNS AND WEAK WAVES IN LIQUID FLUIDIZED BEDS

In the early stages of this investigation, several fluidized beds of relatively low ratio of height to diameter were run and observed. Eventually, it became clear that it was difficult, if not impossible, to avoid large steady or quasi-steady circulation patterns which would obscure diffusion proper, so the apparatus described in Part 1 was developed. Nevertheless, the circulating patterns in the shallower beds are of interest in themselves. The patterns that formed both in a cylindrical bed, with a length-to-diameter ratio of 5 to 1, of glass beads fluidized by water and in conical beds are described below.

In addition to the circulation patterns, weak waves also formed in this cylindrical bed. Narrow strata, basically one dimensional, of varying particle concentration were observed propagating upwards at a somewhat regular rate in the bed of otherwise uniform concentration. The propagating speed was measured and is compared to that estimated using the theory of kinematical waves.

V. EXPERIMENTAL METHOD

The basic elements of the experimental apparatus are illustrated schematically in Figures 14 - 16. The flow circuit is shown in Figure 14; the photograph of Figure 15 depicts the cylindrical bed. The column, a lucite tube 15 inches in length and 3.09 inches inside diameter, is loaded with Kimax glass spheres 0.20 inches in diameter, having an average specific gravity of 2.21. Water at approximately constant head is supplied to the column from a tank situated on the roof of the building. The tank is about 35 feet above the inlet to the column. Before entering the column, the flow passes through a distributor designed to provide a uniform fluid velocity. In the distributor, the flow is diffused by a tapered section and then acted upon by a miniature fluidized bed of 0.040 in. glass spheres contained between two fine mesh brass screens. As was discussed in the first part of this thesis, it is the action of the miniature bed that produces a uniform fluid velocity at the inlet.

In a typical experiment, a known weight of beads (0.854 pounds for most runs) was expanded to a constant height. Water flow rates were measured by recording the time to collect a given volume of water.

A phototube arrangement was employed to measure wave velocities and periods. The phototubes, RCA No. 929, were sensitive to the intensity of light transmitted through the bed from a 300-watt lamp. Wave patterns received from two phototubes, placed 1.20 inches apart along the fluidizing column, were displayed on a dual-beam oscilloscope and recorded on film. Each phototube was properly shielded by

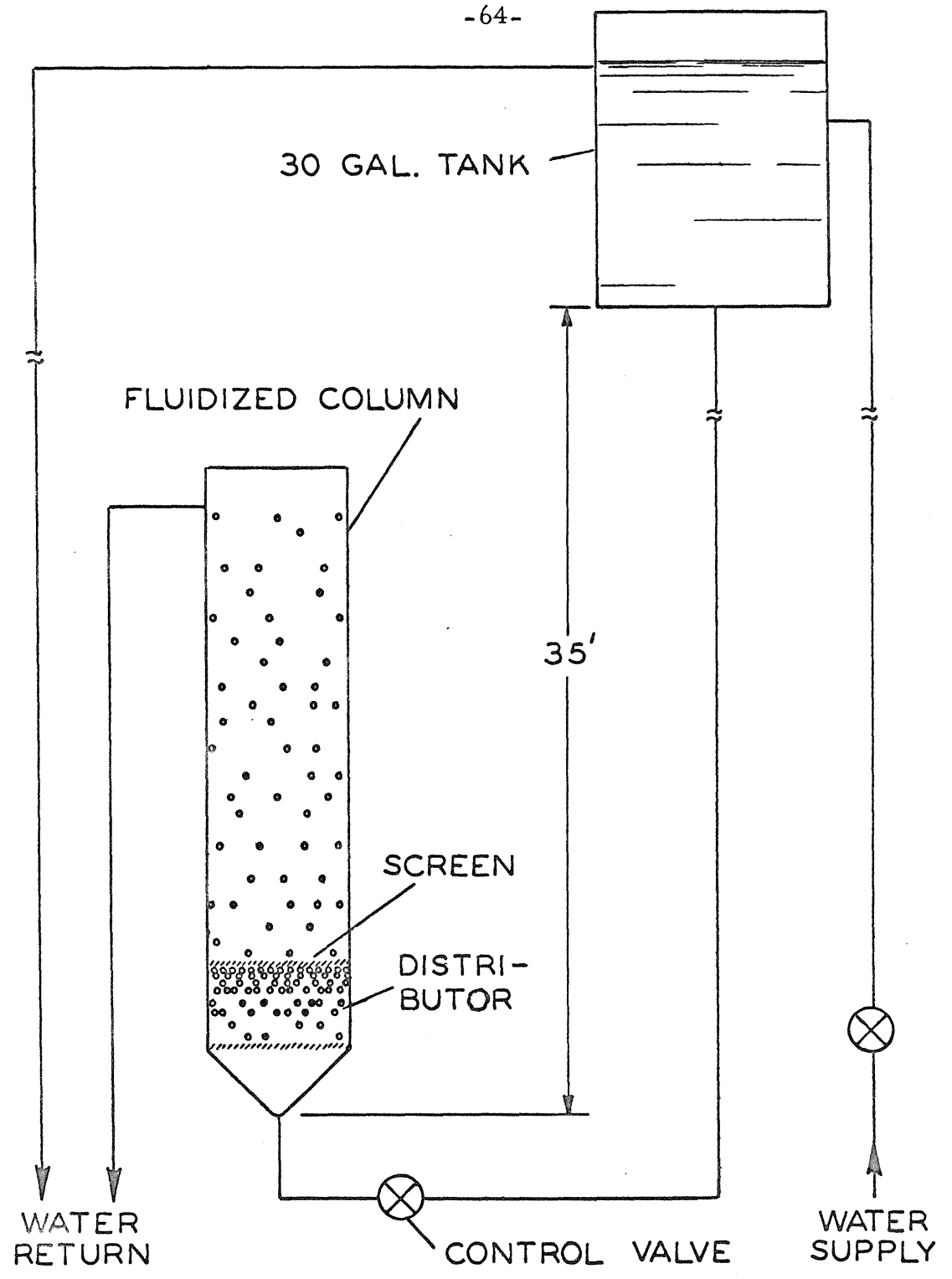

Figure 14. Flow Circuit of the Shallow Bed.

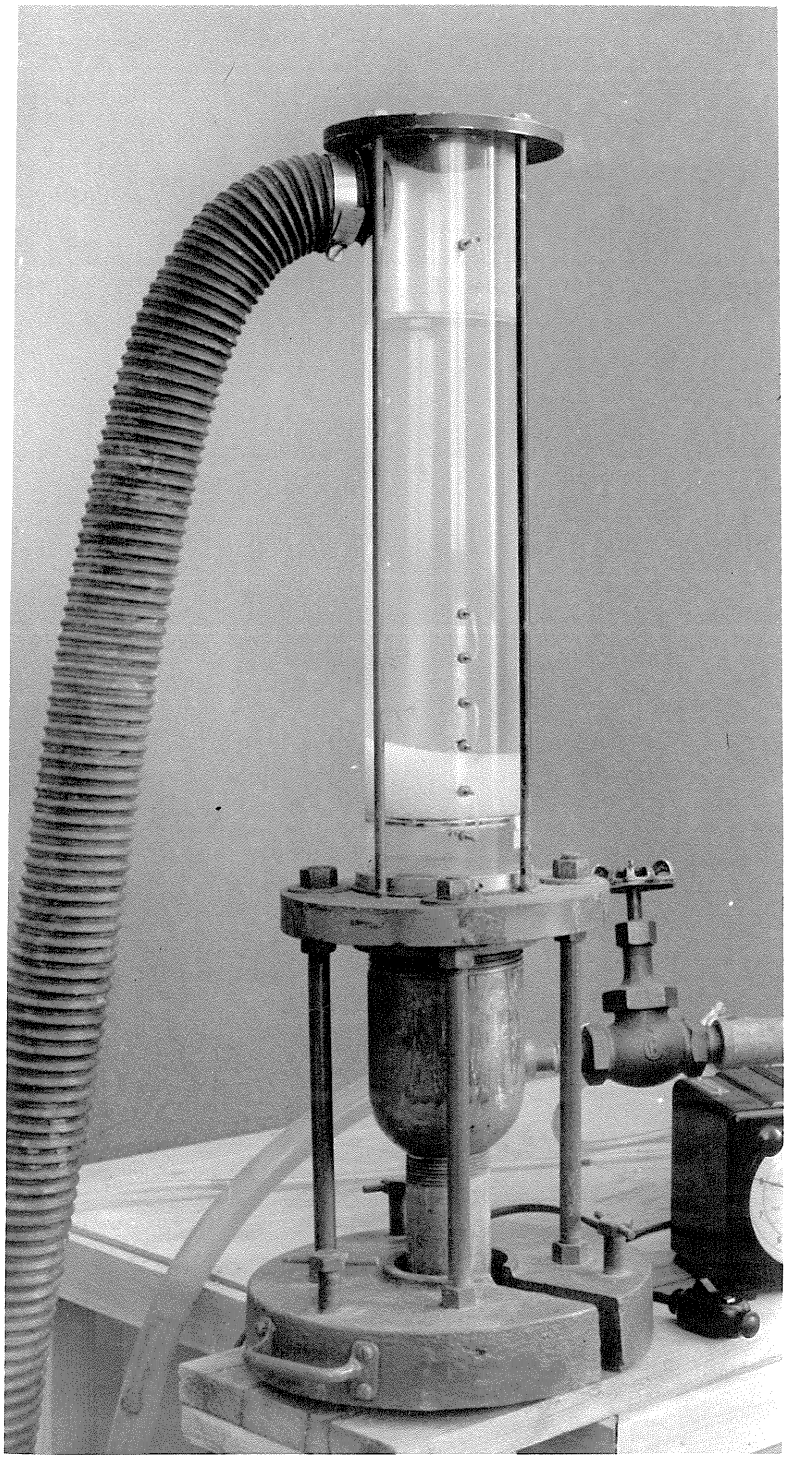

Figure 15. Experimental Installation of the Shallow Bed.

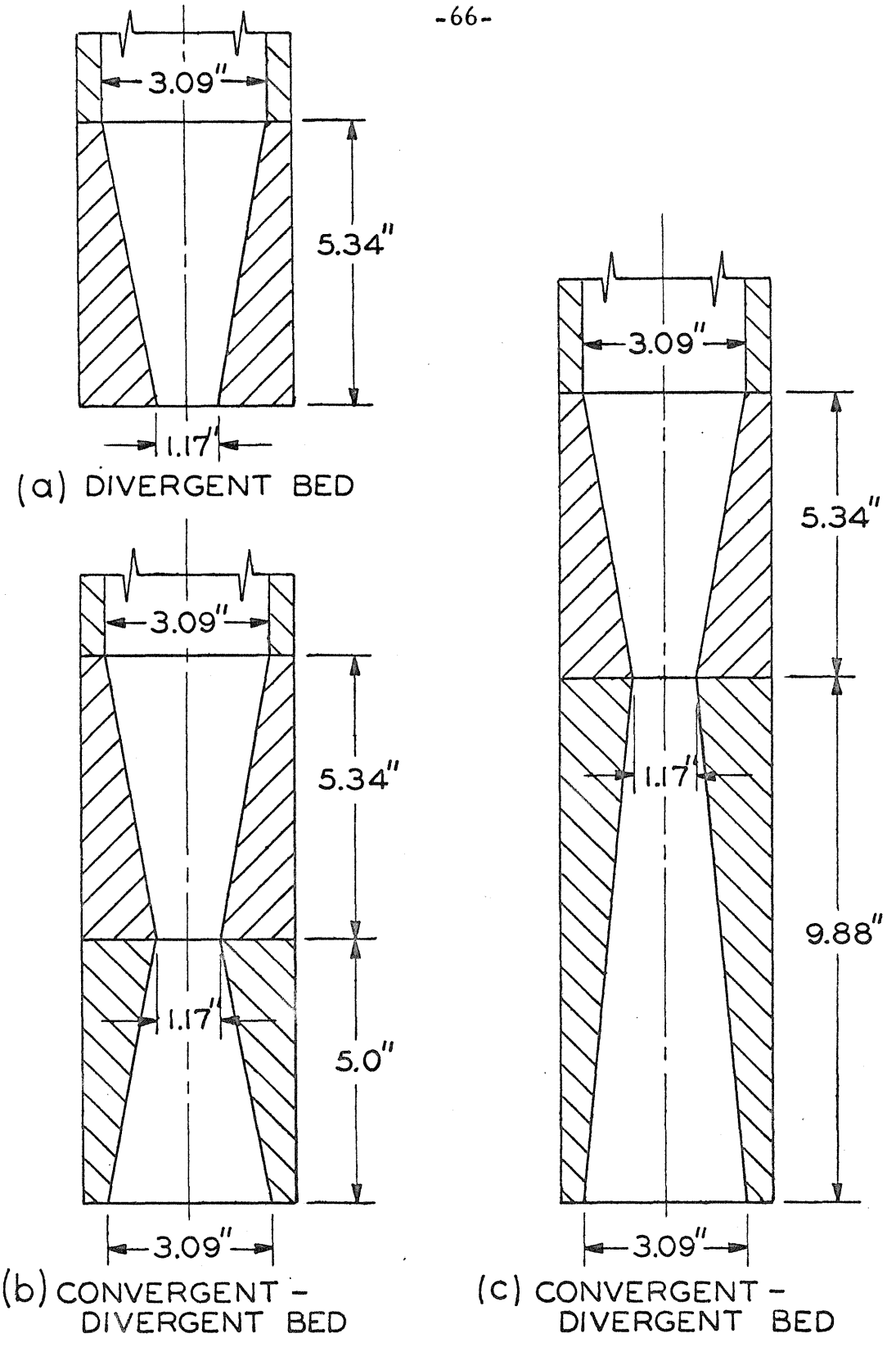

Figure 16. Conical Beds.

apertures placed at each end of a tube 12 inches long and one inch in diameter. Also, still photographs were taken of the fluidized particles.

The patterns of particle circulation that formed in the cylindrical bed were studied by following visually the motion of a tagged bead. In addition, three configurations of conically-shaped beds were used in an investigation of patterns of particle circulation in beds of other than cylindrical section; they are sketched in Figure 16. In each case, the conical configuration was sandwiched between the distributor and the cylindrical bed, and generally the combination was loaded with about one pound of glass spheres, 0.20 inch in diameter. The mixing patterns that formed as the fluidizing velocity was varied were observed. A study was also made of the effect on the mixing of lowering a star-shaped baffle, having four mutually perpendicular vanes, into the bed above the divergent cone.

VI. OBSERVATIONS

A. Patterns of Particle Circulation

The particle circulation patterns that formed in the cylindrical fluidized bed maintained a steady shape that was, however, extremely sensitive to any slight variation in the vertical alignment of the bed. It generally took the form of a net particle drift upwards at the walls and downwards in the central core, as shown in Figure 17a. A slight misalignment of the bed from the vertical, however, would cause the pattern to shift into one of particle movement upwards over one-half of the cross section of the column and downwards over the other (see Figure 17b). Maximum drift velocities were of the same order as the average bed fluid velocity.

Conical beds were investigated in an attempt to find stable patterns of particle circulation. (A stable pattern is here defined to be insensitive to slight variations in the vertical alignment of the bed.) It was hypothesized that the unstable patterns found in cylindrical beds may be the limiting condition of stable patterns found in conical beds. It was determined that certain convergent conical geometries do provide somewhat stable patterns. For divergent conical geometries, on the other hand, unstable and under certain conditions unsteady, patterns were observed. In this case, the rate of particle recirculation was very high. This secondary result may be of practical engineering importance to fluidized bed technology, for it provides a technique to increase mixing rates.

The patterns that formed in the divergent bed of Figure 16a were generally unstable. Only at flow rates so small that the particles

in the upper section of the bed had not yet fluidized was a stable shape exhibited. It was symmetric with an upward particle drift in the central core and a downward particle drift near the walls, as depicted in Figure 18a. At flow rates sufficient to fluidize all of the particles, an unstable pattern of very rapid particle recirculation developed, as shown in Figure 18b. It is interesting to note that a somewhat analogous phenomenon occurs in the flow of a fluid (devoid of particles) in a diffuser; for instance, Kline and Moore[25] report that for certain diffuser designs, the flow stalls and a fluid recirculation pattern forms. They observed the effects of vaned baffles in suppressing the onset of this condition in diffusers.

In an attempt to control the patterns of very rapid particle recirculation in the divergent bed, a star-shaped baffle with four mutually perpendicular vanes was lowered into the bed. When situated in the particle-free fluid region, the baffle had no effect. When it was lowered into the fluid particle system, however, it transformed the recirculatory motion into an unsteady spouting motion. Particles were observed to surge suddenly at random, up one of four channels formed by the vanes of the baffle, and then to settle momentarily before spouting again.

The convergent section of the convergent-divergent bed of Figure 16b produced a stable, symmetric pattern of particle movement upwards near the walls and downwards in the central core (see Figure 19a). When the cone angle of the convergent cone was reduced to that of the bed of Figure 16c, the pattern became unstable, as shown in Figure 19b. This result was expected; the pattern in the more

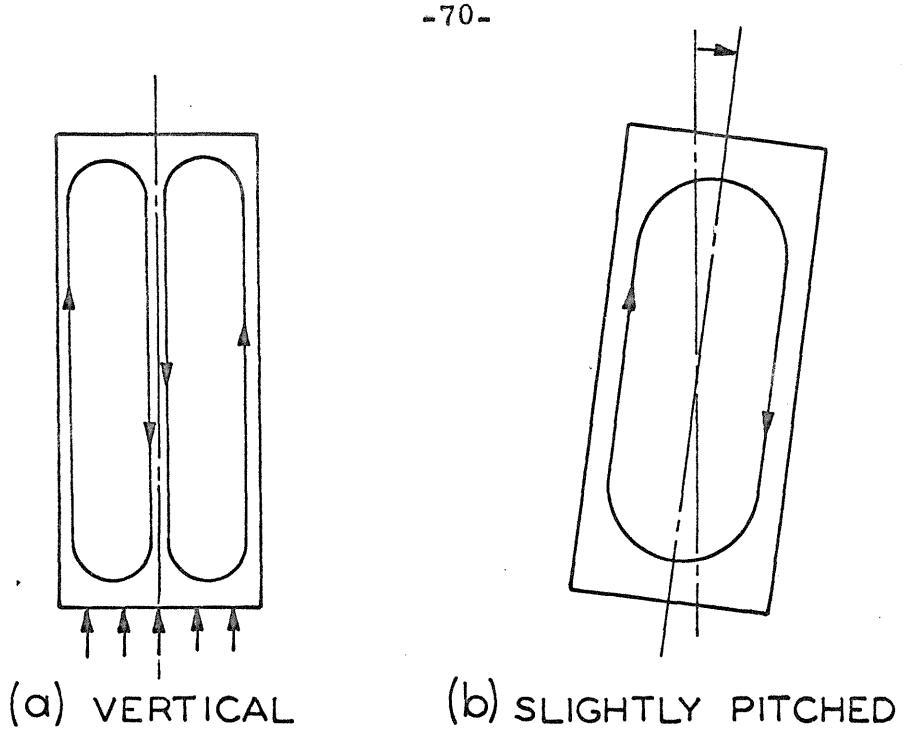

Figure 17. Circulation Patterns in Cylindrical Bed.

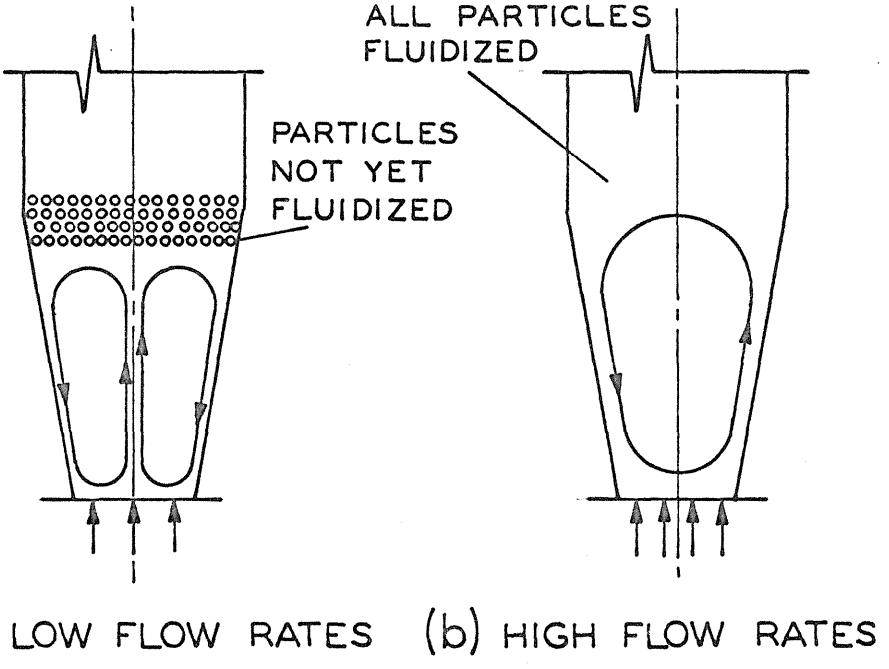

Figure 18. Circulation Patterns in the Divergent Bed of Figure 16a.

gently tapered cone approached the unstable type of pattern that formed in the cylindrical bed.

An unsteady spouting motion was observed in the divergent section of the convergent-divergent beds of Figures 16b and 16c without the use of a baffle. After remaining in a pattern of rapid recirculation for a time, similar to that shown in Figure 18b, the particles suddenly directed their energy into an upward surge, as depicted in Figure 20. The particles then settled, and a new pattern of recirculation developed. The direction of rotation of the new pattern was opposite to that of the original pattern. It was also observed that by adding more particles to the configuration, the unsteady spouting motion could be confined to the lower portion of the bed. The action in the upper portion of the bed resembled that in an ordinary cylindrical bed.

B. Superficial Fluid Velocity

A log-log plot of superficial water velocity, U_o, measured in the range 0.21 to 0.65 ft./sec., as a function of average particle voidage, $1-C_o$, which ranged from 0.48 to 0.81 in the cylindrical bed, appears in Figure 21. From this plot, the following empirical formula was deduced:

$$U_o = 1.05(1-C_o)^{2.4} \text{ ft./sec.}$$

In comparing this formula with the correlation of Richardson and Zaki[10], the exponent agrees precisely while the multiplication factor does not agree very well. Richardson and Zaki suggest using the terminal free-fall velocity of a single particle in a quiescent fluid as the multiplication factor. Employing drag coefficient data for rigid

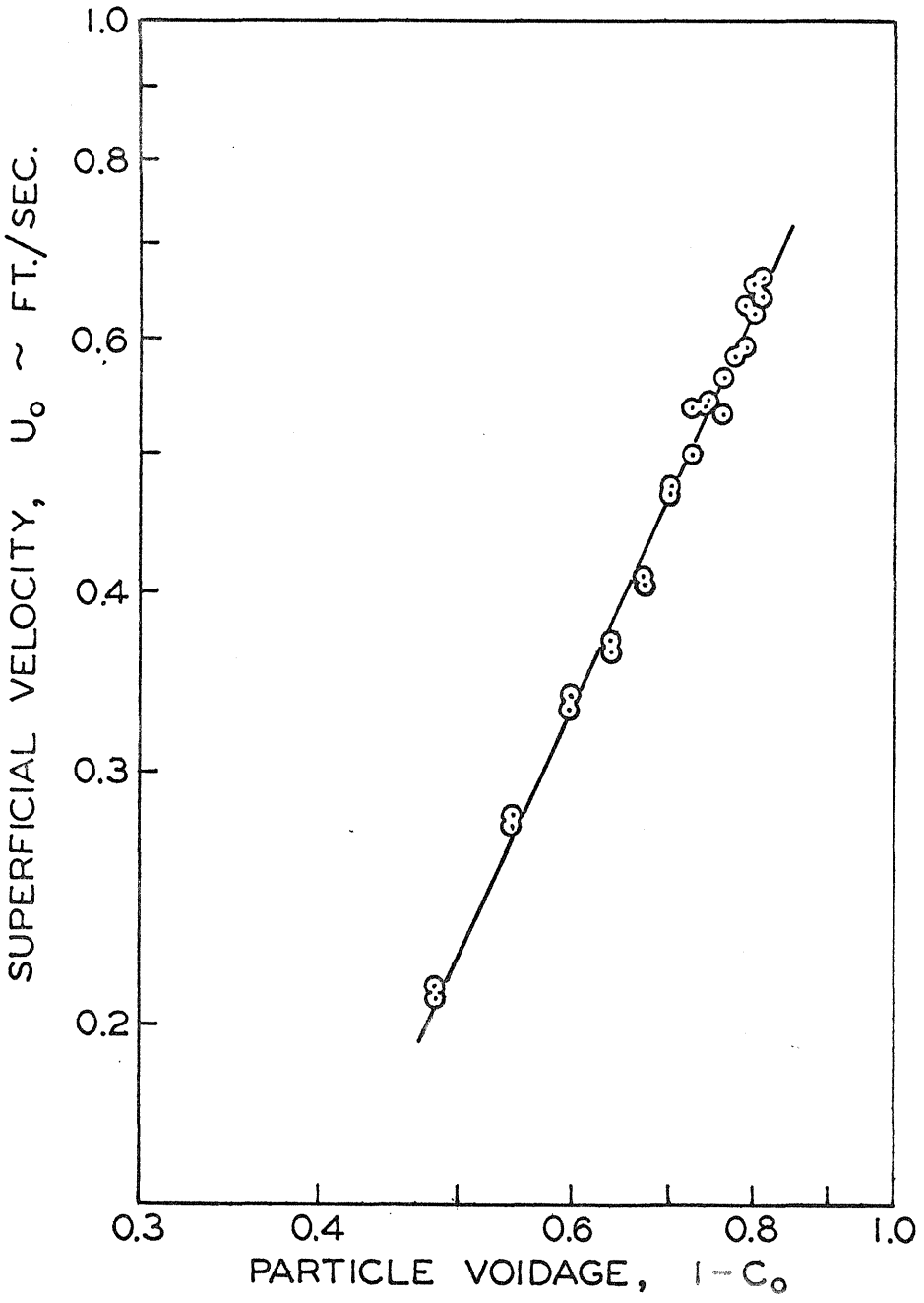

Figure 21. Superficial Water Velocity.

spheres reported by Zenz[26], a terminal velocity of 1.37 ft./sec. of a bead in water was calculated, a value 30 percent larger than the multiplication factor in the formula. A similar discrepancy was noted in applying the correlation to the bed used in the diffusion experiment, and the argument presented in Chapter I to explain the discrepancy can be adopted in the current case. The multiplication factor is the limiting value of the superficial water velocity as the bead concentration tends to zero. However, as the bead concentration tends to zero, the fluid flow in the column is not steady, since the Reynolds number of the fluid based on the diameter of the fluidizing column and calculated using the free-fall velocity is 33,000, approximately. In addition, the presence of even a few particles as $C_o \rightarrow 0$ increases the level of turbulence significantly. It is expected that a better estimate of the multiplication factor is the free-fall velocity in a turbulent field. Unfortunately, data on drag coefficients of spheres in turbulent fields are not yet available.

C. Waves

Weak waves were observed in the cylindrical fluidized bed. They formed near the lower boundary of the bed at a somewhat regular rate and appeared as narrow strata of low particle concentration propagating upwards through a bed of otherwise uniform concentration. Others[27-29, 12] have also reported the occurrence of waves of similar appearance in liquid beds; Hassett[27] has labeled them "par-voids."

The source of the waves has not been identified. At an average particle concentration, C_o, of 0.26, measured periods were of the

order of 0.2 to 0.5 seconds. No driving mechanisms external to the bed were found; their production is suspected to be due to some inherent property of liquid fluidized beds.

Although their existence was easily demonstrated by actually viewing a train of these waves moving in the apparatus, it was very difficult to make accurate measurements of their speeds. Measurements of their shape were not attempted. An individual wave, propagating upwards, interacted with fluid turbulent fluctuations and currents of particle recirculation to such an extent that its speed and shape changed erratically as it moved. As a result, there was considerable scatter in the data, and it was impossible to correlate wave speed as a function of average particle concentration, C_o. At an average particle concentration of 0.26, at which the waves appeared best formed, a wave speed of 0.4 ft./sec. was measured, with most of the readings falling within limits of ± 50 percent of this value.

The general theory of kinematical waves has been discussed by Lighthill and Whitham[30]. Here, it is simpler to proceed directly with a calculation of the propagating speed. Consider a cylindrical bed of particles of equal size and density, fluidized by the upward flow of a liquid. Assume that the motion can be treated as one dimensional, and take z as the vertical height above the lower support of the bed. Let

$C(z, t)$ = particle volume fraction (concentration)

$U_p(z, t)$ = velocity of particles

$U_f(z, t)$ = velocity of fluid

U_t = terminal free-fall velocity of a single particle

U_o = superficial fluid velocity

C_o = average particle concentration

The conservation of mass equations for fluid and particle phases are

$$\frac{\partial(1-C)}{\partial t} + \frac{\partial(1-C)U_f}{\partial z} = 0 \quad , \tag{1}$$

$$\frac{\partial C}{\partial t} + \frac{\partial CU_p}{\partial z} = 0 \quad . \tag{2}$$

Now assume that viscous drag and buoyant forces on a particle dominate inertia effects and that the particle slip velocity, $U_f - U_p$, is a known function of the particle concentration, i.e.,

$$U_f - U_p = F(C) \quad . \tag{3}$$

The function $F(C)$ of (3) is an empirical result of experiments on gross fluidized bed behavior. Various forms for this relationship have been presented in the literature[10, 31, 32], and the one developed by Richardson and Zaki[10] will be adopted here because of its wide acceptance by workers in this field, its fairly good agreement with experiments, and its simplicity. The Richardson - Zaki correlation is

$$F(C) = U_t(1-C)^{n-1} \quad , \tag{4}$$

where U_t is the terminal free-fall velocity of a single particle in the absence of other particles, and n is a slowly varying function of the particle Reynolds number based on U_t and the ratio of the diameter of a particle to that of the bed. To estimate n, Richardson and Zaki have prepared empirical formulas.

Equations (1) - (4) are easily manipulated to derive a kinematical wave equation for particle motion. Add (1) to (2) and integrate to obtain

$$CU_p + (1-C)U_f = U_o \quad , \tag{5}$$

where U_o is the superficial fluid velocity, a constant. From (3), (4), and (5),

$$U_p = U_o - U_t(1-C)^n \quad , \tag{6}$$

which, when substituted into (2), yields

$$\frac{\partial C}{\partial t} + V(C)\frac{\partial C}{\partial z} = 0 \tag{7}$$

where

$$V(C) = U_o - U_t(1-C)^n + nU_tC(1-C)^{n-1} \quad . \tag{8}$$

Equation (7) is a kinematical wave equation with characteristics V(C) along which C is the invariant. Wave equations of this type have been discussed thoroughly by Lighthill and Whitham[30].

It will suffice for the purpose of this analysis to linearize (7) and (8) to find the wave velocity of a small disturbance in particle concentration. For other applications of (7) and (8) to fluidized beds and the closely related problem of sedimentation of solids in a liquid, refer to Slis, et al.[33], Kynch[34], Wallis[35], and Shannon, et al.[36]. Take for the undisturbed state a bed which is fluidized by a constant superficial velocity, U_o, and has a uniform constant particle concentration, C_o, and $U_p = 0$. Consider the effect on the undisturbed bed of a small disturbance in particle concentration. Take

$$C(z, t) = C_o + \epsilon\tilde{C}(z, t) + O(\epsilon^2) \quad , \tag{9}$$

where $\varepsilon << 1$. Apply this approximation to (7) and (8) to find

$$\frac{\partial \tilde{C}}{\partial t} + V_o \frac{\partial \tilde{C}}{\partial z} = 0 \quad , \tag{10}$$

$$V_o = nU_t C_o (1-C_o)^{n-1} \quad . \tag{11}$$

The desired result, the velocity of propagation of a small disturbance in particle concentration, is given by (11).

With formula (11)*, the velocity of a small disturbance in concentration at an average concentration, C_o, of 0.26 is 0.45 ft./sec. This calculated wave speed is within the range of measured wave speeds, 0.4 ± 0.2 ft./sec.

*The measured values of the multiplication factor and the exponent in the Richardson and Zaki superficial velocity function were used.

CONCLUDING REMARKS

As mentioned in the Introduction, the purpose of this work was to attempt to understand the mechanism of unsteady motion within a fluidized bed. The experiment chosen was one of following the motion of a typical particle in the bed. The motion of the particles was found to closely resemble a diffusive motion, and diffusion coefficients for longitudinal motion were measured at several average bed concentrations. A summary of the results of the experiment is contained in the Introduction. In this section, some conclusions concerning the experiment are drawn, and some suggestions for future work are made.

The diffusion coefficients of the beads were compared to particle diffusion coefficients measured by three other investigators in beds with different particle sizes, different particle-to-fluid density ratios, and in different Reynolds number ranges. The writer was unable to resolve the appropriate length and time scales required to correlate the data from other investigators. At least part of the difficulty of doing so rests on the doubt concerning the validity of the diffusion coefficients quoted by the other investigators. Further experiments are needed. Beads of different diameter could be studied in the present apparatus without any modifications to the equipment. However, to make an experiment utilizing a different particle-to-fluid density ratio, a technique other than the optical one employed here would have to be developed, as fluids of the same refractive index as glass are all of nearly the same density. (The use of clear plastic beads should be investigated.) The diameter of the bed may have an influence on the size of eddies and thus on the length scale of diffusion. Experiments in beds

of different diameter would be interesting and could utilize most of the present equipment. An analysis of radial diffusion should also be made in order to determine to what extent, if any, the random particle motion is non-isotropic.

Since a means of correlating the diffusion data by several investigators was not found, particle diffusion coefficients cannot be estimated for any given fluidized bed. If a generalized correlation had been obtained, physical insight into other fluidized bed processes might be gained. As mentioned previously, particle diffusion coefficients can be used to estimate the characteristics of the residence time of a particle in a catalytic reactor. In addition, a large bulk of data on heat and mass transfer between the particles and the fluid and also between the bed and its walls has been reported in the literature; a knowledge of particle diffusion coefficients may be useful in the interpretation of these data.

As a bed is expanded, the film heat transfer coefficient at the wall of the bed increases to a maximum at some intermediate value of voidage; as the voidage is increased further, the film heat transfer coefficient decreases. This maximum can be explained in terms of particle diffusion. As a bed is expanded, the frequency at which a particle contacts the wall and dissipates heat to the core of the bed increases as a result of increased particle diffusion. Thus, the heat transfer coefficient increases also. Eventually, however, the voidage is increased to such an extent that too few particles are available to contact the wall, and the heat transfer coefficient decreases. A knowledge of radial diffusion coefficients would be useful in describ-

ing this effect.

It is interesting to note that an optimum bed expansion at an intermediate value of voidage is also realized in the cleansing of particles of water filters by fluidization. When a bed is fluidized by water, the Reynolds number of the particles is much larger than those of the experiment reported here. At high Reynolds numbers, interparticle collisions are more apt to occur, and an experiment to investigate the effect of particle collisions on mixing would be an important contribution to the field of water filtration.

The observations made on the patterns of particle circulation that formed in the shallow cylindrical bed and also in the conical beds which were both fluidized with water are of engineering value as they suggest a means of increasing mixing rates in fluidized beds. Although nothing definitive was attempted concerning the underlying factors which cause these patterns to form, certain bed geometries were found in which very strong patterns developed. Particularly strong patterns with very large rates of particle recirculation, as well as a spouting effect at the top of the bed, were observed in the divergent conical beds. In addition, rather than suppressing the circulation, baffles amplified the spouting effect. Further experiments on patterns of particle circulation in beds of non-uniform cross section would certainly seem to be of significance to fluidized bed technology.

APPENDICES

APPENDIX A. EXPERIMENTAL APPARATUS AND PROCEDURE

A-1. Bead Tagging Procedure

Tagged Beads were colored brown by γ-rays from a Co^{60} source operated by the Laboratory for Nuclear Medicine of the University of California at Los Angeles. Exposure for a week at a dose rate of approximately one million Roentgens per minute darkened them sufficiently. Neither the size nor the density of the beads was altered.

Before the γ-radiation technique was discovered, a method that is used to color glass fibers commercially was considered and tried. It involves treatment with chemical solutions to form colored compounds in glass. Hyde[37] suggests solutions of specific chemicals in water to obtain various colors; the glass beads were treated with two of these.

1) Beads were placed in a 3 percent solution of ferrous sulfate at 85°C for a half hour and then dipped into a one percent solution of potassium ferrocyanide with hydrochloric acid. This colored them pale blue.

2) Beads were placed in a 5 percent solution of lead acetate at 85°C for forty-eight hours and then dipped into a dilute solution of ammonium sulfide. This gave them a pale brownish-gray color.

Although a coloration was produced in the beads, it did not render them sufficiently opaque for photographic purposes.

A-2. Determination of the Density and Viscosity of the Working Fluid

The density of the working fluid was determined at a selected temperature by use of a 25-ml. specific gravity bottle (pycnometer). The procedure involved measuring the mass of working fluid which filled the bottle at the selected temperature and determining, independently, the volume of the bottle at this temperature; the volume of the bottle was obtained by measuring the mass of distilled water which filled the bottle at the selected temperature and using the density of water at this temperature.

A Hoeppler falling-ball viscosimeter, model HV303, was utilized in the determination of the viscosity of the working fluid. The time was measured for a ball to travel 10 cm. in the tube containing working fluid at the selected temperature. This fall time, along with the specific gravity of the working fluid at the selected temperature, was used as data in an empirical formula, based on information from the manufacturer's calibration of the instrument, to compute the absolute viscosity.

A "Porta Temp," manufactured by the Precision Scientific Company, was used to control the temperature of a 10-gal. bath of water to maintain the temperature of the working fluid during the tests. Thermometer readings indicated that the temperature of the bath could be held constant to within .05^{o}C for at least 30 minutes, the duration of a test. The pycnometer, filled with fluid (working fluid or distilled water) at room temperature, was immersed in the bath (bath temperature higher than room temperature) for 30 minutes. The "Porta Temp" included a pump which supplied bath water to a

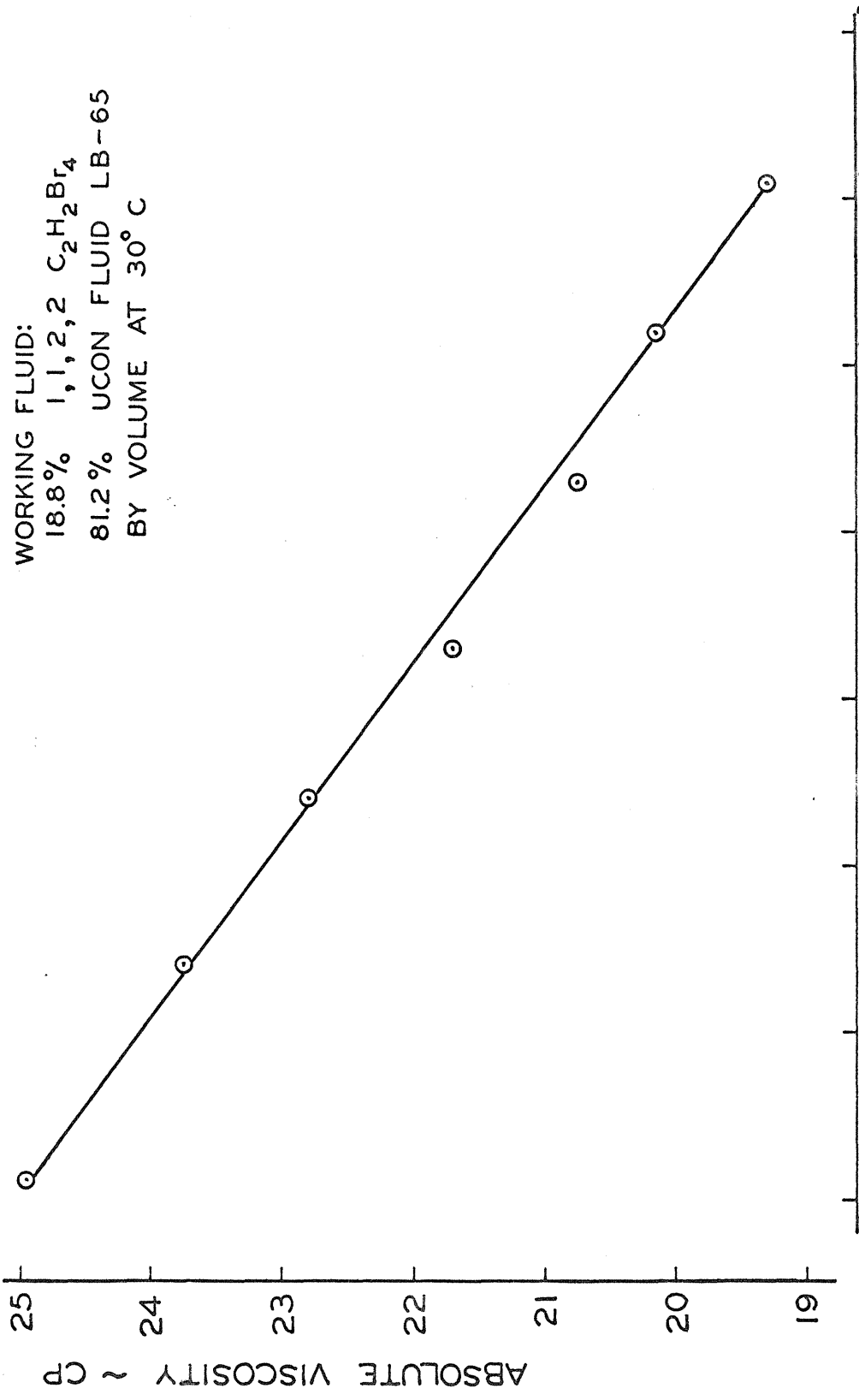

Figure 22. Viscosity of the Working Fluid at a Range of Temperatures.

jacket surrounding the viscosimeter. The thermocouple probe from the fluidized bed apparatus was mounted in the jacket and recorded the same temperature as that of the bath to within .1°C. For more information concerning specific details of the tests, refer to McLaughlin[38], who employed basically the same apparatus to determine the properties of glycerin.

The absolute viscosity and density of the working fluid were determined at temperatures ranging from 27°C to 33°C. A plot of absolute viscosity as a function of temperature is presented in Figure 22; at 30°C, a density of 1.3296 g./cc. was found.

A-3. Corrosive Effects of Acetylene Tetrabromide

Acetylene tetrabromide has a corrosive effect on most common materials. In the presence of even a small amount of water, the acetylene tetrabromide hydrolyzes to form some HBr, and the rate of corrosion is amplified. In order to prevent the deterioration of the apparatus and to protect the fluid from contamination and discoloration, the corrosive effect was retarded by using relatively inert materials and by keeping the system dry.

Based upon preliminary investigations, glass, teflon, 18-8 stainless steel, and brass were employed in the construction of the apparatus. After remaining in acetylene tetrabromide for a month, test samples of these four materials showed no signs of corrosion, nor did the acetylene tetrabromide discolor. In support of this evidence, it was reported that 18-8 stainless steel rates very high in the resistance of corrosion by halogenated hydrocarbons of which acetylene tetrabromide is one[39]. Organic bromides corrode brasses by de-

zincification, somewhat, but only in the presence of water[40]. Also tested were steel, aluminum, copper, neophrene, and polyethylene; each was attacked severely by the acetylene tetrabromide.

The working fluid remained in the apparatus for eight months while experiments were in progress. During this time, no discoloration from corrosive effects was observed. Although a very slight cloudiness formed periodically after a month, this was suspected not to be the result of corrosive effects but rather fine debris remaining in the system from the pump accident, for the clarity of the fluid was restored with use of the filter.

Samples of materials used in the construction of the apparatus were placed in covered beakers containing the working fluid for the duration of the experiment. The beakers were only half-filled, and in contrast to the apparatus, precautions were not taken to remove the remaining air before covering. The corrosive effects of the acetylene tetrabromide were in evidence as follows.

1) 304 stainless steel (sample of 1-inch tube, .035 in. wall thickness): results were negative for the first six months. However, in the last two months, the fluid became a pale orange and then turned to a brilliant orange. The surface of the steel itself took on a sheen.

2) Yellow brass (sample of .004-in. shim stock): within a month, the fluid had discolored a faint pale green, which deepened, somewhat, over the 8-month duration. Although the surface of the brass sample became etched, no appreciable change in its thickness was noted.

3) Steel (sample of the drum, 18 ga. disc, one side lined with baked epoxy): within a few days, the steel began to rust, discoloring the fluid burgundy. After about three months, the steel had disintegrated, leaving the lining intact.

A-4. Pump Accident

During the time that the apparatus was being tested, before actual experiments were run, an overheating of the pump shaft resulted in the impeller contacting the impeller housing; the pump stuffing, solid teflon discs, had inhibited proper lubrication of the pump shaft. The condition was corrected by replacing this stuffing with teflon braid, manufactured by Garlok, Inc. As a precaution, a thermocouple was installed to monitor shaft temperature to a Honeywell "Pyr O Vane" control unit, which was set to trigger a bell if the shaft temperature reached an unsafe limit.

Due to the intense heat released from the abrasive action of the impeller, the entire working fluid acquired a slight gold coloration; the clarity, however, was not affected. Fine stainless-steel chips introduced into the system by rubbing of the impeller were removed by the filter.

A-5. Orifice Meter Calibration

Coefficients were determined experimentally for each orifice plate by measuring, directly, mass flow rates of working fluid through the orifice meter. The flow circuit was modified to enable the working fluid to empty into a weigh tank after passing through the orifice meter. Instead of entering the bed, flow leaving the orifice

meter was routed into the filter line which was connected to a T-shaped section of pipe, one leg of which extended into and close to the bottom of the drum and the other into the weigh tank. Valves placed in each leg could be adjusted to direct the flow into either the drum or the weigh tank. The flow resistance in each leg was small and equal by employing large diameter pipes of equal length. The weigh tank with 20 gal. capacity was placed on a Howe scale of beam balance design.

After the flow had reached an equilibrium, it was rechanneled into the weigh tank. Time was allowed for the redirected flow to stabilize by allowing thirty pounds of fluid to collect. The mass flow rate was determined by measuring the time for an additional eighty pounds to collect. Three manometer readings were recorded -- one before the flow was rechanneled, a second after thirty pounds had collected, and a final one after the additional eighty pounds had collected--and were averaged to correct for small variations in flow rate as the drum emptied. The temperature of the fluid in the weigh tank was noted. Fluid was then returned to the system and circulated for 30 minutes while a new flow rate stabilized and air bubbles worked their way out of the fluid.

The orifice coefficient, K, is defined by

$$K = 10.03\, \dot{m}/d^2(\rho_f h_w)^{\frac{1}{2}} ,$$

where $\dot{m}$ is the mass flow rate in lb./sec., h_w is the pressure differential in inches of water, ρ_f is the density of the working fluid in lb./cu. ft., and d is the orifice diameter in inches. Coefficients were determined for each orifice plate at Reynolds numbers R_d (at

orifice throat), ranging from approximately 1000 to 3000 applicable in the determination of the mass flow rates in the fluidized bed experiments. The results, presented in Figure 23, agree fairly well with those reported by Ambrosius and Spink[41]. Differences arise, it is believed, because the flows in the regime studied experimentally (transition between laminar and turbulent) are particularly sensitive to inlet and outlet pipe geometry; Ambrosius and Spink employed very long, straight lengths of inlet and outlet pipes, while the present author did not, due to practical considerations.

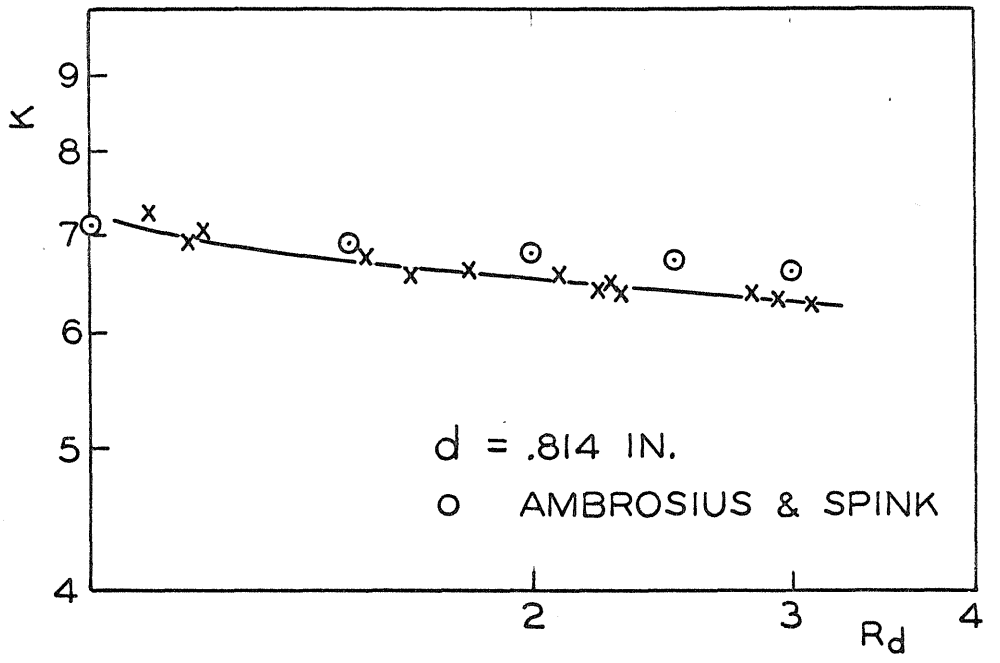

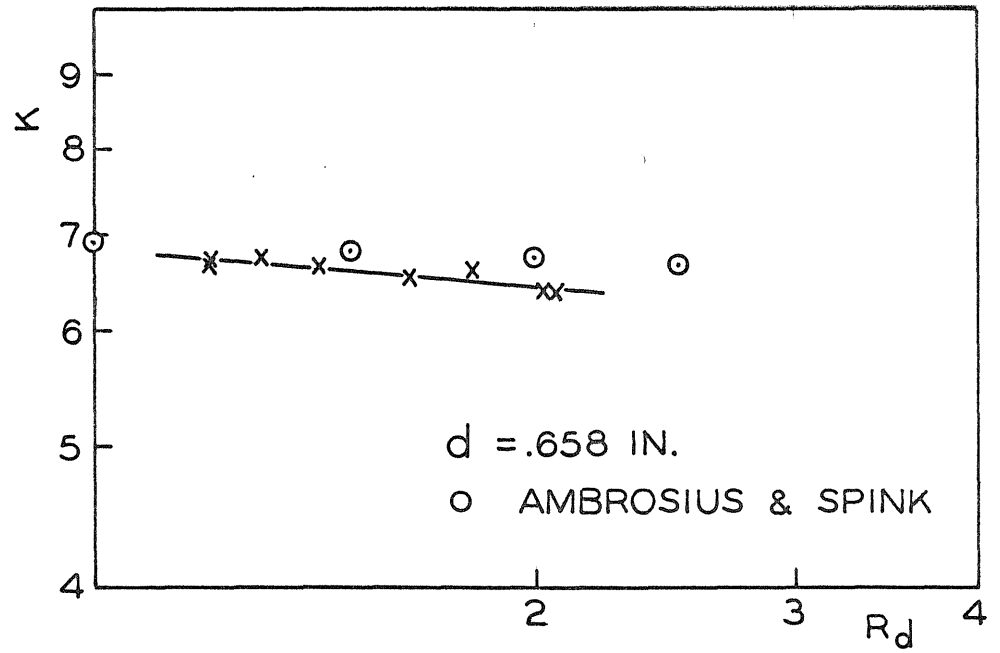

Figure 23. Orifice Coefficient, K, as a Function of Reynolds Number, R_d, in Tube of 1.94-Inch I. D.

APPENDIX B. REDUCTION OF POSITION DATA

B-1. Vertical Position

Figure 24 outlines, schematically, the equipment utilized to record raw position data from the film onto IBM cards. A frame of film was projected on the screen of a microfilm reader. A cursor, movable over the face of the screen, actuated a potentiometer to produce a voltage signal which varied linearly with the location of the cursor on the screen. A DVM converted this voltage signal to a digital signal which was directed to a key punch machine.

A typical frame of film is shown in Figure 25; on the left is a front view of the test section containing tagged beads, and on the right is the mirror view. What was in reality a three-dimensional space is now a two-dimensional image, distorted by the perspective effect of the camera and the refractive effect of the glass column. In locating the real vertical position of a bead in the column, the distortive effects were negligible, due in particular to the use of a camera lens of long focal length. The maximum apparent difference in height between two beads in a horizontal plane normal to the column ranges from zero at the center to 0.050 inches at the ends of the test section, due to perspective distortion; the refractive effect of the glass column reduces this by about 30 percent. The maximum distortion is of the same order of magnitude as the random error involved in locating a particle on a frame of film using the cursor. In addition, for the step times analyzed in a given experiment, a tagged bead traverses such short lengths that merely a small fraction of the maximum distortion affects a given step length calculation, rendering

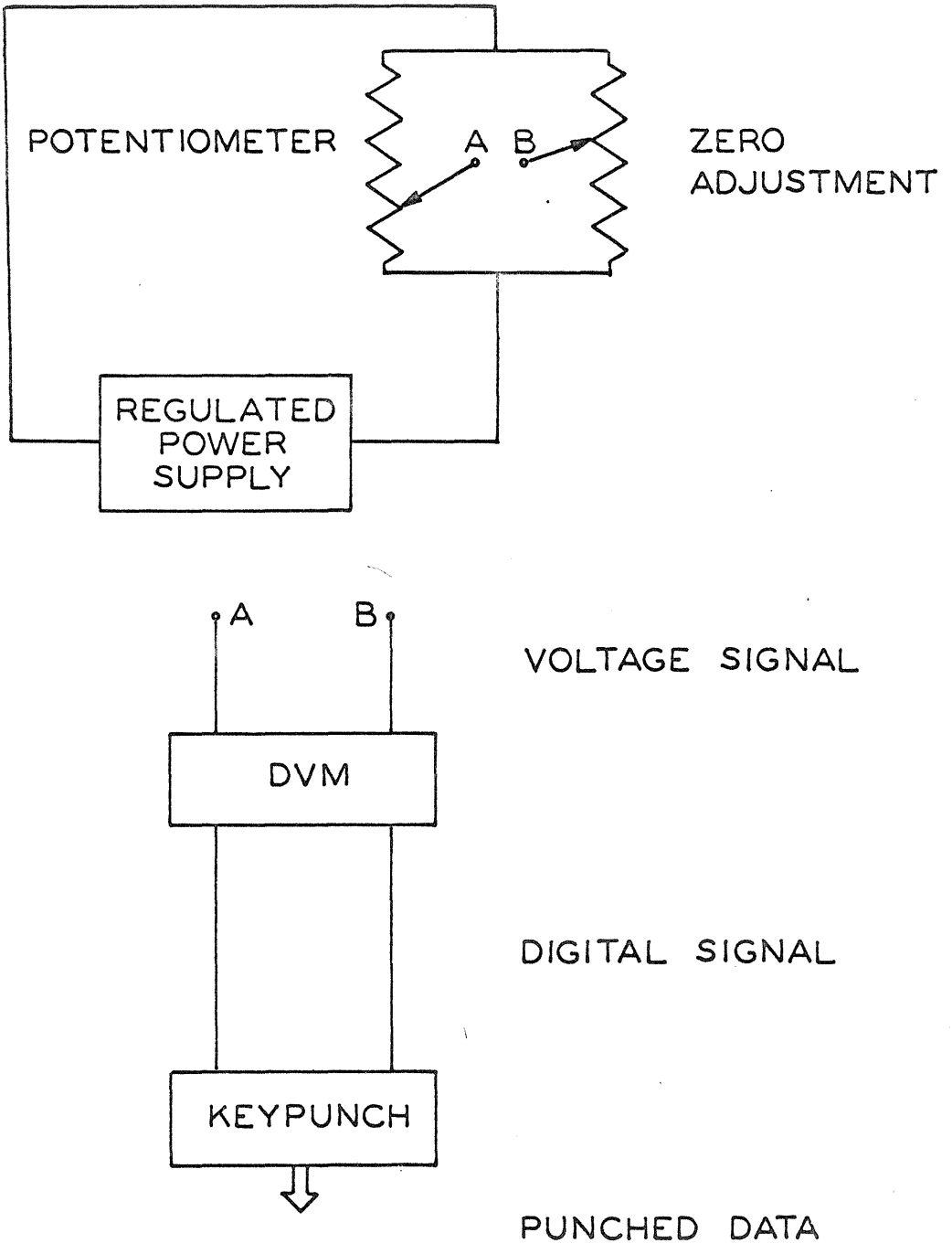

Figure 24. Schematic Diagram of Data Processing Equipment for Raw Film Positions.

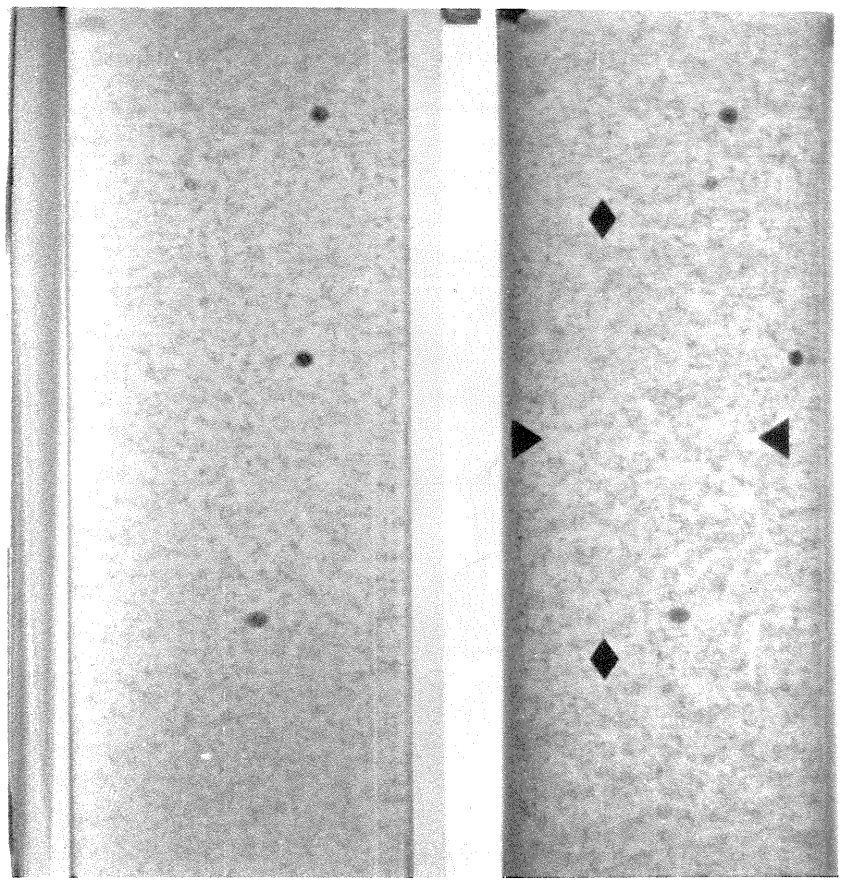

Figure 25. Typical Frame of Film with Front View on the Left and Mirror View on the Right.

distortive errors negligible.

A frame projected onto the screen of the microfilm reader was about 58 percent life size. The precise scale, SC, was determined as the ratio of the real distance between the vertical mirror marks to the projected distance in DVM units*. The vertical position of a tagged bead was determined relative to the horizontal mirror marks. Since distortion was negligible, the real vertical position could be scaled directly with no other corrections necessary.

Four readings, depicted schematically in Figure 26, were recorded on an IBM card to determine the vertical position of a tagged bead on each frame in a given run; the run number and the number in the sequence were also recorded. ZREF is the position of the horizontal mirror marks; ZPB and ZPT are the positions of the bottom and top edges, respectively, of a bead in the front view; ZMT is the position of the top edge of a bead in the mirror view. If the bead was at a blind spot (a blind spot is defined in Appendix B-2) in the front view, ZPB and ZPT were set at ZMT; if it was at a blind spot in the mirror view, ZMT was set at ZPT. With the bead visible in the front view, the vertical position, Z, of its center was computed using the formula

$$Z = \left(\tfrac{1}{2}(ZPT-ZPB) - ZREF\right)(SC) \ .$$

If the bead was at a blind spot in the front view, its vertical position was determined by use of the formula

$$Z = \tfrac{1}{2}(ZMT-ZREF)(SC)-\tfrac{1}{2}D_p \ ,$$

*The sharp image of the mirror marks, filmed with filters removed and aperture stopped down, was used for this purpose.

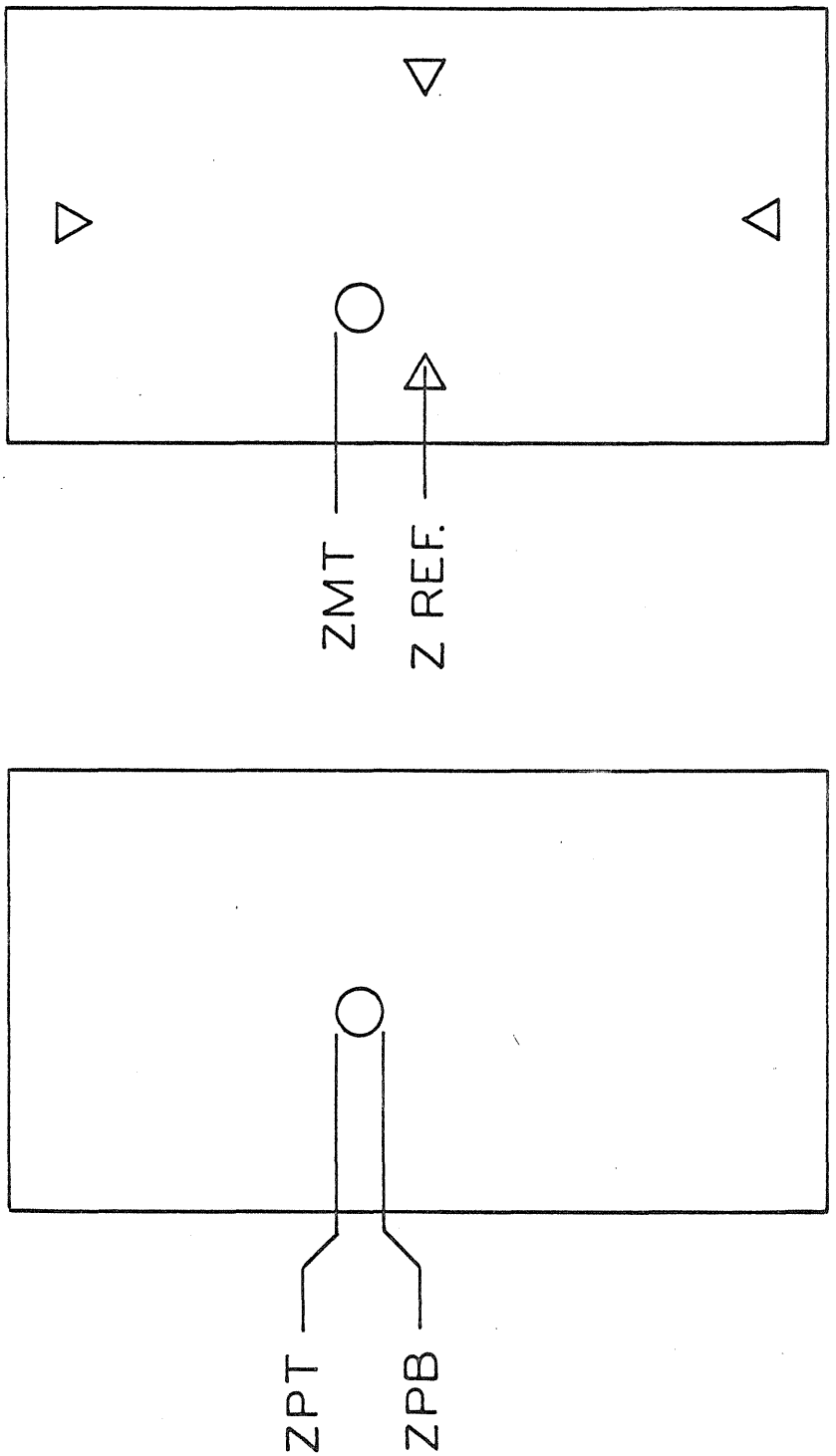

Figure 26. Readings on a Frame of Film for Vertical Position.

where D_p is the diameter of a bead. Computer routine CORPO was used for these calculations.

The resolution of a bead was not the same on every frame of film; it depended on the depth of a bead within the column. To account for these variations, the position of a bead in the front view was based on both ZPT and ZPB. A random error was introduced in the actual positioning of the cursor. From many readings of ZPT and ZPB on successive frames, it was possible to compute the variance of the diameter of a bead which was found to be 0.02 in., approximately. This is a conservative estimate of the random error in positioning the cursor to obtain ZPT and ZPB, for it includes the effect of the varying resolution of a bead. Assuming the variance of the reading, ZREF, to be about half the variance of the bead diameter, or 0.01 in., an estimate of the total variance of the vertical position measurement, Z, is 0.03 in., approximately. A confirmation that the total variance is in fact 0.03 in. was made by re-reading about 100 frames in run 001 and comparing differences. Since the variance of Z is approximately 0.03 in., the variance of a step length measurement, the difference between two successive positions is probably about 0.06 in., conservatively.

B-2. Polar Position

When the colored bead entered certain regions of the fluidizing column, it vanished from either the front view or the mirror view, and in one case from both views. These regions have been referred to as "blind spots." Blind spot regions exist due to the lens effect of the column and the geometry of the photographic arrangement; all

rays of light emanating from a bead located in one of these regions with respect to either the front or mirror view are totally reflected at the outher wall of the column.

As in the reduction of vertical positions, perspective distortion is assumed negligible, forcing all rays of light emanating from the test section to be perpendicular to the focal plane of the camera. Neglecting perspective distortion in the reduction of polar positions introduces the same small error that was introduced in the reduction of vertical positions. However, in contrast to the vertical case, the refractive distortion in the polar case due to the column is significant.

By tracing rays originating within the column, a blind spot region can be constructed as shown in Figure 27. To simplify the construction, a bead was assumed to be a point. Rays emanating from within the column obey the law of refraction as they pass from the more optically dense column (refractive index 1.49) into the surrounding air where they emerge parallel to one another. Rays originating from the region in the upper left portion of the column cannot satisfy these conditions; they are totally reflected by the wall of the column, creating a blind spot region. In constructing the figure, Young's graphical technique[42] was employed. Figure 28 shows blind spot regions in each quadrant. Quadrant I has a blind spot region with respect to the front view, Quadrant III with respect to the mirror view, and Quadrant II with respect to both views.

Another problem was encountered in reducing the polar position of a colored bead; when it was in certain regions of the column,

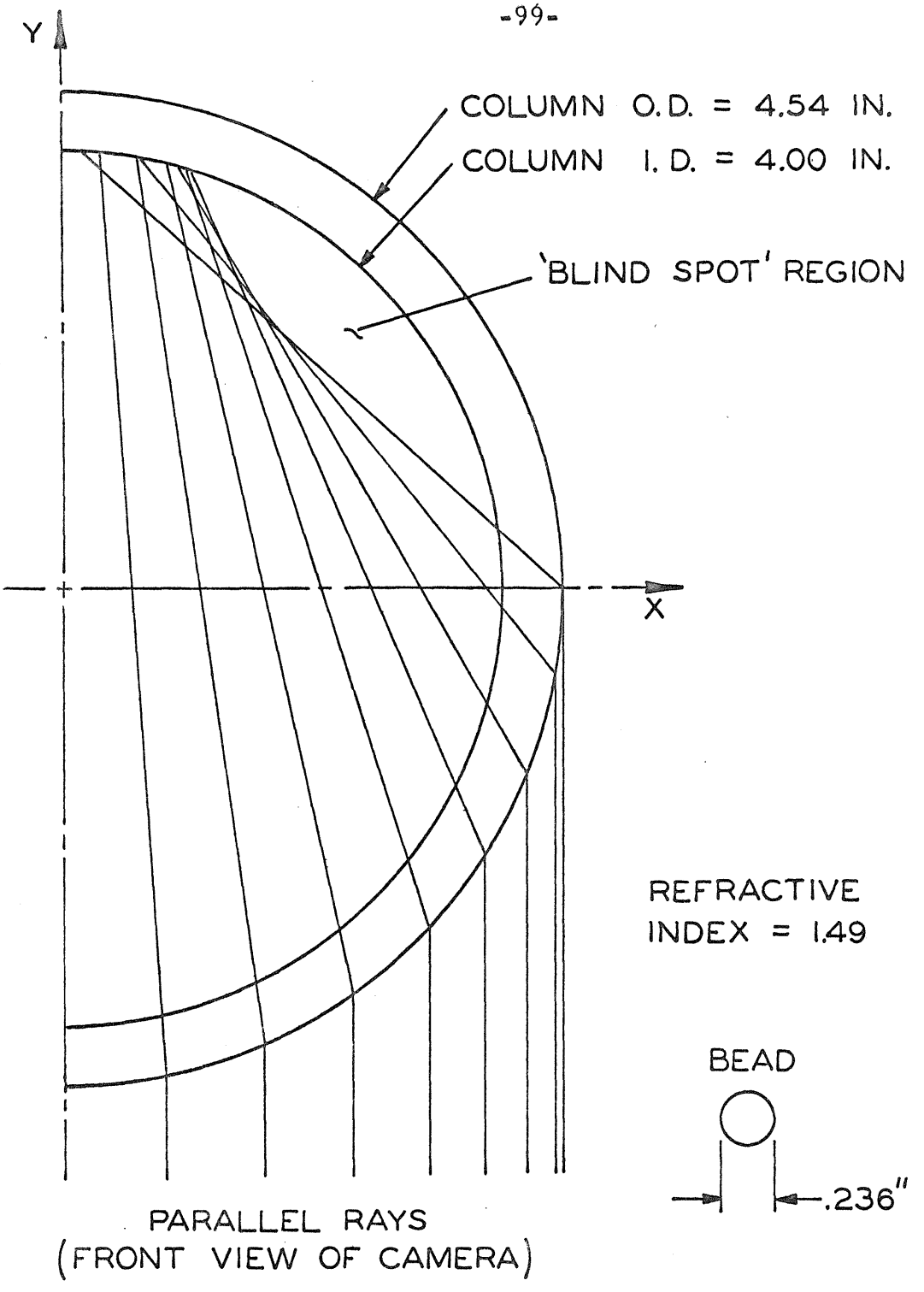

Figure 27. Cross-Sectional View of Column Illustrating Blind Spot Region in Quadrant I. Drawn to Scale.

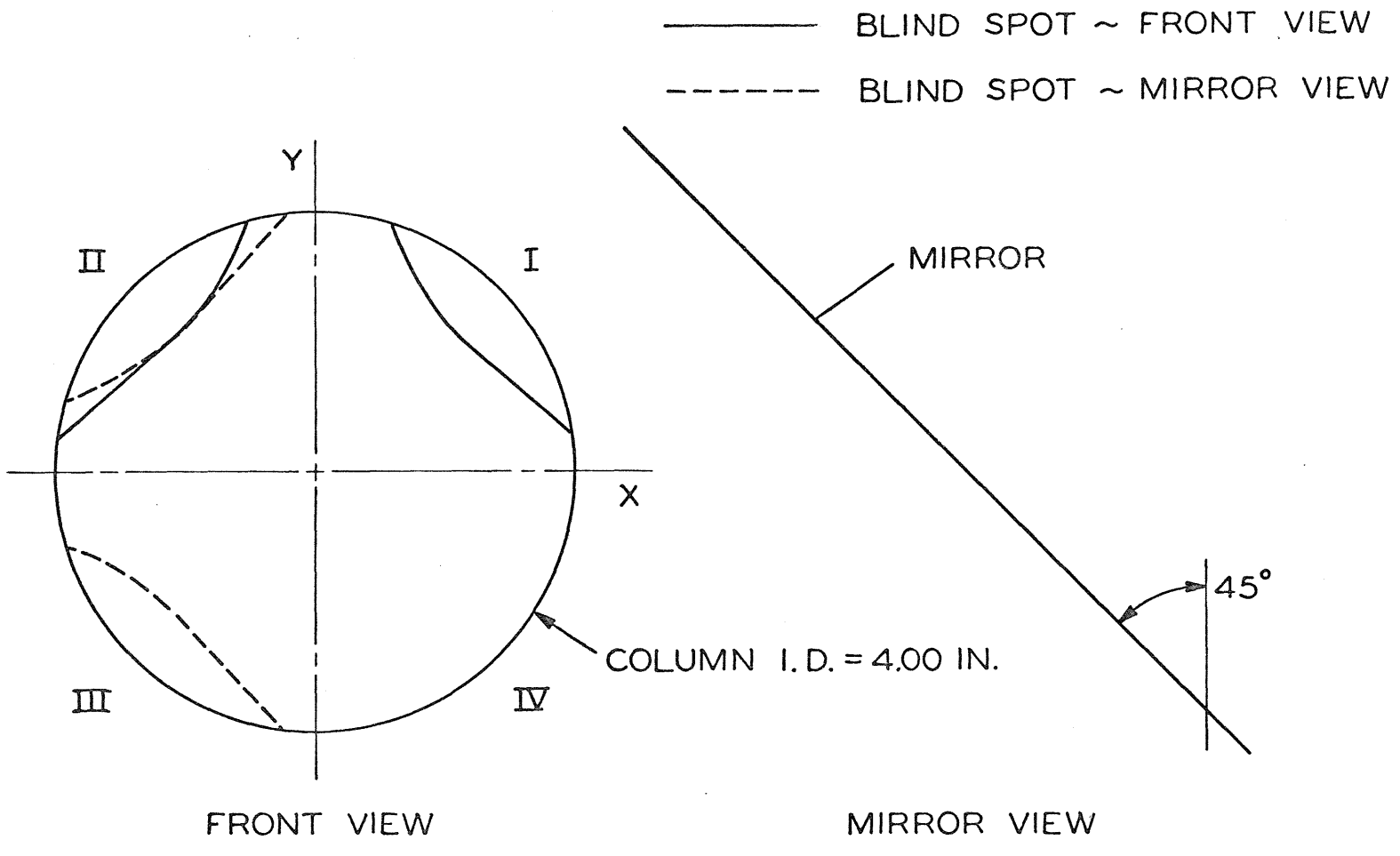

Figure 28. Blind Spot Regions in Each Quadrant. Drawn to Scale.

its shape was distorted on film. For instance, considering the region of Figure 27 where rays overlap, the filmed image of a bead located in that region was very elongated. On the other hand, a very contracted image was noted when a bead was located in the lower left portion of the column because rays originating in that region become crowded after being refracted at the wall of the column, as shown in the figure. The effect of these distortions was to reduce the accuracy with which polar positions were determined. However, since only the position of the center of a bead was needed, the average effect of these distortions on the accuracy of a measurement was not excessive.

In determining the polar position of a bead, the location of its center in both the front and mirror views was obtained directly from film data displayed on the screen of the microfilm reader. Five readings, schematically shown in Figure 29, were recorded on an IBM card; the run number and the number in the sequence were also recorded on the card. RREF is the position of the vertical mirror marks; A_1 and A_2 are the positions of the edges of a bead in the front view; B_1 and B_2 are the positions of the edges of a bead in the mirror view. If the bead was located in a blind spot in either the front or mirror view, both readings of the edges of the bead were set at a position outside the appropriate edge of the column's image in that view; this enabled location of the appropriate quadrant of the column in which the bead had vanished. Also noted, but not recorded on each IBM card as they are constants, were A, the projected distance of the centerline of the column in the front view from the vertical

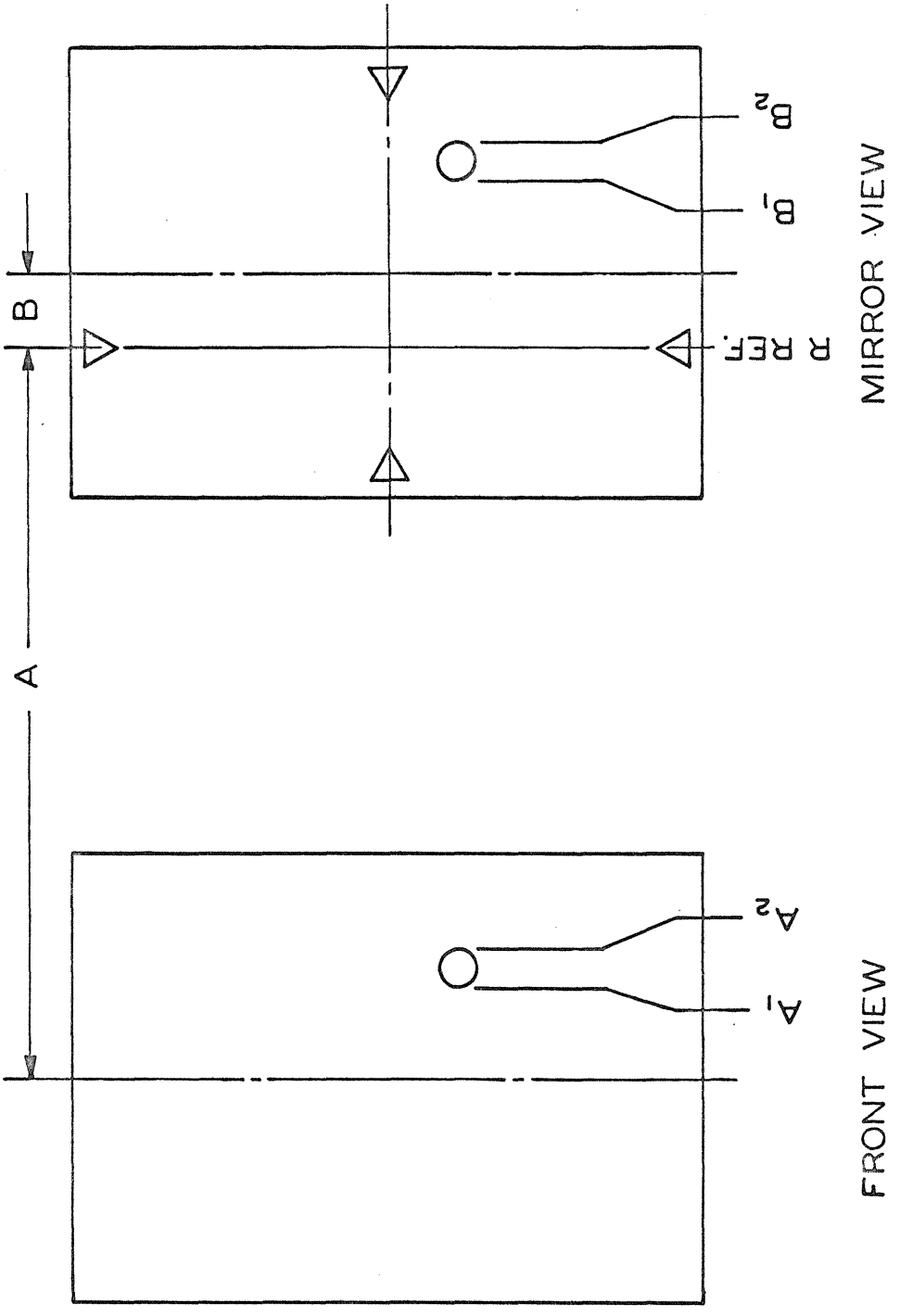

Figure 29. Readings on a Frame of Film for Polar Position.

mirror marks, and B, the projected distance of the centerline of the column in the mirror view from the vertical mirror marks. With the bead visible in the front view, the position of its center relative to the centerline of the column in the front view was computed using the formula

$$x_1 = [RREF + A - \tfrac{1}{2}(A_1+A_2)](SC),$$

where SC is the scale factor between real distances and projected distances. Similarly, with the bead visible in the mirror view, the position of its center relative to the centerline of the column in the mirror view was evaluated by use of the formula

$$\xi_2 = [RREF + B - \tfrac{1}{2}(B_1+B_2)](SC) .$$

Note that x_1 and ξ_2 are not the real positions of the center of a bead within the column in each view, but merely the positions of the images of the bead formed at the boundary between the wall of the column and the surrounding air.

Refractive corrections were applied to determine the real polar position of a colored bead within the column. The position x_1 of the center of the bead in the front view defines a ray which intersects the wall of the column a distance x_1 from the y-axis of the x-y coordinate system shown in Figure 30. This ray, as well as the y-axis, are perpendicular to the focal plane of the camera. Similarly, the position ξ_2 of the center of the bead in the mirror view defines a ray which intersects the wall of the column a distance ξ_2 from the η-axis of the ξ-η coordinates of the figure. The inclination, ϕ, of the ξ-η coordinates with respect to the x-y coordinates is related to the

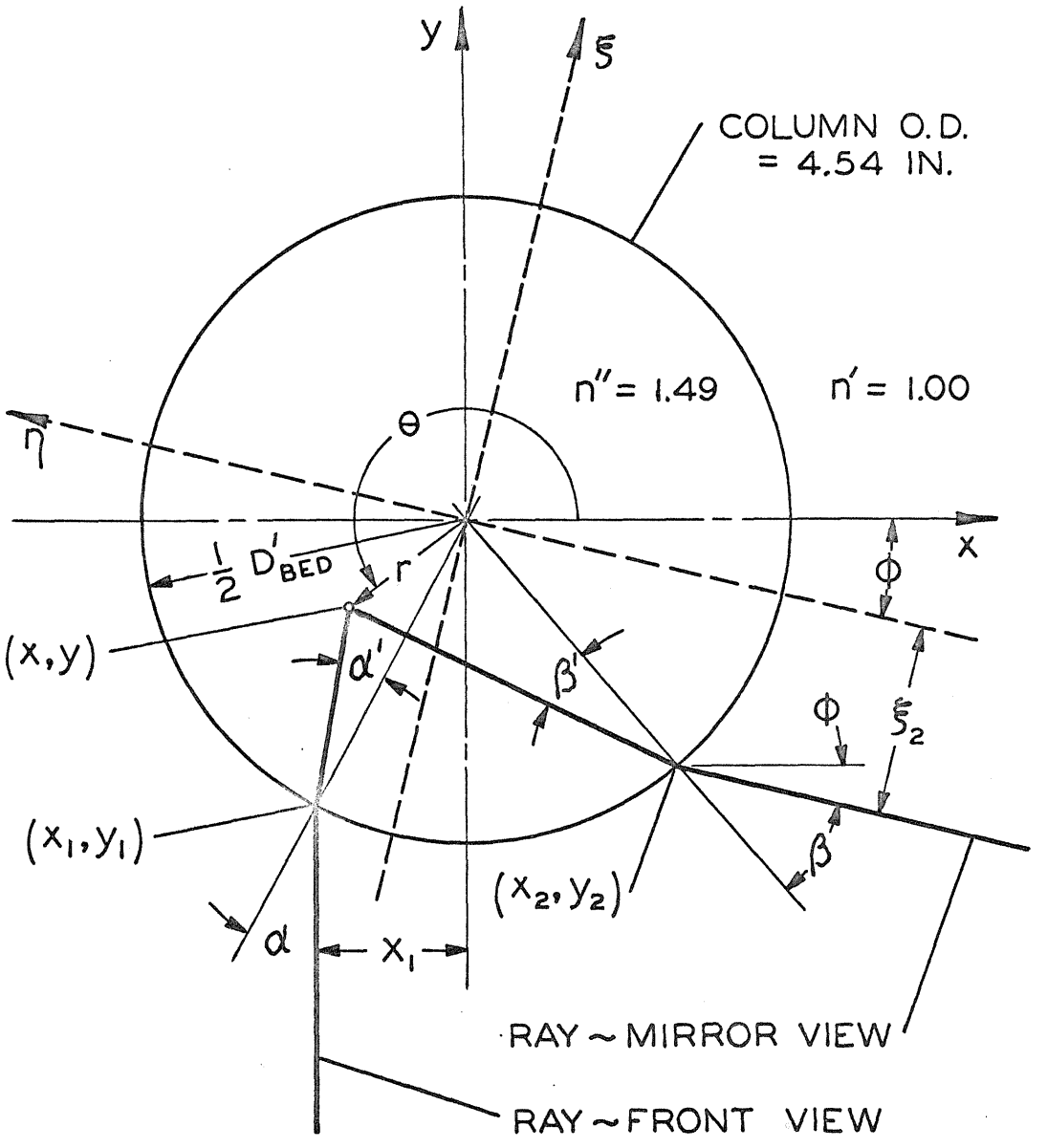

Figure 30. Refracted Rays of a Bead in the Column in the Determination of Polar Position.

angle Φ,* formed by the mirror and the focal plane of the camera by the formula

$$\phi = 2\Phi - 90^{o} \quad .$$

Each ray is refracted at the boundary of the column and the surrounding air; they intersect at a point (x, y) inside the column, the real position of the center of the bead. Considering the ray of the front view, it intersects the wall of the column at the point (x_1, y_1), with y_1 given by

$$y_1 = -\sqrt{\frac{1}{4} D'^{2}_{bed} + x_1^2} \quad ,$$

where D'_{bed} is the outside diameter of the column. The law of refraction relates the angle, α', of the ray inside the column relative to the normal at the wall to the angle, α, of the same ray outside the column relative to the normal at the wall by

$$n'' \sin \alpha = n' \sin \alpha' \quad ,$$

where n'' and n' are the refractive indices of the fluid - particle system and the surrounding air, respectively, and

$$\alpha = \sin^{-1}(2x_1 / D'_{bed}) \quad .$$

The path of this ray inside the column is given by

$$y = y_1 + m_1(x - x_1) \quad ,$$

where

$$m_1 = \cot(\alpha' - \alpha) \quad .$$

Similarly, the ray of the mirror view intersects the wall of the column at the point (ξ_2, η_2), with η_2 given by

---

* Φ was set very close to 45^{o}. The exact value was determined by comparing the real distance between the horizontal mirror marks to the distance between the filmed images of the marks.

$$\eta_2 = -\sqrt{\frac{1}{4} D'^2_{bed} + \xi_2^2} \quad .$$

The angle β' of this ray inside the column relative to the normal at the wall, and the angle β of this same ray outside the column relative to the normal at the wall are related by the law of refraction, namely,

$$n'' \sin \beta = n' \sin \beta' \quad ,$$

where

$$\beta = -\sin^{-1}(2\xi_2 / D'_{bed}) \quad .$$

The equations which transform the ξ-η coordinates into x-y coordinates are

$$x = -\eta \cos \phi + \xi \sin \phi \quad ,$$

$$y = \eta \sin \phi + \xi \cos \phi \quad .$$

The path of the ray of the mirror view inside the column is given by

$$y = y_2 + m_2(x - x_2) \quad ,$$

where

$$m_2 = \tan(\beta - \beta' - \phi) \quad .$$

Two equations describing the paths of the rays inside the column are solved simultaneously to determine the point of intersection; the position of the center of the bead is given by

$$x = \frac{(y_1 - m_1 x_1) - (y_2 - m_2 x_2)}{m_2 - m_1} \quad ,$$

$$y = \frac{m_1(y_1 - m_1 x_1) - m_1(y_2 - m_2 x_2)}{m_2 - m_1} \quad .$$

The corresponding polar position, (r, θ), is given by

$$r = \sqrt{x^2 + y^2} \quad ,$$

$$\theta = \tan^{-1}(y/x) \quad .$$

A computer routine, CORPO, was used for these calculations.

B-3. Coding of Runs

Table 4 lists the run number, the basic frame rate, the number of positions recorded (M^R), and the first data frame for each run in each experiment. A three digit number was used to code a run and was punched on each data card. The first two digits represent the number of the spool of film from which the raw data for the run were obtained. This spool number is inscribed on the film at the beginning of a roll. The third digit represents the run number on a particular spool. On each spool, frames were identified by consecutive numbers marked at either the short or the long basic frame rate. The term, first data frame, in Table 4 refers to one of these. To determine which bead on the first data frame belongs to the run in question, the raw data on an IBM card for the run and frame were utilized.

TABLE 4. Runs for Each Experiment

RUN NUMBER	BASIC FRAME RATE	FIRST DATA FRAME	M^R
	a) C_o = 0.120		
151	5	230	240
152	5	494	150
153	5	500	128
154	5	237	121
161	10	200	115
162	10	14	71
163	10	472	55
171	10	20	117
172	10	219	86
181	10	72	198

RUN NUMBER	BASIC FRAME RATE	FIRST DATA FRAME	M^R
		b) $C_o = 0.203$	
211	5	43	281
212	5	364	205
221	5	360	141
226	10	27	127
231	10	9	113
232	10	89	170
241	10	171	116
251	10	27	69
252	10	216	82
		c) $C_o = 0.286$	
001 (7)*	4	--**	249
002 (7)	4	--	105
003 (7)	4	--	23
004 (7)	4	--	157
005 (7)	4	--	67
011 (6)	18	--	17
012 (6)	18	--	17
013 (6)	18	--	93
014 (6)	18	--	31

*The coding rule does not apply to this experiment. The number in parentheses designates the spool number.

**Consecutive frames were not numbered on film; the run number is marked on the first data frame.

APPENDIX C. MEAN SQUARE STEP LENGTH DATA

TABLE 5. Mean Square Step Length Data of Each Experiment

a) $C_o = 0.120$

k	N(k)	τ_k (sec.)	$\overline{\lambda^2(k)}$ (in.^{2})
1	635	.208	.0825
2	316	.417	.250
3	210	.625	.441
4	157	.833	.624
5	125	1.042	.858

T_1 = 5 frames (Runs 151 - 154)

k	N(k)	τ_k	$\overline{\lambda^2(k)}$
1	952	.417	.247
2	474	.833	.618
3	314	1.250	.970
4	234	1.657	1.31
5	186	2.083	1.78
6	155	2.500	2.22
7	133	2.917	2.50
8	113	3.333	3.19

T_2 = 10 frames (Runs 151 - 181)

b) $C_o = 0.203$

k	N(k)	τ_k	$\overline{\lambda^2(k)}$
1	624	.208	.0827
2	312	.417	.255
3	207	.625	.469

k	N(k)	τ_k (sec.)	$\overline{\lambda^2(k)}$ (in.^{2})
4	156	.833	.676
5	124	1.042	.859

T_1 = 5 frames (Runs 211 - 221)

k	N(k)	τ_k	$\overline{\lambda^2(k)}$
1	983	.417	.213
2	490	.833	.514
3	325	1.250	.813
4	243	1.667	1.11
5	194	2.083	1.42
6	161	2.500	1.62
7	138	2.917	1.90
8	119	3.333	2.36

T_2 = 10 frames (Runs 211 - 252)

c) $C_o = 0.286$

k	N(k)	τ_k	$\overline{\lambda^2(k)}$
1	596	.167	.0446
2	298	.333	.117
3	197	.500	.224
4	148	.667	.278
5	117	.833	.437

T_1 = 4 frames (Runs 001 - 005)

k	N(k)	τ_k	$\overline{\lambda^2(k)}$
1	462	.750	.489
2	231	1.500	1.01
3	151	2.250	1.42
4	113	3.000	1.94

T_2 = 18 frames (Runs 011 - 022)

d) $C_o = 0.365$

k	N(k)	τ_k (sec.)	$\overline{\lambda^2(k)}$ (in.^{2})
1	1138	.417	.132
2	566	.833	.348
3	376	1.250	.536
4	281	1.667	.714
5	223	2.083	.972
6	186	2.500	1.09
7	159	2.917	1.24
8	138	3.333	1.39
9	123	3.750	1.47
10	108	4.167	1.95

T_1 = 10 frames (Runs 101 - 131)

APPENDIX D. CONFIDENCE LIMITS ON MEAN SQUARE STEP LENGTHS

For a group of size N(k), let $\chi^2_{a/2}$ and $\chi^2_{1-a/2}$ be the 100 /2 and the 100(1 - /2) percentiles, respectively, of the chi-square distribution with N(k)-1 degrees of freedom. Since the step lengths $\lambda_i(k)$ are distributed normally,

$$\text{Prob.} \left\{ \frac{[N(k)-1]\,\overline{\lambda^2(k)}}{\chi^2_{1-a/2}} < \overline{\lambda^2_\infty(k)} < \frac{[N(k)-1]\,\overline{\lambda^2(k)}}{\chi^2_{a/2}} \right\} = 1-a \,,$$

where

$$\chi^2_b = \tfrac{1}{2}\left(\mu_b + (2N(k)-3)^{\frac{1}{2}}\right)^2 .$$

$\overline{\lambda^2(k)}$ is the experimentally determined mean square step length based on a group of size N(k) from a population with a mean square step length, $\overline{\lambda^2_\infty(k)}$. μ_b is the 100 b percentile of the standard normal distribution. The theory upon which these results are based is discussed in reference 43.

Confidence limits at the 90 percent level on the mean square step lengths in the experiment $C_o = 0.203$ are listed in Table 6.

TABLE 6. Confidence Limits on the Mean Square Step Lengths in the Experiment $C_o = 0.203$

k	N(k)	$\overline{\lambda^2(k)}$ (sq. in.)	$\frac{[N(k)-1]\overline{\lambda^2(k)}}{\chi^2_{1-a/2}}$ (sq. in.)	$\frac{[N(k)-1]\overline{\lambda^2(k)}}{\chi^2_{a/2}}$ (sq. in.)
1	624	.0827	.0752	.0903
2	312	.255	.226	.292
3	207	.469	.402	.551
4	156	.676	.569	.818
5	124	.859	.681	1.08

a) Basic frame rate, T_1, of 5 frames (0.208 sec.)

k	N(k)	$\overline{\lambda^2(k)}$ (sq. in.)	$\frac{[N(k)-1]\overline{\lambda^2(k)}}{\chi^2_{1-a/2}}$ (sq. in.)	$\frac{[N(k)-1]\overline{\lambda^2(k)}}{\chi^2_{a/2}}$ (sq. in.)
1	983	.213	.199	.229
2	490	.514	.467	.573
3	325	.813	.722	.929
4	243	1.11	.967	1.29
5	194	1.42	1.22	1.69
6	161	1.62	1.36	1.95
7	138	1.90	1.59	2.34
8	119	2.36	1.95	2.96

b) Basic frame rate, T_2, of 10 frames (0.417 sec.)

NOMENCLATURE

a	confidence coefficient
A	projected distance of the centerline of the column in the front view from the vertical mirror marks, DVM units
A_1, A_2	projected horizontal positions of edges of bead in front view, DVM units
A'	annulus area per quadrant, $ft.^2$
ATB	1, 1, 2, 2 tetrabromoethane
B	projected distance of the centerline of the column in the mirror view from the vertical mirror marks, DVM units
B_1, B_2	projected horizontal positions of edges of bead in mirror view, DVM units
C(z, t)	local particle concentration
$\tilde{C}(z, t)$	small disturbance in particle concentration
C_o	average particle concentration
d	orifice diameter, inches
D_{bed}	column inside diameter, feet
D'_{bed}	column outside diameter, inches
D_p	bead diameter, inches
D_z	particle diffusion coefficient for vertical movement, $ft.^2/sec.$
f	friction factor
F(C)	slip velocity, $U_f - U_p$, ft. sec.
h_w	pressure differential across orifice, inches of H_2O
k	time interval index of a group of step lengths
K	orifice coefficient
$\tilde{K}(\tau)$	timewise correlation coefficient, $e^{-\tau/\tau^*}$
$K_j(k)$	timewise correlation coefficient at a time $j\tau_k$ seconds and formed of steps of time index k

$\dot{m}$	mass flow rate through orifice, lb./sec.
m_1	slope of ray of front view inside the column
m_2	slope of ray of mirror view inside the column
M^R	number of positions in a run
n	exponent of Richardson-Zaki[10] superficial velocity function
n'	refractive index of air
n''	refractive index of fluid - particle system
N(k)	number of step lengths with time index k, all runs combined
$N^R(k)$	number of step lengths in a run with time index k
O	on the order of
r	radial coordinate on the cross section of the column
R	Reynolds number based on D_{bed} and U
R_d	Reynolds number at orifice throat based on d
R_t	Reynolds number based on D_p and U_t
R_o	Reynolds number based on D_{bed} and U_o
RREF	projected horizontal position of vertical mirror marks, DVM units
SC	scale, real-to-projected distance, inches/DVM units
t	time, seconds
T_1	short frame rate, frames or seconds
T_2	long frame rate, frames or seconds
U	fluid velocity in a pipe, ft./sec.
$U_f(z, t)$	local fluid velocity, ft./sec.
$U_p(z, t)$	local particle velocity, ft./sec.
U_t	free-fall velocity of particle in quiescent fluid, ft./sec.

U_o	superficial fluid velocity, ft./sec.
U^*	turbulent friction velocity in a pipe, ft./sec.
V(C)	kinematic wave speed, ft./sec.
V_o	kinematic wave speed of small disturbance in particle concentration, ft./sec.
x	abscissa of (x, y) coordinates on cross section of column, inches
x_1	abscissa of (x, y) coordinates of point of intersection of ray of front view with air-column boundary, inches
x_2	abscissa of (x, y) coordinates of point of intersection of ray of mirror view with air-column boundary, inches
y	ordinate of (x, y) coordinates on cross section of column, inches
y_1	ordinate of (x, y) coordinates of point of intersection of ray of front view with air-column boundary, inches
y_2	ordinate of (x, y) coordinates of point of intersection of ray of mirror view with air-column boundary, inches
z	vertical position above lower support of bed, feet
Z	vertical position of bead relative to horizontal mirror marks, inches
Z_i^R	i^{th} vertical position in a run, inches
ZMT	projected vertical position of top edge of bead in mirror view, DVM units
ZPB	projected vertical position of bottom edge of bead in front view, DVM units
ZPT	projected vertical position of top edge of bead in front view, DVM units
ZREF	projected vertical position of horizontal mirror marks, DVM units
α	angle formed by ray of front view, outside the column, and normal at wall
α'	angle formed by ray of front view, inside the column, and normal at wall

β	angle formed by ray of mirror view, outside the column, and normal at wall
β'	angle formed by ray of mirror view, inside the column, and normal at wall
ϵ	positive number, much less than one
ϵ_f	fluid eddy viscosity, ft.^{2}/sec.
η	ordinate of (ξ, η) coordinates on cross section of column, inches
η_2	ordinate of (ξ, η) coordinates of point of intersection of ray of mirror view with air-column boundary, inches
θ	azimuthal component on the cross section of the column
$\lambda_i(k)$	i^{th} vertical step length with time index k, combined runs, inches
$\lambda_i^R(k)$	i^{th} vertical step length with time index k in a run, inches
$\overline{\lambda(k)}$	mean step length with time index k, inches
$\overline{\lambda^2}$	mean square step length, in.^{2}
$\overline{\lambda^2(k)}$	mean square step length with time index k, in.^{2}
$\overline{\lambda_\infty^2(k)}$	mean square step length with time index k from a population of infinite size, in.^{2}
μ_b	100 b percentile of standard normal distribution
ξ	abscissa of (ξ, η) coordinates on cross section of column, inches
ξ_2	abscissa of (ξ, η) coordinates of point of intersection of ray of mirror view with air-column boundary, inches
ρ_f	fluid density, lb./ft.^{3}
τ	diffusion time, seconds
τ_k	time interval of a group of step lengths with time index k, seconds
τ^*	time constant of $\widetilde{K}(\tau)$, seconds
ϕ	angle formed by ray of mirror view and x-axis

Φ	angle formed by mirror and focal plane of camera
χ^2_b	100 b percentile of chi-square distribution

subscripts and superscripts

a	confidence coefficient
b	level of a statistical distribution
bed	fluidizing column
d	orifice throat
e	base of natural logarithm
f	fluid
i	index of position and step length sequences
j	time index of timewise correlation coefficient
k	time interval index of a group of step lengths
p	particle
R	run
w	water
z	vertical direction

REFERENCES

1. Leva, M., Fluidization, McGraw-Hill Book Co., New York (1959).

2. Zabrodsky, S.S., Hydrodynamics and Heat Transfer in Fluidized Beds, The M.I.T. Press, Cambridge (1966).

3. Zenz, F.A. and Othmer, D.F., Fluidization and Fluid - Particle Systems, Reinhold Publishing Co., New York (1960).

4. Botterill, J.S.M., "Progress in Fluidization," British Chemical Engineering 10, no. 1, 26-30 (1965); and "Progress in Fluidization," British Chemical Engineering 8, no. 1, 21-26 (1963); and "Fluidization," British Chemical Engineering 6, 327-331 (1961).

5. Davidson, J.F. and Harrison, D., Fluidised Particles, Cambridge University Press, Cambridge, England (1963).

6. Carlos, C.R. and Richardson, J.F., "Solids Movement in Liquid Fluidised Beds, I. Particle Velocity Distribution; II. Measurements of Axial Mixing Coefficients," Chemical Engineering Science 23, 813-831 (1968).

7. Handley, D., Doraisamy, A., Butcher, K.L., and Franklin, N.L., "A Study of the Fluid and Particle Mechanics in Liquid-Fluidised Beds," Trans. Instn. Chem. Engrs. 44, T260-T273 (1966).

8. Rowe, P.N., Partridge, B.A., Cheney, A.G., Henwood, G.A., and Lyall, E., "The Mechanisms of Solids Mixing in Fluidised Beds," Trans. Instn. Chem. Engrs. 43, T271-T286 (1965).

9. Haberman, W.L. and Morton, R.K., "An Experimental Investigation of the Drag and Shape of Air Bubbles Rising in Liquids," TMB Report 803 (1953).

10. Richardson, J.F. and Zaki, W.N., "Sedimentation and Fluidisation: Part I," Trans. Instn. Chem. Engrs. 32, 35-53 (1954).

11. Gordon, L.J., "Solids Motion in a Liquid Fluidized Bed," Ph. D. Thesis, University of Washington (1963).

12. Wilde, D.J., "Aggregative Fluidization of a Solid with a Liquid," M.S. Thesis, University of Washington (1956).

13. Lemlich, R. and Manoff, M., "Optically Tagging Individual Particles in a Bed," A.I.Ch.E. Journal 9, 426 (1963).

14. UCON Fluids and Lubricants, The Union Carbide Corporation, New York (1966).

15. Schneider, J.A., "Acetylene Tetrabromide -- Fire Retardant Additive," Dow Technical Report, The Dow Chemical Company, Midland (1969).

16. Handbook of Chemistry and Physics, 50th Edition, R. C. Weast, Ed., The Chemical Rubber Company, Cleveland (1969), p. C-287.

17. Cokelet, G. R., personal communication, Dept. of Chemical Engineering, Montana State University.

18. "Standards for Discharge Measurement with Standardized Nozzles and Orifices," NACA TM No. 952, Washington, D. C. (1940).

19. Einstein, A., Investigations on the Theory of the Brownian Movement, Dover Publications, Inc. (1956), pp. 1-18.

20. Feller, W., An Introduction to Probability Theory and Its Applications, Vol. 1, John Wiley and Sons, New York (1950), Chapter 14.

21. Taylor, G.I., "Diffusion by Continuous Movements," Proc. London Math. Soc. A20, 196-212 (1921).

22. Williams, E. J., Regression Analysis, John Wiley and Sons, New York (1959), pp. 59-64.

23. Schlichting, H., Boundary Layer Theory, McGraw-Hill Book Co., New York (1968), p. 572.

24. Blasius, H., "Das Ähnlichkeitsgesetz bei Reibungsvorgängen in Flüssigkeiten," Forschg. Arb. Ing.-Wes., No. 131, Berlin (1951).

25. Moore, C. A. and Kline, S. J., "Some Effects of Vanes and of Turbulence on Two-Dimensional Wide-Angle Subsonic Diffusers," NACA TN 4080 (1958).

26. See reference 3, page 202.

27. Hassett, N. J., "The Mechanism of Fluidisation," British Chemical Engineering 6, no. 11, 777 (1961).

28. Kramers, H., Westermann, M. D., deGroot, J.H., and Dupont, F. A. A., "The Longitudinal Dispersion of Liquid in Fluidized Beds," Proceedings of the Symposium on the Interaction between Fluids and Particles, London (1962), pp. 114-119.

29. Cairns, E. J. and Prausnitz, J. M., "Macroscopic Mixing in Fluidization," A. I. Ch. E. Journal 6, no. 4, 554-560 (1960).

30. Lighthill, M. J. and Whitham, G. B., "On Kinematic Waves, I. Flood Movement in Long Rivers; II. A Theory of Traffic Flow on Long Crowded Roads," Proc. Roy. Soc. (London) A229, 281-345 (1955).

31. Steinour, H. H., "Rate of Sedimentation," Ind. Eng. Chem. 36, 618-624 (1944).

32. Brinkman, H. C., "A Calculation of the Viscous Force Exerted by a Flowing Fluid on a Dense Swarm of Particles," App. Sci. Res. A1, 27-34 (1947).

33. Slis, P. L., Willemse, Th. W., and Kramers, H., "The Response of the Level of a Liquid Fluidized Bed to a Sudden Change in the Fluidizing Velocity," App. Sci. Res. 8, 209-218 (1959).

34. Kynch, G. J., "A Theory of Sedimentation," Trans. Faraday Soc. 48, 166-176 (1952).

35. Wallis, G. B., "Simplified One-Dimensional Representation of Two-Component Vertical Flow and Its Application to Batch Sedimentation," Proceedings of the Symposium on the Interaction between Fluids and Particles, London (1962), pp. 9-16.

36. Shannon, P. T., DeHaas, R. D., Stroupe, E. P. and Tory, E. M., "Batch and Continuous Thickening," Ind. Eng. Chem. Fundamentals 3, no. 3, 250-260 (1964).

37. Hyde, J. F., "Method of Coloring Glass Fibers," U. S. Patent, No. 2, 245, 783 (1941).

38. McLaughlin, M. H., "An Experimental Study of Particle - Wall Collision Relating to Flow of Solid Particles in a Fluid," Mechanical Engineer Thesis, California Institute of Technology (1968).

39. Paint, Oil, and Chemistry Review 109, 12, 14, 16 (1946).

40. The Corrosion Handbook, H. H. Uhlig, Ed., John Wiley and Sons, New York (1948), p. 76.

41. Ambrosius, E. E. and Spink, L. K., "Coefficients of Discharge of Sharp-Edged Concentric Orifices in Commercial 2-In., 3-In., and 4-In. Pipes for Low Reynolds Numbers Using Flange Taps," Trans. A. S. M. E. 69, 805-812 (1947).

42. Southall, J. P. C., The Principles and Methods of Geometrical Optics, The Macmillan Co., New York (1910), pp. 292-294.

43. Lindgren, B. W. and McElrath, G. W., Introduction to Probability and Statistics, The Macmillan Co., New York (1959), pp. 191-193.